BNL -52351-97/12-REV

LABORATORY DIRECTED RESEARCH & DEVELOPMENT

ANNUAL REPORT TO THE DEPARTMENT OF ENERGY

DECEMBER 1997

FROM FIFTY TO THE FUTURE

BROOKHAVEN NATIONAL LABORATORY
1947 TO 1997

BROOKHAVEN NATIONAL LABORATORY
ASSOCIATED UNIVERSITIES, INC.
UPTON, NEW YORK 11973-5000

UNDER CONTRACT NO. DE-AC02-76H00016
WITH THE UNITED STATES DEPARTMENT OF ENERGY

BNL-52351-97/12-REV

Laboratory Directed Research & Development Program

Annual Report to the Department of Energy
December 1997

Gregory J. Ogeka and John M. Searing
Special Assistants to the
Associate Director for Administration

BROOKHAVEN NATIONAL LABORATORY
ASSOCIATED UNIVERSITIES, INC.
UPTON, NEW YORK 11973-5000

UNDER CONTRACT NO. DE-AC02-76CH00016
UNITED STATES DEPARTMENT OF ENERGY

Printed in the United States of America
Available from
National Technical Information Service
U.S. Department of Commerce
5285 Port Royal Road
Springfield, VA 22161

NTIS price codes:
Printed Copy: A07; Microfiche Copy: A01

Acknowledgments

The Laboratory Directed Research and Development (LDRD) Program is directed by Peter D. Bond, Interim Laboratory Director, and is administered by Henry C. Grahn, Associate Director for Administration (ADA). Preparation of the FY 1997 report was coordinated and edited by Gregory Ogeka and John Searing, Special Assistants to the ADA, who wish to thank Susan Cuevas, Regina Paquette, and D.J. Greco for their assistance in organizing, typing, and proofing the document. A special thank you is also extended to the Photography and Graphic Arts Group for their help in publishing. Of course, a very special acknowledgement is extended to all of the authors of the project annual reports and to their secretaries.

Table of Contents

Table of Contents

Introduction

Background: Brookhaven National Laboratory (BNL) was established in 1947 on the site of the former Army Camp Upton. Brookhaven is a multidisciplinary laboratory that carries out basic and applied research in the physical, biomedical and environmental sciences, and in selected energy technologies. The Laboratory is managed by Associated Universities, Inc., under contract with the U. S. Department of Energy. BNL's total annual budget has averaged about $380 million, and its facilities are valued at over $2.2 billion. There are about 3,200 employees, and another 4,000 guest scientists and students who come each year to use the Laboratory's facilities and work with the staff. BNL's Relativistic Heavy Ion Collider (RHIC), presently under construction, will be the world's foremost facility for nuclear physics research. RHIC will create the hot, dense plasma of quarks and gluons from which particles condensed after the "Big Bang" of the early universe.

Mission and Core Competencies: Brookhaven National Laboratory's mission is to support the basic Department of Energy (DOE) activities through its research and technology development, educational efforts, and industrial involvement. Brookhaven was founded as a laboratory which would provide specialized research facilities that could not be designed, built and operated at a university or industrial complex, and this still remains a basic mission of the Laboratory. Brookhaven National Laboratory has four core competencies.

Brookhaven's four core competencies: Research Facilities, Scientific Research, Technology Development, and Knowledge Transfer are not independent isolated competencies. They are interrelated in a complex manner.

MAJOR CORE COMPETENCIES
RESEARCH FACILITIES Expertise to conceive, design, build and operate complex leading-edge, user-oriented research facilities in a safe and environmentally responsible manner.
SCIENTIFIC RESEARCH Expertise to carry out basic and applied scientific research in long-term, high-risk programs. This is an essential capability needed to keep our research facilities at the leading edge of science. These programs lead to new insights and technological advances which provide the underlying scientific base supporting DOE missions and generating long-term benefits to the nation.
TECHNOLOGY DEVELOPMENT Expertise to develop advanced technologies that address national needs, support and strengthen the ability of DOE to carry out its missions, support other federal and state agencies, and enable industry to benefit from the multidisciplinary research and development at the Laboratory.
KNOWLEDGE TRANSFER Expertise and mechanisms for disseminating scientific and technical knowledge to educate new generations of scientists and engineers to produce a technically trained workforce, to enhance scientific literacy of the general public, and to improve the competitiveness of U. S. industry.

Research Facilities and Scientific Research have a synergistic relationship. To maintain and constantly improve a research facility, and to keep it at the cutting edge, it is essential that the Laboratory have a significant research staff of excellent stature. The staff will drive the performance of the facility. Having the several complementary facilities at one location, such as the National Synchrotron Light Source and the High Flux Beam Reactor, allows a unique research capability, such as in material science and biological structure determination. The other two core competencies: Technology Development and Knowledge Transfer, bridge all of the research facilities and research programs.

Brookhaven's core competencies support and cut across the five central activities of the Department of Energy as defined in its Strategic Plan.

DOE Strategic Plan Activities	
SCI	**Science and Technology**
ENV	**Environmental Quality**
ENER	**Energy Resources**
SEC	**National Security**

BNL plays a major role in the Science and Technology, the Environmental Quality, the Industrial Competitiveness and the Energy Resources sectors, with a smaller, but special role in the National Security arena. In order to better see the connection between the various Brookhaven activities that form the core competencies and the Department of Energy Strategic Plan activities, each BNL activity/competency is followed with the letter code describing the match in the Table 1, "Major Activity Clusters."

Summary: New ideas and opportunities fostering the advancement of technology are occurring at an ever increasing rate. It, therefore, seems appropriate that a vehicle be available which fosters the development of new ideas and technologies, promotes the early exploration and exploitation of creative and innovative concepts, and develops new "fundable" R&D projects and programs if BNL is to carry out its primary mission and support the basic Department of Energy activities. At Brookhaven National Laboratory one such method is through its Laboratory Directed Research and Development Program. This discretionary research and development tool is critical in maintaining the scientific excellence and vitality of the Laboratory. Additionally, it is a means to stimulate the scientific community, fostering new science and technology ideas, which is the major factor in achieving and maintaining staff excellence and a means to address national needs within the overall mission of the DOE and BNL.

The Project Summaries with their accomplishments described in this report reflect the above. Aside from leading to new fundable or promising programs and producing especially noteworthy research, they have resulted in numerous publications in various professional and scientific journals and presentations at meetings and forums.

TABLE 1:
MAJOR ACTIVITY CLUSTERS

LARGE RESEARCH FACILITIES

ALTERNATING GRADIENT SYNCHROTRON
(SCI)
- Research in Particle and Nuclear Physics
- High-Intensity Frontier of Particle Physics
- World's Only High Energy Polarized Proton Source
- At Present, Nation's Only High Energy, Heavy Ion Synchrotron
- Over 800 Users

RELATIVISTIC HEAVY ION COLLIDER
(under construction)
(SCI)
- Dedicated Colliding Beams Facility for Ultra Relativistic Collisions of Heavy Nuclei
- New Phases of Nuclear Matter High-Temperature Frontier
- Large and Unique High Energy Physics Potential (e.g. spin physics)
- International Community of Over 800 Scientists

HIGH FLUX BEAM REACTOR
(SCI, ENER, ENV)
- 16 Instruments for Research in Condensed-Matter Physics, Biology, Chemistry, Applied Sciences and Industrial Applications
- Facilities for Radio Isotope Production and Radiation Damage Studies
- 270 Users

NATIONAL SYNCHROTRON LIGHT SOURCE
(SCI, ENV, ENER)
- Two Storage Rings Providing Intense UV and X-ray Photon Sources
- 83 Beamlines for Research in Materials Science, Biology, Chemistry, Medical and Industrial Applications
- R&D on Free Electron Lasers and on Production and Utilization of Synchrotron Radiation
- Over 2300 Users, Including 400 Industrial Users

BIOMEDICAL FACILITIES

BROOKHAVEN CENTER FOR IMAGING AND NEUROSCIENCE
(SCI)
- Positron Emission Tomography (PET), Single Photon Emission Computed Tomography (SPECT), and High-Field (4 Tesla) Magnetic Resonance Imaging (MRI) for Research in the Basic and Clinical Neuroscience (Substance Abuse; Aging; Brain Cancer; Drug Research) and the Development of New Forms of Imaging

BROOKHAVEN LINEAR ISOTOPE PRODUCTION FACILITY
(SCI)
- Production of Isotopes for Medical Purposes
- Approximately 20 Isotopes Produced for Commercial and/or Research Use

MEDICAL RADIATION FACILITY
(SCI)
- Cancer Patient Treatment: 250 patients annually

BROOKHAVEN MEDICAL RESEARCH REACTOR
(SCI)
- Neutron Capture Cancer Therapy Research

SCANNING TRANSMISSION ELECTRON MICROSCOPE
(SCI)
- Structural Biology, Molecular Masses
- Over 75 Users

PROTEIN DATA BANK
(SCI)
- World-Wide Repository for Three-Dimensional Structures of Biological Macromolecules

GENOME SEQUENCING CENTER
(under development)
(SCI)
- Large-Scale DNA Sequencing

OTHER FACILITIES

TANDEM VAN DE GRAAFF FACILITY
(SCI, SEC, ENV, ENER)
- Injector (source) for Heavy Ions for AGS/RHIC
- Microchip Radiation Testing Facility
- Film Irradiation Plant for Track Etching Filter Membranes
- 250 Users from 45 Institutions

ACCELERATOR TEST FACILITY
(SCI, SEC)
- Advanced Acceleration Concepts

CENTER FOR RADIATION CHEMISTRY RESEARCH
(SCI, ENER, ENV)
- Study of Rapid Chemical Reactions: Catalysis, Energy Conversion and Storage

NATIONAL NUCLEAR DATA CENTER
(SCI, SEC, ENV)
- Nuclear Cross-Section and Structure Data
- 1100 Users

BOOSTER APPLICATIONS FACILITY
(under development)
(SCI, SEC)
- Proton and Heavy Ion Radiobiology & Microelectronics Radiation Effects

DYNAMITRON ACCELERATOR
(SCI)
- 3MeV Electron or Positron Accelerator
- Device Calibration

SCIENTIFIC RESEARCH

HIGH ENERGY PARTICLE AND NUCLEAR PHYSICS
(SCI)
- Beyond the Standard Model
  - Rare Kaon Decays
  - Muon Anomalous Magnetic Moment
  - Exotics and Glueball Spectroscopy
  - Strange Matter
  - Solar Neutrinos
- Relativistic Heavy Ions
  - Nuclear Matter In Extreme States of Temperature and Density
  - QCP Phase Transitions: Hadrons to Quark-Gluon Plasma
  - Recreate Conditions of the Early Universe, Microseconds after the Big Bang

ADVANCED ACCELERATOR CONCEPTS
(SCI, SEC)
- Short Wavelength Accelerating Structures
- Production of Coherent Radiation Free Electron Laser
- Muon Collider
- Neutron Sources

MATERIALS SCIENCES
(SCI, ENER)
- Materials Characterization with Neutron and X-ray Scattering
- Magnetism and Superconductivity
- Surface Studies
- Corrosion, Adhesion & Catalysis
- Condensed Matter Theory Metallic Alloys and Cooperative Phenomena
- Defect Structure with Positrons

CHEMICAL SCIENCES
(SCI, ENER, ENV)
- Dynamics and Energetics and Reaction Kinetics
- Thermal, Photo and Radiation Induced Reactions
- Catalysis
- Porphyrin Chemistry
- Electrochemistry

ENVIRONMENTAL SCIENCES
(SCI, ENV)
- Global Change
- Atmospheric Chemistry
- Oceanography
- Soil Chemistry
- Cycling of Pollutants
- Environmental Remediation

MEDICAL SCIENCE
(SCI)
- Medical Imaging: PET, SPECT, MRI, Coronary Angiography
- Nuclear Medicine
- Radionuclides, Radiopharmaceuticals, Synthesis and Applications
- Advanced Cancer Therapies: Neutron Capture, Microbeam Radiation, Proton Radiation, Photon Activation Therapy (PAT)
- Mechanisms of Oncogenesis

MOLECULAR BIOLOGY AND BIOTECHNOLOGY
(SCI)
- Genome Structure, Gene Expression
- DNA Damage and Repair
- Molecular Genetics
- Plant Science
- Bio-Structure Determination by X-ray and Neutron Scattering
- Enzyme Kinetics by Laue Crystallography
- Mass Measurements by Electron Microscopy

ADVANCED SCIENTIFIC COMPUTING AND SYSTEMS ANALYSIS
(SCI, ENV, ENER)
- Risk Assessment
- Energy Modeling
- Groundwater Modeling
- Traffic Congestion Simulation
- Atmospheric Transport Modelling

TECHNOLOGY DEVELOPMENT

PHYSICAL, CHEMICAL AND MATERIALS SCIENCE
(SCI, ENER, SEC)
- State-of-the-Art Instrumentation and Devices for Precision Electronics, Optics and Microelectronics
- Superconducting Materials
- X-ray Lithography
- Micromachining
- Battery Technology
- Permanent Magnets
- "Designer" Polymers
- Flat Planar Optic Displays

ACCELERATOR TECHNOLOGY
(SCI, SEC)

- High-Field, High-Quality Superconducting Magnets
- High-Power Radio Frequency Systems
- Ultrahigh Vacuum Systems
- Advanced Accelerator Designs
  - High-Gradient Acceleration
  - High-Beam Current Acceleration
  - Novel Structures for Synchrotron Radiation Generation, FELs
- Accelerator/Spallation Source Applications
- Insertion Device Development: Wigglers and Undulators

ENVIRONMENTAL AND CONSERVATION TECHNOLOGIES
(SCI, ENV, ENER, SEC)

- Environmental Remediation and Mitigation
- Energy-Efficiency Technologies
- Waste Treatment
- Disposal of Nuclear Materials
- Radiation Protection
- Infrastructure Modernization
- Transportation: Intelligent Vehicle Highway System, MAGLEV
- Ultrasensitive Detection and Characterization

MEDICAL TECHNOLOGIES
(SCI)

- Biomedical Applications of Nuclear Technology
- Production of Radionuclides and Radiopharmaceuticals
- Development of Particle Radiation Therapies for Cancer
- Medical Imaging
- X-ray Microbeam Therapy

BIOTECHNOLOGY
(SCI)

- Neutron and Synchrotron X-ray Scattering
- Large-Scale Genome Sequencing
- High-Resolution Scanning and Cryo Electron Microscopy
- Cloning, Expressing and Engineering Genes
- Metal Cluster Compounds for Electron Microscope Labels
- Phage Displays for Probing Specific Interactions

SAFETY AND RISK ASSESSMENT
(SEC, SCI, ENV, ENER)

- Safeguards, Nonproliferation and Arms Control
- Safety Analysis of Complex Systems
- Probabilistic Risk Assessment and Management
- Human Reliability
- Material and Component Survivability Testing
- Remote Sensing of Chemical Signatures
- Technical Support for U.S. Policy

KNOWLEDGE TRANSFER

EDUCATING FUTURE GENERATIONS OF SCIENTISTS AND ENGINEERS
(SCI, ENV, ENER, SEC)

- Scientific Publishing, Lecturing, Conference Participation
- Visiting Scientist Program
- Accelerator Fellowship Program
- Postdoctoral Research Associates
- Engineering Intern Program
- Graduate Student Thesis Projects
- Adjunct Teaching Appointments at Local Colleges
- Office of Educational Program
  - Precollege and College Programs for Students and Teachers

EDUCATING THE GENERAL PUBLIC
(SCI, ENV, ENER, SEC)

- Science Museum and Laboratory Tours (20,000 people/year)
- Speakers Bureau
- BNL Videos
- Laboratory Lectures for the Public
- Community Outreach Programs
- School Mentoring Program

TECHNOLOGY TRANSFER TO INDUSTRY
(SCI, ENV, ENER, SEC)

- Scientific Publishing
- Industrial Users at the Research Facilities
- Consulting by Scientific Staff
- Technology Transfer Office
  - Patenting and Licensing Office
  - Technical Assistance for Industry
  - CRADAs
  - Visiting Scientist Program with Industry
  - Research Partnerships with Industry
  - Industry-Sponsored Proprietary Research and Development
- Long Island Research Institute (LIRI) (founding member)
  - promotes Laboratory-Industry Interaction
  - ARPA-Funded BNL/LIRI Defense Conversion Project
  - NY State-Funded Biotechnology Initiative

INFORMATION TECHNOLOGY
(SCI, ENV, ENER, SEC)

- Electronic Library and Database Information Source
- Networking - "Information Superhighway"
- Technical and Scientific Publishing
- National Nuclear Data Center
- Protein Data Bank
- Data Visualization
- ALARA Center

TRAINING AND EDUCATION OF TECHNOLOGISTS

(ENER, SEC, ENV)

- Safety of Soviet-Designed Reactors
- Safeguards of Special Nuclear Materials in the former Soviet Union
- Mentoring within the DOE Complex
- Waste Management in the former Soviet/Artic Regions

Management Process

PROGRAM DESCRIPTION:

Introduction: The Department of Energy's (DOE) Laboratory Directed Research & Development (LDRD) Program at Brookhaven National Laboratory (BNL) was originally established as the "Exploratory Research Program" under the guidelines set forth in DOE Order 5000.1 in May 1984. From inception through September 1998, a period spanning fourteen fiscal years, the Laboratory has authorized $34.2 million in Exploratory R&D, consisting of 179 separate projects.

BNL LDRD PROGRAM HISTORY 1985-1998

FISCAL YEAR	AUTH K$	COSTED K$	NO. REC'D	NEW STARTS
1985	1,842	1,819	39	13
1986	2,552	2,515	22	15
1987	1,451	1,443	29	8
1988	1,545	1,510	46	14
1989	2,676	2,666	42	21
1990	2,008	1,941	47	9
1991	1,353	1,321	23	14
1992	1,892	1,865	30	14
1993	2,073	2,006	35	14
1994	2,334	2,323	44	15
1995	2,486	2,478	46	13
1996	3,500	3,050	47	17
1997	4,500	3,459	71	10
1998	4,000*	—	53	4
TOTALS	34,212	28,391	574	181

*Additional projects may be funded in FY 1998, pending the availability of funds.

Historical Perspective: Brookhaven National Laboratory was established in 1946. Throughout its history, certain projects of an exploratory nature, sometimes referred to in the past as "seed money projects," were supported with overhead funding. In 1979, as a result of a Review Audit in that year, the seed money accounting procedures were formalized, and oversight by the then DOE Brookhaven Area Office Manager was first established. This seed money program operated at a variable level of funding, which averaged about 0.1 percent of the Laboratory's operating budget over the period 1979 to 1984.

In May 1984, the program was expanded. The expanded program embraced the new Exploratory R&D guidelines of DOE Order 5000.1. The new program, called the Exploratory Research Program, was put into effect for FY 1985 funding. The current Laboratory Directed Research & Development Program reflects the operating styles and many of the procedures of the earlier programs, which have evolved somewhat informally over the years. It also encompasses the requirements of the current DOE Order 413.2.

Goals and Objectives: The goals and objectives of BNL's LDRD Program can be inferred from the Program's stated purposes. These are to (1) encourage and support the development of new ideas and technology, (2) promote the early exploration and exploitation of creative and innovative concepts, and (3) develop new "fundable" R&D projects and programs. The emphasis is clearly articulated by BNL to be on supporting exploratory research "which could lead to new programs, projects, and directions" for the Laboratory.

General Characteristics of the LDRD Program: Projects or studies that are appropriate candidates for the Laboratory's LDRD Program include, but are not limited to, (1) projects, normally relatively small, in the forefront areas of basic and applied science and technology for the primary purpose of enriching laboratory capabilities, (2) advanced study of new hypotheses, new concepts, or innovative approaches to scientific or technical problems, (3) experiments and analyses directed toward "proof of principle" or early determination of the utility of new scientific ideas, and (4) conception and preliminary technical analysis of experimental facilities or devices.

PROGRAM ADMINISTRATION:

Overall Coordination: Overall responsibility for coordination, oversight, and administration of BNL's LDRD Program resides with the Laboratory's Director. The Office of the Associate Director for Administration assists in the administration of the program. This includes administering the program budget, establishment of project accounts, maintaining summary reports, and reports of Program activities to the DOE through the Brookhaven Group Manager.

Responsibility for the allocation of resources and the orchestration, review, and selection of proposals lies with a management-level group called the Laboratory Directed Research & Development Program Committee.

The Program Committee is made up of six members. For Fiscal Year 1998, the Laboratory's Director is the chairperson of the Committee. The other members are the Associate and Assistant Directors of the Laboratory.

1997 LDRD PROGRAM COMMITTEE

Peter D. Bond	**Chairperson**
Henry C. Grahn	**Administration**
Thomas Kirk	**High Energy & Nuclear Physics**
Denis B. McWhan	**Basic Energy Sciences**
Mark Sakitt	**Planning & Policy and for Applied Programs**
Richard B. Setlow	**Life Sciences**

Allocating Funds: There are two types of decisions to be made each year concerning the allocation of funds for the LDRD Program. These are: (1) the amount of money that should be budgeted overall for the Program; and (2) of this, how much, if any, should go to each competing project or proposal. Both of these decisions are made by high-level management.

Concerning the overall budget, for each upcoming fiscal year the Laboratory Director, in consultation with the Associate Director for Administration, develops an overall level of funding for the LDRD Program. The budget amount is then incorporated into the Laboratory's LDRD Plan which formally requests authorization from the DOE to expend funds for the LDRD Program up to this ceiling amount.

The majority of projects are authorized for funding at the start of the fiscal year. However, projects can be authorized throughout the fiscal year, as long as funds are available and the approved ceiling for the LDRD Program is not exceeded.

The actual level of funding available for LDRD, however, may turn out to be much less than this ceiling. The actual level is determined during the course of the year and is affected by several considerations including: the specific merits of the various project proposals, as determined by Laboratory management and the members of the LDRD Program Committee; the overall financial health of the Laboratory; and a number of budgetary tradeoffs between LDRD and other overhead expenses.

LDRD COSTS VS. TOTAL LABORATORY COSTS

operating $ in millions

FISCAL YEAR	DOE FUNDS	WFO FUNDS	TOTAL FUNDS	LDRD FUNDS	% OF TOTAL
1985	153.0	40.4	193.1	1.82	0.9
1986	156.5	45.1	201.6	2.52	1.2
1987	161.7	45.6	207.3	1.44	0.7
1988	176.7	45.9	222.6	1.51	0.7
1989	193.6	46.7	240.3	2.67	1.1
1990	203.8	45.2	249.0	1.94	0.8
1991	220.9	50.3	271.2	1.32	0.5
1992	234.3	47.2	281.5	1.87	0.7
1993	231.4	47.3	278.7	2.01	0.7
1994	237.0	47.9	284.9	2.32	0.8
1995	243.0	53.7	296.7	2.48	0.8
1996	251.6	50.6	302.2	3.05	1.0
1997	257.2	52.5	309.7	3.46	1.1

Concerning the allocation of resources to specific topic areas or to individual project proposals, such issues are addressed on a case-by-case basis by the LDRD Program Committee, once specific proposals have been received. The Committee meets periodically to review and recommend project proposals and to determine the amount of funding to be made available to the LDRD Program. The requirements of DOE Order 413.2 are carefully considered during the selection process to ensure that proposals are consistent with DOE's criteria.

Request for Proposals: The availability of special funds for research under the LDRD Program is well publicized throughout the Laboratory. This is done using three methods --one occurring at yearly intervals, the other occurring irregularly, and the last by computer on the internet. Each year in May a memo is sent by the Laboratory Director to all scientific staff issuing a "call for proposals." This memo is accompanied by a document entitled, "Guidelines and Procedures for Developing Proposals via the Laboratory Directed Research and Development (LDRD) Program." The other method is by announcement in the Brookhaven Bulletin, the Laboratory's weekly newspaper; but the nature of the announcements varies, and they appear at irregular intervals. In some years the Bulletin prints an article that amounts to a separate call for proposals. In other years the Bulletin publishes articles on specific research projects which, in effect, help advertise the LDRD Program. Lastly, the Associate Director for Administration maintains an LDRD website with information regarding submittal of projects for LDRD funding.

The "Guidelines and Procedures" document specifies the requirements necessary for participation in the program. It states the program's purpose, general characteristics, procedures for applying, and restrictions. An application for funding, that is, a project proposal, takes the form of a completed "Proposal Information Questionnaire." An application must be approved up the chain-of-command which includes the initiator's Department or Division Budget Administrator, the Department Chairperson or Division Head, and the cognizant Associate Director. Plans to ensure the satisfactory continuation of the principal investigator's regularly funded programs must also be approved. The applications are then forwarded to the Chairperson of the LDRD Program Committee for further review and consideration for funding.

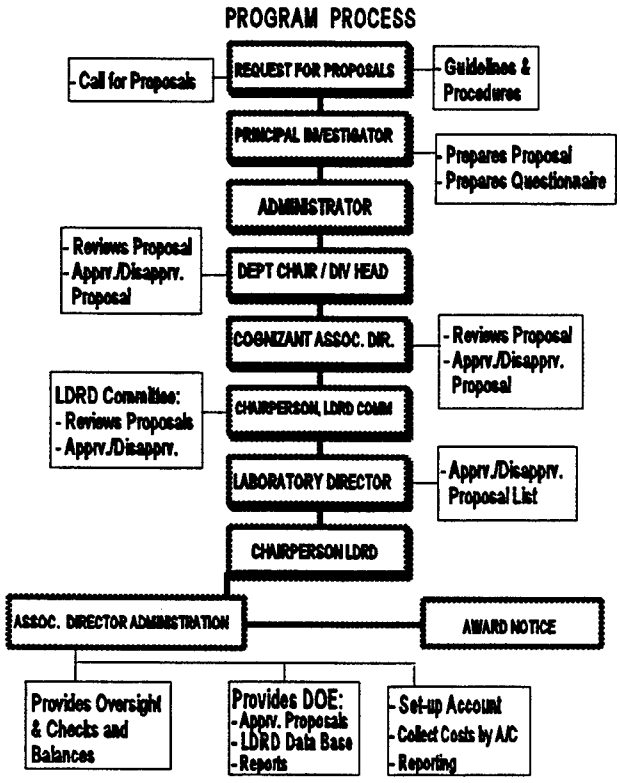

The process which solicits and encourages the development of proposals has evolved into two modes of operation. Specifically, the ideas for proposal development may originate among the scientific staff in response to the general call for proposals. Alternatively, they may be initiated by top-level Laboratory management. Eventually, both follow the standard procedure for proposal approval up the chain-of-command to the same decision makers. The fact that all proposals must be approved up the chain-of-command permits BNL managers to consider all ideas together when designing the mix of projects for the LDRD Program.

An initiative from management typically takes the form of a general topic area or item of special interest. It is not a directive, nor is it included in the call for proposals, but the idea is communicated to a group of scientific staff, which is known to be in a position capable of pursuing and developing the idea in the form of a more formal proposal.

Proposal Review: Once a proposal is approved by the cognizant line managers, all proposals are forwarded to the Chairperson of the Committee who transmits a copy of all proposals received to the Committee for review. The Committee considers all proposals that have met certain minimum requirements pertaining to the Department's and BNL's LDRD policies.

Lead responsibility for the review of a proposal is then assigned to that member of the Committee who last approved it in the chain-of-command, that is, the member who oversees and directs the technical area from which the proposal originated. All members have several weeks to review the proposals and prepare for the next Committee meeting. During this time, additional reviews, if desired, may be arranged.

Formal peer reviews, consisting of written comments by experts outside the normal lines of supervision, are not usually performed. The members of the Committee are considered to have sufficient technical knowledge so that peer reviews are seldom required.

At the next Committee meeting, the Committee member responsible for the review of the proposal presents the proposal to the other members of the Committee. This is done without the member necessarily becoming an advocate for the proposed project.

Selection Criteria: Before proposals can be considered by the Committee, they must be screened to ensure that they meet a set of minimum requirements concerning the Department's LDRD policies and the Laboratory's own guidelines.

Minimum requirements of each proposal are: (1) consistency with program purpose; (2) consistency with missions of BNL, DOE, and NRC; (3) approval by Department Chairperson and/or Division Head, and cognizant Associate Director; (4) assurance of

satisfactory continuation of principal investigator's regularly funded programs; (5) modest size and limited to 3 years; (6) will not substitute for, supplement, or extend funding for tasks normally funded by DOE, NRC, or other users of the Laboratory; (7) will not require the acquisition of permanent staff; (8) will not create a commitment of future multi-year funding to reach a useful stage of completion; and (9) will not fund construction line-item projects, facility maintenance, or general purpose capital equipment.

The selection criteria used to evaluate and rank individual proposals are not formally stated or published. While the "Guidelines and Procedures" document clearly states that "awards will be made on a competitive basis," the factors or selection criteria to be considered in this competition are not listed. Nevertheless, selection is based on (1) scientific merit, (2) compliance with minimum requirements, (3) proposal cost as compared to the amount of available funding, (4) innovativeness, and (5) its potential for follow-on funding. The requirements of DOE Order 413.2 are also carefully considered during the selection process to ensure that proposals are consistent with DOE criteria.

Project Approval: After all presentations are heard, the Committee attempts to arrive at a consensus concerning the highest priority proposals. Differences, if any, are resolved by the Chairperson. Also, a balance is struck between the prevailing financial needs of the Laboratory, which may vary over the course of the year, and the priorities of the projects considered. Some funding may be held in reserve during the earlier meetings of the fiscal year so that funds remain available for proposals submitted at later dates. The funding amount requested in any one specific proposal may be changed or adjusted during the approval process. The Committee's recommendation is then submitted to the Director for his approval.

The Associate Director for Administration is then notified, so that a separate Laboratory overhead account can be established to budget and collect the costs for the project. Statistics on the number of projects approved, compared to those rejected, show an overall approval rate of about 31 percent for new starts. From inception of the program through September 1997 (for FY 1998), 574 project proposals were considered and 181 were approved.

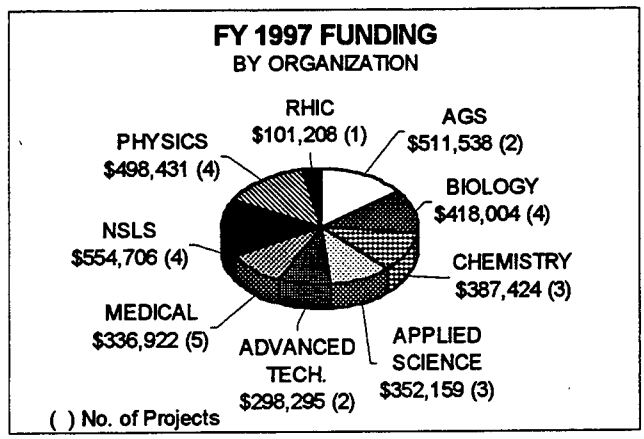

Eight scientific departments and the RHIC Project were represented in the FY 1997 LDRD Program.

Project Supervision: Supervision over the actual performance of LDRD projects is carried out in the same way as other research projects at the Laboratory. Each principal investigator is assigned to an organizational unit (Department, Division), which is supervised by a manager.

Each manager is responsible for seeing that the obligations of the principal investigator are satisfactorily fulfilled and that the research itself is carried out according to standard expectations of professionalism and scientific method. The manager is kept informed of the project's status, schedule, and progress.

The manager ensures that the work is completed in a timely manner and that annual status reports are submitted to the Director.

In addition, LDRD Program activity is reported to the DOE Brookhaven Group Manager, including copies of all funded proposals, a LDRD Program data base, and a project funding and schedule summary report.

Project Reporting: Routine documentation of each project funded under the LDRD Program consists of a file containing: (1) a copy of the written proposal; (2) all interim status reports; (3) notifications of changes in research direction, if any; and (4) reports on cost incurred. Also, a formal Annual Report on the LDRD Program is submitted to BNL management and the DOE, summarizing work progress, accomplishments, and project status on all projects.

Documentation for the overall Program consists of (1) various program history files, (2) a running list of all proposals with their acceptance/rejection status, (3) funding schedule and summary reports for all approved projects, (4) permanent records on cost accounting, and a data base containing information on each funded project (description, funding by fiscal year, status and accomplishments, follow-on funding, publications, etc.).

Some of the projects involve animals or humans. Those projects have received approval from the Laboratory's appropriate review committees. The projects which involve animals or humans are identified in this report as follows:

Note: This project involves animal vertebrates or human subjects.

This is noted on the summary sheet and also at the end of each report.

BROAD TECHNICAL AND SCIENTIFIC CATEGORIES:

Over the past several years, BNL has been categorizing its LDRD programs into six broad technical and scientific areas, including one miscellaneous area. The programs targeted for funding by BNL's LDRD Program fall into the following broad technical and scientific categories:

New Directions for Energy Technologies: In the course of basic research efforts, there are occasionally discoveries which hold promise for utilization in energy technologies. Such research is of significance, both for the Laboratory and for the DOE.

Environmental Science and Technology: BNL has a broad range of programs in environmental science. There are many important applications of our programs which we would like to exploit. These programs include atmospheric, oceanographic, and mathematical sciences, as well as efforts in environmental remediation. LDRD proposals in these areas, which move in new directions, are given priority as the Laboratory tries to make contributions to solutions of environmental problems.

Radiation Therapies and Imaging: Applications of the Laboratory's facilities to the treatment of cancer and in imaging of the human body for diagnostic purposes, including such techniques as functional MRI, microplaner x-ray therapy, neutron capture therapy and the use of other imaging techniques, are a significant part of the LDRD effort.

Genetic Studies: This area of research at the Laboratory has produced many new ideas and applications which are too important to remain undeveloped. LDRD funded projects in this area are varied in subject matter covering many bio-medical topics.

New Directions for the Development and Utilization of BNL Facilities: High priority is assigned to ideas for more efficient utilization and for new directions for our major facilities. Ideas for more useful sources of x-rays at the synchrotron light source, for the utilization of new electron sources in the chemical study of

pulse radiolysis, and new laser systems are all areas which are given priority for support.

Other Miscellaneous: Finally, the Program is open to significant and original ideas which do not necessarily fall within the bounds of the aforementioned priority areas. These usually involve small individual programs and projects that are judged to have high scientific/technical merit. Typically, materials development, electrochemical studies, advanced nuclear concepts and new bio-chemistry technologies fall into this category.

Brookhaven National Laboratory's FY 1997 LDRD Program covered the following Scientific and Technical Areas.

Programs/Projects	Funding $000
New Directions for Energy Technologies	$ 0
Environmental Science & Tech.	318
Radiation Therapies and Imaging	804
Genetic Studies	325
New Directions for the Development and Utilization of BNL Facilities	1,613
Other - Miscellaneous	399
TOTAL	$ 3,459

SUCCESS INDICATORS:

Overall the BNL LDRD Program has been very successful. Some of the more common indicators/measures of success are: (1) the amount of follow-on funding received, (2) the number of proposals anticipating future funding, (3) the number of full-length papers published, (4) the number of papers published in other journals or publications or presented at meetings, (5) the number of post-doctoral students supported, and (6) the number of copyrights, invention disclosures and patents applied for or granted.

Although it is difficult to maintain an accurate and timely database of these success measures for each project, a summary of the information reported is presented below. The difficulty in compiling data is the loss of contact with the principal investigators soon after the LDRD projects are concluded. This is particularly true in trying to determine whether or not follow-on funding was received.

However, in an FY 1995 analysis, it was found that of the 54 projects which were funded during the period FY 1992 - 1994, 22 received follow-on funding, and 5 others were awaiting responses to proposals which have been submitted. The total amount of follow-on funding reported for the 22 projects involved was $5.3M as compared to funding of these projects of $2.5M. Other indicators reported during this period were:

Number of Projects with at Least 1 Full-Length Publication	33
Number of Post-Doctoral Students Supported	21
Number of Scientific Associates Hired	7
Number of Copyrights, Invention Disclosures, and Patents Applied For/Granted	12

In fact, only 10 of the 54 projects had none of the aforementioned success indicators to report.

It is estimated that cumulative follow-on funding reported for all projects funded from

FY 1985 to FY 1994 is upwards of $42M versus a total program authorization of $19.7M during that period. This estimate is conservative since, as mentioned earlier, contact is not generally maintained with the principal investigator once the project has ended.

Summary of FY 1997 LDRD Program

In FY 1997, the BNL LDRD Program funded 28 projects, 10 of which were new starts, at a total cost of $3,458,687. Following is a table which lists all of the FY 1997 funded projects and gives a history of funding for each by year.

Several of these projects have already experienced varying degrees of success as indicated in the individual Project Program Summaries which follow. A total of 40 informal publications (abstracts, presentations, BNL reports and workshop papers) were reported and an additional 18 formal (full length) papers were either published, are in press or being prepared for publication. The investigator on one project (#97-45) has filed for a patent.

Six of the projects reported that proposals/grants had either been funded or were submitted for funding.

The complete summary of follow-on activities is as follows:

Follow-on Activity of LDRD Projects	
	Number of Projects
Informal Publications	**40**
Formal Papers	**18**
Grants/Proposals/Follow-on Funding	**6**
Patents/Disclosures Applied For	**1**
CRADA Application	**-**

In addition, 19 post doctoral candidates and guest scientists were supported or collaboratively involved in these projects.

In conclusion, a significant measure of success is already attributable to the FY 1997 LDRD Program in the short period of time involved. The Laboratory has experienced a significant scientific gain by these achievements.

Laboratory Directed Research and Development Fiscal Year 1997 - Summary of Projects

Project Number	Project Title	Dept.	Principal Investigator	Approved Budgets by Fiscal Year						Total Funding
				FY 1994	FY 1995	FY 1996	FY 1997	FY 1998 (estimated)	FY 1999 (estimated)	
94-06	Siberian Snake Prototype Development for RHIC	RHIC	M. Harrison	132,139	133,591	219,580	101,208			586,518
95-01	Study of possible 2+2 TeV Muon-Muon Collider	PHYS	R.B. Palmer		149,580	200,185	240,023			589,788
95-03	Ultraviolet FEL R&D	NSLS	I. Ben-Zvi		100,005	99,491	299,099			498,595
95-33*	Low Dose Gamma Imaging Facility for In Vivo Molecular Medicine	MED	R. Ma		109,736	110,070	4,809			224,615
96-06*	Positron Emission Magnetic Resonance Imaging (PEMRI)	CHEM	C.S. Springer			100,208	169,224	175,000		444,432
96-11	In-Vacuum Undulator (IVUN) for the NSLS X-ray Ring	NSLS	P.M. Stefan			100,118	98,466			198,584
96-16	Spin Polarized Coincidence Spectroscopies	PHYS	P.D. Johnson			78,999	82,281			161,280
96-19	An Evaluation of the WSR-88D Radar for the Remote Sensing of Cloud Properties	DAS	M.A. Miller			77,893	115,159			193,052
96-22	Studies of Nano-scale Structural Defects Using Advanced Electron Diffraction and Imaging Techniques	DAS	Y. Zhu			102,697	133,643			236,340
96-26	Research into New Database Methodology Based on the Object Protocol Model	BIO	E.E. Abola			14,394	98,792	95,000		208,186
96-27	Tailored Pulse UV/XUV Photon Source Development	CHEM	L.F. DiMauro			71,570	114,097	120,000		305,667
96-32	Methods for Detecting Activation of the DNA-Activated Protein Kinase, DNA-PK, in Human Tissue Culture Cells	BIO	C.W. Anderson			101,639	107,565			209,204
96-34	Enzymatic & Regulatory Interactions of a Single Protein with 3 Different Sites in Nucleic Acids	BIO	S.A. Lacks			111,076	117,516			228,592
96-37	Low Frequency Dynamics of Novel Materials	PHYS	M. Strongin			77,465	84,693			162,158
96-38*	BNCT for Leukemia Through Ex-Vivo Purging of Bone Marrow	MED	J.A. Coderre			82,116	86,342	100,000		268,458
96-46	Medical Physics Program Development	DAT	E.C. Selcow			157,773	199,229			357,002
96-49	Autecology of the Peconic Bay Brown Tide Organism, *Aureococcus anophagefferens*	DAS	J. LaRoche			98,405	103,357	108,000		309,762
96-50	The Development and Demonstration of Accelerator-Based BNCT Capability	AGS	D. Raparia			188,449	412,137	200,000		800,586
97-02	Physics Goals for a New Intense Muon Facility	PHYS	W. Marciano				91,434	115,000		206,434
97-08	A Novel Curved Proportional Counter for X-ray Powder Diffraction Studies at NSLS	NSLS	D.P. Siddons				96,666	100,000		196,666
97-13	Extraction Kicker R&D for Target Shock Testing	AGS	A. McNerney				99,401			99,401

*This project involves animal vertebrates of human subjects.

Laboratory Directed Research and Development Fiscal Year 1997 - Summary of Projects

Project Number	Project Title	Dept.	Principal Investigator	Approved Budgets by Fiscal Year						Total Funding
				FY 1994	FY 1995	FY 1996	FY 1997	FY 1998	FY 1999	
97-16	Plasma Window for Transmission of Synchrotron Radiation	NSLS	E.D. Johnson				60,475	60,000		120,475
97-29	Development of New Techniques in Picosecond Pulse Radiolysis	CHEM	J. F. Wishart				104,103	115,000		219,103
97-39	X-ray Circular Dichroism of Biological Macromolecules	BIO	J.C. Sutherland				94,131	107,000		201,131
97-44*	X-ray Schlieren Computed Tomography	MED	A. Dilmanian				59,792	97,000	44,000	200,792
97-45*	Biodistribution Toxicity & Boron Neutron-Capture Therapy in Animals Using a Metallotetracarboranylporphyrins	MED	M. Miura				86,157	111,000		197,157
97-50	Development of Pump-&-Probe LIDAR for the In Situ Study of Fast Atmospheric Chemical Reactions	DAT	A.J. Sedlacek, III				99,066	100,000	100,000	299,066
97-70*	Molecular Biological Markers as Potential Prognostic Indicators for BNCT	MED	J. Capala				99,822	117,000		216,822
				132,139	492,912	1,992,128	3,458,687	1,720,000	144,000	7,939,866

*This project involves animal vertebrates of human subjects.

LABORATORY DIRECTED RESEARCH AND DEVELOPMENT

1997 PROJECT PROGRAM SUMMARIES

Siberian Snake Prototype Development For RHIC

M.A. Harrison *94-06*

PROJECT DESCRIPTION:

A helical dipole magnet is one in which the dipole field, rather than remaining vertical, rotates uniformly along the length of the magnet. Such magnets are required to do spin physics at RHIC. The parameters required include the following: B ~ 4T, aperture = 100 mm, low current operation (<500A) to minimize heat leak through many necessarily separated leads, and a pitch in the helix of approximately 180 degrees in one meter. There is no published record that such magnets have been built in the past; this is not surprising since they serve no useful purpose in normal accelerator or beam transport optics.

TECHNICAL PROGRESS AND RESULTS - Fiscal Year 1997:

Purpose: The purpose of this R&D program is to demonstrate the feasibility of implementing polarized protons in the RHIC accelerator by constructing a prototype Siberian Snake module.

Approach: Design Principles: Various possible ways to build a helical magnet were considered without any particular method standing out as obviously superior. The usual rules of engagement for the building of superconducting magnets still apply: that high forces be contained, that superconductor motion (particularly stick/slip motion) be minimized, that energy be safely extracted from the magnet at quench, that the ends of the magnet be restrained, that cooling be adequate for the operational conditions, etc. The design that is presently being developed borrows some concepts developed in the SSC and RHIC magnet programs, in particular the coils of the RHIC sextupole magnet and the assembly methods used for RHIC correctors. However, the critical question of how to build a spiral coil uses a new concept: grooves milled into a thick-walled aluminum cylinder to give a $\cos(\theta)$ current distribution when the grooves are filled with conductor. Unfortunately, this approach mandates that there will be considerable labor required in building model magnets because the many turns forming the coils will have to be wound by hand. The positive side of this approach is that models can be built without a large tooling expense. If this design goes into production, then a machine can be built to automatically wind the coils.

Technical Progress and Results: It was found that the superconductor wire being used in the RHIC corrector program could be used for the helical magnet design if it is wound into a 7-strand cable. This conductor, nearly one mm in diameter, would require 382A to produce a 4T field in the present design. By using this existing wire, the need to develop a new superconductor is circumvented. Using a cable in the magnet is preferable to using a single wire: if a break in a wire should occur, the magnet would very likely still operate. The required cable has been manufactured in sufficient quantity for several models of the present coil design. The required Kapton insulation was also wrapped onto the cable in the manufacturing operation.

As stated, this small diameter cable is hand-wound in an ordered pattern into slots milled into an aluminum cylinder. A piece of prepreg fiberglass cloth is placed between each layer of cables in the slots. When all the turns have been wound onto the cylinder, they are compacted with Kevlar wound under tension

onto the cylinder. And then the entire assembly is placed into an oven to cure at elevated temperature, thereby forming a series of current blocks around the cylinder in which each cable is firmly supported in a fiberglass/epoxy matrix. This design for supporting the cable turns is analogous to that developed for the wire turns in the RHIC sextupole magnet. The ends are then filled with a mineral-loaded epoxy to remove all voids, a technique used in the SSC program for adding strength and rigidity to coil ends.

Two of these cylinders, concentric with one another, are required to give the required field of 4T. These two cylinders are mounted into an iron yoke using a support scheme as is being used for the RHIC corrector magnets. A helium containment shell is then welded in place around the yoke, serving also as the magnet support structure. From this point, the design is similar to that of the arc magnets for RHIC and all the same concepts and methods will be used as appropriate.

It is estimated that the helical magnet operating at 4.2K will have a margin in field of 30% above 4T, or 5.2T. The increased field has been achieved in this revised design by increasing the current turns in the coils, and by using a higher current in the outer coil relative to the inner coil to take advantage of the current capacity of the superconductor. Undesired harmonics were easily minimized in this design by adjusting the thickness of the walls between current blocks, a procedure analogous to adjusting coil wedges in a conventional magnet.

Status: A half length model was built and successfully tested. It reached a field of 4.8T at 4.3K with no training in the coil (several lead quenches preceded the magnet quenches). This half length model had all the features required for production magnets. The field in the magnet was measured to be as predicted in the design. The margin is sufficient that a dual current is not needed. A few wire turns are being redesigned to optimize field with a single current for production magnets.

Future Work: This successful test concludes the helical magnet LDRD work. With funding supplied by RIKEN, the design is being prepared for the production of 48 full length (2.4m) units required in RHIC. A machine is being built to automatically wind the coils, and tooling needed for the complete production process is being implemented. Production of the first production magnet is expected to begin early in calendar year 1998.

FOLLOW-ON FUNDING:

The Japanese research institute at RIKEN has signed an agreement to fund the construction of helical magnets for RHIC.

LDRD FUNDING:

FY 1994	$132,139
FY 1995	$133,591
FY 1996	$219,580
FY 1997	$101,208

Study of Possible 2 + 2 TEV Muon-Muon Collider

R.B. Palmer *95-01*
R.C. Fernow

PROJECT DESCRIPTION:

The muon collider is being studied as a possible means for reaching the TeV-energy regime at less cost than using hadron-hadron or electron-positron colliders. A conceptual design of a complete collider facility will be worked out. This includes a description of all the necessary machine components, starting from the muon production and ending with the collider detector.

PREVIOUS TECHNICAL PROGRESS:

A muon collider collaboration has been established between Brookhaven, Fermilab, Lawrence Berkeley Laboratory, and a number of university groups. A major study of the feasibility of the concept was presented to the 1996 Snowmass Workshop on New Directions for High Energy Physics.

TECHNICAL PROGRESS AND RESULTS - Fiscal Year 1997:

Purpose: Muon colliders represent a possible approach to extending the high energy frontier of particle physics. Electron-positron colliders are believed to be constrained by energy loss due to beamstrahlung radiation and the expense of building two full-energy linacs. Hadron colliders require an order of magnitude higher beam energy to achieve the same effective constituent energy. Since the muon is a heavy lepton, the muon collider has negligible beamstrahlung and might be more economical, since it can make use of circular accelerator and collider rings. A 2 + 2 TeV machine would be of moderate size (it would fit on the BNL site) and does not require the use of any exotic technologies.

However, many difficulties must be addressed. To fully understand the feasibility of this concept, it is important to simulate a complete facility from particle production to the intersection in the collider. Experiments should be performed to measure the efficiency of proposed pion production and collection ideas. The number of collected muons per incident proton on target is a crucial parameter for determining the ultimate luminosity of the collider. Another crucial measurement is the efficiency of the proposed ionization cooling method in reducing the emittance of the muon beam.

Approach: We have organized a design group, which meets weekly to discuss muon collider problems and concepts. We are collaborating in this work with groups at FNAL and LBNL, as well as with interested individuals in other labs and universities. Work is presently concentrating on the design of a high energy 2 + 2 TeV collider and on a smaller 50 + 50 GeV collider. We believe that once the accelerator problems are understood at these limiting energies, a Higgs particle factory could be designed at any intermediate energy, once the Higgs' mass is known.

Technical Progress and Results: A complete conceptual design for a 50 + 50 GeV collider has been determined, including a detailed parameter list. This, together with our earlier design of a 2 TeV + 2 TeV collider, shows us the range of accelerator and detector problems likely to be encountered in a muon collider.

Work continued on a set of Monte Carlo programs to simulate many aspects of muon collider accelerator physics. A major emphasis

was placed on simulations of ionization cooling. Three codes are being continually updated and cross-checked to provide reliable estimates of the efficiency of various proposed cooling arrangements.

Work continued on data processing and analysis of Experiment 910 at the AGS, in order to measure the pion production spectrum in the appropriate kinematic regions. Work continued on a pion collection system based on a target inside a high field solenoid. The cooling system, which decreases the transverse and longitudinal phase space of the muon beam, is continuing to be studied with particle tracking and interaction codes. A lot of progress was made on understanding transverse cooling in a periodic lattice of alternating direction solenoids (FOFO lattice). Some interesting ideas were proposed for doing longitudinal cooling in a bent solenoid channel. Work has continued on the design of rapid cycling synchrotrons for possible use in the accelerator rings. Progress was made on the design of an isochronous, low-beta collider ring at 50 GeV.

A physics group worked on (1) physics processes that can be measured at a muon collider, (2) the expected backgrounds at the intersection region due primarily to muon decays, and (3) the design of a generic detector at 50 GeV.

A major workshop on all aspects of the muon collider was held in May at Orcas Island, Washington. In addition a large number of specialized workshops were held throughout the year on special problems in the muon collider design.

An important presentation of the muon collider and its associated research and development issues was made in July to the Gilman subpanel of High Energy Physics Advisory Panel (HEPAP). The major R&D issues faced by the muon collider requiring experimental verification were prioritized. The most pressing item was determined to be a demonstration of ionization cooling. A draft proposal for an ionization cooling test program has been prepared. Work has also begun on preparing a proposal for the second priority item: a targeting and capture demonstration.

PAPERS/JOURNALS/PUBLICATIONS:

The following publications were presented at conferences.

R.B. Palmer & J.C. Gallardo, Future colliders, BNL report 63601, 1996.

R.B. Palmer & J.C. Gallardo, High luminosity muon collider design, BNL report 63602, 1996.

R.B. Palmer et al, High luminosity muon muon collider: report of a feasibility study, BNL report 63864, 1996.

R.B. Palmer & J.C. Gallardo, High energy colliders, BNL report 64147, 1996.

R.B. Palmer & J.C. Gallardo, Muon-muon and other high energy colliders, BNL report 64148, 1996.

R.B. Palmer & J.C. Gallardo, Overview of a high luminosity muon-muon collider, BNL report 64177, 1996.

R.B. Palmer, Progress on muon-muon colliders, BNL report 64529, 1996.

LDRD FUNDING:

FY 1995	$149,580
FY 1996	$200,185
FY 1997	$240,023

Ultra-violet Free Electron Laser R&D

Erik D. Johnson *95-03*
Ilan Ben-Zvi
Richard Heese
Sam Krinsky and
Li-Hua Yu

PROJECT DESCRIPTION:

The NSLS has identified short wavelength Free Electron Lasers as a possible new source for its synchrotron radiation research community. Considerable research and development work has already taken place at BNL on many of the component technologies necessary to prototype such a device. Key among these elements is an accelerator designed to produce short pulses of electrons with low emittance and high peak current. Several types of synchrotron radiation sources can utilize such a machine, including a coherent transition radiation source, a Compton scattering source, as well as a short wavelength Free Electron Laser. This suite of experiments is now known collectively as the Source Development Laboratory (SDL). The SDL utilizes equipment recovered from various terminated projects notably the ARPA 210 MeV linac, and the 10 meter long NISUS undulator from the Army SSDC. The goal of this LDRD project is to support the integration of these existing technologies into an accelerator designed to prototype an UV-FEL.

PREVIOUS TECHNICAL PROGRESS:

In previous supported activities, we have developed strategies to meet the stringent requirements for the production and preservation of bright electron beams within the framework of existing hardware that can support our experiments. Based on work supported by this project, it was determined that a photoinjector similar to that developed by the 'Gun III' collaboration (BNL,SLAC,UCLA), would serve as the electron source for the SDL. A prototype based on modifications of this design is currently under construction. Similarly, we determined that a Titanium:Sapphire (Ti:Sapp) laser system adapted from the Center for Radiation Chemistry Research (CRCR) facility could serve both as driver for the photo-injector and as the source for our seeded beam experiments. A system based on the specifications developed through this project is currently being commissioned. We also undertook the development of a suitable control system based on the NSLS accelerator control system. Low level drivers compatible with existing equipment were developed to make this interface possible. We also undertook a simulation effort to address concerns about possible emittance blow up in bending magnets, such as those designed for our bunch compressor, due to centrifugal space charge forces and coherent synchrotron radiation emission. These results have been presented at international meetings [1,2]. These basic developments set the stage for the activities of fiscal 97 for electron beam preparation and diagnostic development research.

TECHNICAL PROGRESS AND RESULTS - Fiscal Year 1997:

Purpose: A full CDR has been developed for an ultra-violet free electron laser designed to operate into the deep UV. The so-called DUV-FEL proposal cost estimate is roughly $30M for its full implementation. Much of the pre-construction R&D it would require can be accomplished on existing or loaned equipment, running at reduced repetition rate and tuning capability. This experiment, called the ultra-violet project free electron laser (UP-

FEL)seeks to perform a reduction to practice in a proof of principle experiment. Many of the existing components must be adapted or improved from their present form. This LDRD project covers some of the R&D required to execute the proof of principle experiment for the FEL

Approach: The DUV-FEL Conceptual Design Report forms the basis for the design of the Source Development Lab accelerator. It requires the production and delivery of a very bright electron beam to an amplifier, in this case comprised initially of the NISUS undulator. To generate the electron beam, the 'Gun III' design developed in an Accelerator Test Facility (ATF) collaboration has been adopted. To be confident that the accelerator can preserve the bright beam produced by the gun, and that compression can be achieved without emittance dilution, extensive simulations have been undertaken in collaborations with other laboratories, and through R&D subcontracts. The results of this work will be used to guide detailed component system designs for the accelerator.

Technical Progress and Results: The possibility of emittance blow up in bending magnets, such as those designed for our bunch compressor, due to centrifugal space charge forces and coherent synchrotron radiation emission is a major concern. From the standpoint of the FEL, any dilution of emittance arising from these effects in the pulse compressor could negate any benefit to be derived from the shorter pulses and higher peak current it would produce. Previously, we had simulated these effects, in this years effort, we have extended those simulations and developed a design for our compressor which takes the simulation results into account. These results and our proposed design are described below. Additionally, for short wavelength FEL's, simulations indicate that focusing and correction will become increasingly important. We have therefore undertaken the development and testing of high precision imaging electron beam position monitors, which appear to provide position and profile information with resolution below 10 microns. These experiments are also described.

Compressor Development: The SDL linac currently consists of four SLAC-type constant-gradient linac tanks operating at 2856 MHZ, with provision for installation of a fifth section. The first two linac tanks accelerate the beam to approximately 80 MeV, where it enters the magnetic chicane bunch compressor. The final two linac tanks following the chicane accelerate the beam to a maximum energy of 230 MeV.

The SDL bunch compressor is made up of three major components: the dipole magnets, the vacuum vessel mounting the beam diagnostics, and the mechanical support system. The 4 dipoles are fabricated from solid blocks of 1006 low carbon steel. Steel dowel pins at the magnet midplane accurately locate the yoke blocks. Each magnet uses eight air-cooled pancake coils of 16 turns. Current density is held to less than 1.5 A/mm^2 to avoid thermal distortion. The coils also extend away from the iron to allow natural convection cooling. The field strength is 4.5 kG, magnetic length is 19 cm, and the gap is 3 cm. The magnetic design was optimized with the three-dimensional code TOSCA. The aluminum vacuum chamber is machined in halves and seam-welded at its periphery. Two CCD cameras are used as electron beam and synchrotron radiation diagnostics. The electron beam probe is injected through the center of the vacuum chamber. It has a YAG crystal and mirror to observe beam shape (see next section). It also has 3 slots 0.3, 0.6, and 1.0 mm wide, respectively, so that slice emittance

may be studied. The slots may also be used to select a fixed energy bandwidth for transmission to the wiggler. The local emittance and local energy spread are key determinants of single-pass FEL performance. The probe may be moved to any transverse position in the chamber by a stepper motor. The maximum displacement of the beam is 14 cm at 80 MeV. The compressor may be operated at any value from zero field to full strength.

Figure 1.

Compressor Chicane Design

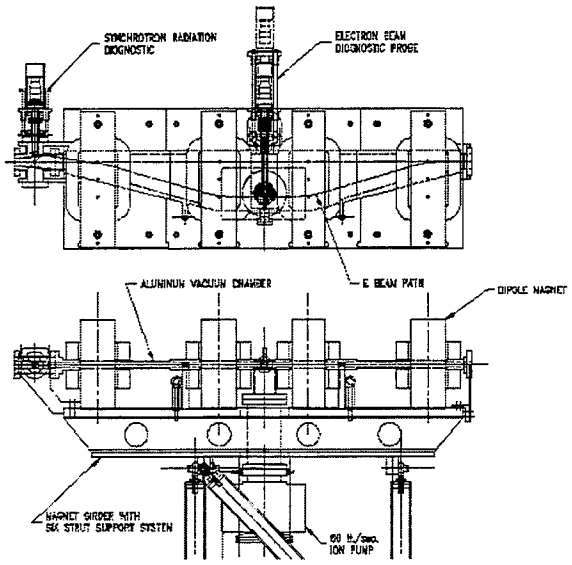

The synchrotron radiation monitor is used to observe emission as the beam passes through the final bend magnets. A variable position mirror is needed to accommodate potential magnet repositioning. The CCD mount is also moveable to accommodate variations in the direction of radiation emission.

Drift distances are 38 cm between outer magnets and 25 cm between the central magnets. For a given compressor length it is desirable to maximize these outer drifts (from magnets 1 to 2, and 3 to 4) in order to minimize the emission of Coherent Synchrotron Radiation (CSR). The separated magnet configuration also reduces coupling between adjacent magnets. The outer magnets may be placed in either of two positions. In addition to the normal position with 38 cm outer drifts, the outer magnets may be placed adjacent to the inner magnets. The latter position generates a greater portion of the path-length difference in the bends, and will be used to investigate the effects of coherent synchrotron emission on beam emittance and energy distribution.

There are several methods of producing short electron bunches, but they are not all applicable to the high charge (>1nC) regime. The electron bunch length immediately adjacent to the cathode surface is approximately equal to the input laser pulse length. It is possible to produce short bunches in the RF gun through two mechanisms. The Ti:Sapp gun drive laser can produce 100 fs pulses directly, or a longer laser pulse may be timed at an advanced RF phase so that velocity bunching occurs in the first ½ cell of the gun. Both of these methods are applicable to small beam charges (<<1nC) only. At higher charges the low energy and high charge density in the gun cause both bunch-lengthening and emittance growth due to space charge forces. Bunch compression via magnetic rotation at high energies is preferable due to the reduced space charge forces.

Nonlinear components of the longitudinal bunch distribution are produced by curvature of the RF waveform and longitudinal wakefields generated in the linac. These nonlinearites may be partially corrected by the T566 element of the magnetic transport matrix. For our design T566 = -7.4 cm and

dE/E = 1% yielding a second order path length difference of just 7.4 microns, too little to correct aberrations in the distribution. Investigations are underway to study longitudinal pulse shaping to balance the curvature due to wakefields and RF.

Conservation of the longitudinal emittance requires that the uncorrelated energy spread of the bunch grow in inverse proportion to the bunch length reduction. The maximum energy spread that the FEL will tolerate sets a limit on the amount of compression that may be achieved. The input beam to the compressor is expected to have an uncorrelated RMS energy spread of .04% and a FWHM bunch length of 10 ps. The FEL and scattering experiments will tolerate approximately 1% energy spread at the compressor (0.4% at the wiggler), hence we may compress the beam by a factor of 25 for a compressed FWHM of 0.4 ps. The beam current before compression is 200 Amps; after compression it is increased to 5000 Amps.

The substantially higher current provided by the compressor will have a profound impact on the performance of the FEL, and represents a major improvement in capability over the originally envisioned machine.

Electron Beam Diagnostic Development:

The high brightness electron beams now being produced for short wavelength FELs and high energy colliders have focused sizes of a few microns in diameter. We have developed and tested a new beam diagnostic to measure transverse profiles down to this range using Yttrium:Aluminum:Garnet (YAG) crystals doped with a visible-light scintillator to produce an image of the transverse beam distribution. The advantage of this material over traditional fluorescent screens is that it is formed from a single crystal, and therefore has improved spatial resolution. The current system is limited to a resolution of about 10 microns. Improvements in the optical transport will enable measurements of RMS beam sizes of less than 1 micron. In addition, the total cost of the system is modest so they can be deployed throughout the accelerator.

Measurements of electron beam sizes and of the crystal's properties were performed at both the Accelerator Test Facility (ATF) at BNL and at Duke University's Free Electron Laser Laboratory. At Duke the brightness, linearity, damage resistance, and time structure of the fluorescence were made while the measurements at the ATF were devoted to spatial resolution limits.

The YAG crystals are supplied as disks 10 mm in diameter and 0.5 mm thick. We were concerned that these nominally insulating materials might develop potentially damaging electrostatic charge on their surfaces in the electron beam. To address this issue we used a standard electron microscopy sample preparation technique and evaporated an approximately 14 nm thick coating of 60% Au / 40% Pd on both faces of the crystal. Each measurement was recorded with a Cohu 4910 video camera. To provide the best image fidelity, the monitors are all arranged with the crystal at normal incidence to the electron beam. An aluminum mirror is placed down-stream of the crystal to deflect the fluorescence light out to the camera. We made preliminary measurements on air-ports at the Duke FEL linac at energies of 36 and 264 MeV to make sure that the crystals were robust, and then made in-vacuum measurements at the high energy port (264 MeV). In this configuration, the light from the crystal is brought out at 90 degrees from the electron beam, deviated and inverted by a rooftop (Amici) prism, and focused to the CCD camera by a 55 mm focal length telecentric lens with a 2X adapter.

To test damage resistance the YAG was inserted for an extended period in the beam, and its performance monitored. It was then removed and examined for surface damage. After 2 hours and approximately 1200 nC of charge, no loss of intensity was observed, and no visible damage was apparent on the crystal. A PMT was used to measure the time duration of the YAG fluorescence. The pulse duration was measured to be about 80 ns FWHM. The crystal exhibits good linearity for this range of charge. The brightness of the spot produced on the YAG was compared to similar beam spots on a ZnS screen. The intensity of the YAG matched that of the ZnS.

To test the limits of the system resolution, we installed a monitor as part of the Smith-Purcell experiment located on beamline 1 of the ATF. In this case the available ports on the vacuum chamber dictated that the optical beam be taken out at an angle of 45 degrees with respect to the electron beam axis. To improve the resolution of the experiment we used a diffraction-limited achromat of 122 mm focal length positioned to produce a 1 to 1 image of the YAG outside the chamber on the CCD camera. The optical focus and magnification were calibrated and after the components were locked in place, no adjustments were made. In this case, the field of view is equal to the CCD chip size, 6.4 mm X 4.8 mm corresponding to 8.3 by 8.6 micron pixels. The minimum electron beam size measured had a RMS radius of 10.7 microns at 50 MeV and approximately 100 pC of charge. This is consistent with normalized emittance of 0.5 mm-mrad and a beta function of 2 cm. These values are in reasonable agreement with calculations from the TRANSPORT computer program. The ultimate resolution is set by both the minimum object size that can be produced by the crystal and by the diffraction of visible light. The minimum object size for high energy electrons is limited by multiple Coulomb scattering of the beam through the crystal and by the generation of bremsstralung. For a 50 MeV beam traveling through a 0.5 mm thick crystal, Coulomb scattering increases spot size by approximately 0.6 microns.

The critical energy, where energy losses due to ionization and radiation of bremsstrahlung are equal, is about 50 MeV. Above this energy the x-rays generated by electrons passing through the material will also cause scintillation, limiting the minimum measurable beam size. The characteristic emission angle of the x-rays is 10 mrad at 50 MeV. Thus 2.5 microns is the minimum measurable spot size at 50 MeV. The minimum spot size limits due to either multiple scattering or bremsstrahlung are both dependent on the electron beam energy. The limits are reduced in size at higher energies.

A final limitation is the diffraction of the emitted green light. The rms spot size of a diffraction limited focus from a 1 inch diameter lens is 0.7 microns. The optics installed on our system have a magnification of unity and diffraction limited resolution of 6 microns. The camera pixel size is 8.5 microns. This pixel size currently sets the resolution limit. For insertion into small vacuum chambers such as in our FEL wiggler, we developed an actuator that uses an optical periscope to extract the beam. This has the advantage that a comparatively 'sloppy' and therefore inexpensive actuator can be used to maintain high absolute precision, as long as the beam imaging optics are fixed relative to the vacuum chamber.

Figure 2.

Periscope Pop-in Schematic

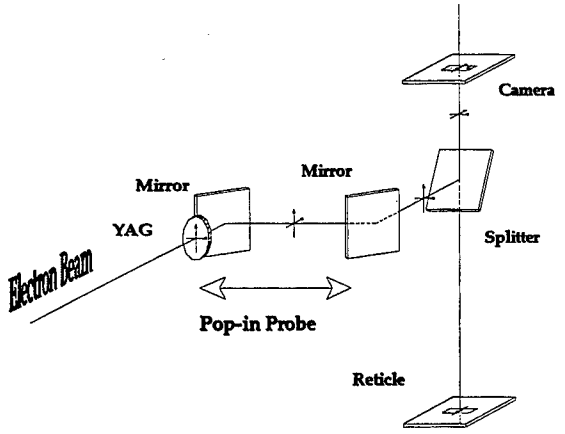

We have also used the high resolution available from these crystals to test a compact three-screen emittance diagnostic. Three screens displaced longitudinally are required to measure the beam's size and divergence. In the past, several meters of beamline were required for this measurement due to the poor resolution of each screen. The high resolution of the YAG screens permits a dramatic reduction of the required beamline length to a few centimeters. Three screens have been installed in the Smith-Purcell experiment at the ATF with a spacing of 6 cm. The beam image from each screen is transported by common output optics to a single video camera. This system allows rapid measurement of the emittance in a compact device.

PAPERS/JOURNALS/PUBLICATIONS:

We have established the baseline parameters for our accelerator, and developed a set of tools for electron beam preparation and measurement. These techniques may be of broad utility to the accelerator community as well as being necessary components of our FEL project.

[1] "The BNL Source Development Laboratory," I.Ben-Zvi, E. Blum, W.S. Graves, R.N. Heese, E.D. Johnson, S. Krinsky, J.B. Murphy, L.-H. Yu, Presented at the FEL96 Conference, Rome, Italy, August 26-31 1996. Nucl. Instrum. & Methods A393(1997) II-10.

[2] "The Source Development Lab Linac at BNL," W.S. Graves, E.D. Johnson, T.O. Raubenheimer, Proc. Linac-96 Conference, Geneva, Switzerland, August 1996.

[3] "Design of the Source Development Lab Bunch Compressor," W.S. Graves, I. Ben-Zvi, E.D. Johnson, S. Krinsky, J. Skartika, M.H. Woodle, L.-H. Yu, and T.O. Raubenheimer, IEEE Particle Accelerator Conference, 1997.

[4] "A High Resolution Electron Beam Profile Monitor," W.S. Graves, E.D. Johnson, P.G. O'Shea, IEEE Particle Accelerator Conference, 1997.

LDRD FUNDING:

FY 1995	$100,005
FY 1996	$99,491
FY 1997	$299,099

Low Dose Gamma Imaging Facility for *In Vivo* Molecular Medicine

Ruimei Ma 95-33
Eugene P. Cronkite
F. Avraham Dilmanian
Ludwig E. Feinendegen
Darrel D. Joel
Ashok Vaswani and
Nora D. Volkow

PROJECT DESCRIPTION:

The subject of this LDRD is to develop a Low Dose Gamma Imaging (LDGI) facility at the Medical Department, BNL, utilizing 1) the existing shielded rooms of the Whole Body Counter (WBC) for reducing the background and 2) the WBC and a gamma camera equipped with specially designed high-sensitivity collimators to provide high counting sensitivity with acceptable spatial resolution and low background. The facility will be used for certain applications of nuclear medicine imaging in the field of molecular medicine, such as the study of the whole body distribution of radiolabelled growth factors (GFs), which cannot be carried out using a conventional gamma camera because of the camera's limited sensitivity. In the original proposal two pilot studies were proposed using the LDGI facility: 1) assessment of the metabolism of radioiodinated erythropoietin as a representative of GFs, and 2) analysis of lipid synthesis in the liver employing the dual tracer approach with the two fatty acid analogues ^{123}I-oPPA and ^{131} I-pPPA. However, due to delays in the delivery of the collimator, it was not possible to complete evaluation of the performance of the gamma camera and to conduct pilot studies planned to demonstrate the capability of the LDGI facility.

TECHNICAL PROGRESS AND RESULTS - Fiscal 1997:

Purpose: Although the image quality of both planar scintigraphy and SPECT imaging in the range of activities commonly used in clinical studies is not affected by the environmental background, scintigraphy at very low doses with very high sensitivity collimators will be affected by such background. For this purpose we use the WBC room, shielded by 122 cm-thick low-activity concrete and 10 cm-thick low-activity (pre-World War II) steel. Measurements of background using a 15 cm diameter x 5 cm length NaI(Tl) detector indicate that in the 50-1000 keV energy range this shielding reduces the background radiation by a factor of 30. The exact reduction of the background count for a gamma camera installed in the shielded room depends on the camera's own shielding, the crystal size, and the collimator design.

Our research plan included four steps:

1. Move the Toshiba gamma camera GCA-901A into the shielded room.

2. Design the gamma camera collimators for low dose gamma imaging with very high sensitivity.

3. Evaluate the performance of the gamma camera with newly designed collimators.

4. Carry out one of the two pilot research programs indicated above to demonstrate the capability of the LDGI facility.

Step 1 and 2 were completed in FY 95 and 96. However, step 3 was delayed due to the difficulties we have encountered in finding a manufacturer to make our specially designed

collimators. One year of additional LDRD funding was made available in FY98 to complete step 3 and 4 to demonstrate the unique capability of this facility.

Approach: Four small shielded rooms (9' x 10') were available. The Toshiba GCA-901A gamma camera required a minimum space of two of the shielded rooms. Therefore, the 4" steel wall between the two small shielded rooms was removed to provide a larger room. The wall removal was carried out by the Central Shops division using an oxygen plasma torch mounted on an articulated jig. Safety procedures included lead paint abatement, fire control measures, and treatment and evacuation of exhaust air gases to the atmosphere. As a result a room of 10' x 18' has become available for the installation of the gamma camera. In addition, a separate room for data acquisition has been established.

The collimator was designed to emphasize high counting sensitivity while maintaining an acceptable spatial resolution. Preliminary design of four collimators was made to provide very-high and ultra-high sensitivity for low and medium energy γ-rays. Because of the unique characteristics of the collimator design, we had difficulties finding a manufacturer that would make the collimator for under $10,000. Based on the cost and availability, only one collimator was ordered. Then the design of this collimator was modified to reduce the tooling cost while maintaining its performance specifications. The collimator was manufactured by the Nuclear Fields Corp., Des Plaines, Illinois.

Technical Progress and Results: The new collimator is a parallel-hole lead collimator with a hexagonal array of hexagonal holes optimized for studies using ^{123}I at very high sensitivity (VHS). The septal penetration was designed to be less than 2.5%. Table I compare the expected efficiency of the new collimator with that of the LEGP (low energy general purpose) collimator provided by Toshiba for nuclides emitting gamma rays with energy up to 150 keV. The overall spatial resolutions (FWHM in cm) of these two collimators are presented in Figure 1 as a function of the distance between the source and the collimator face.

Table I. Comparison of Collimators for ^{123}I

Collimator	LEGP	VHS
Efficiency	2.1×10^{-4}	2.1×10^{-3}
Hole length (cm)	4.0	2.4
Hole diameter (mm)	2.36	4.6
Septum thickness(mm)	0.22	0.65

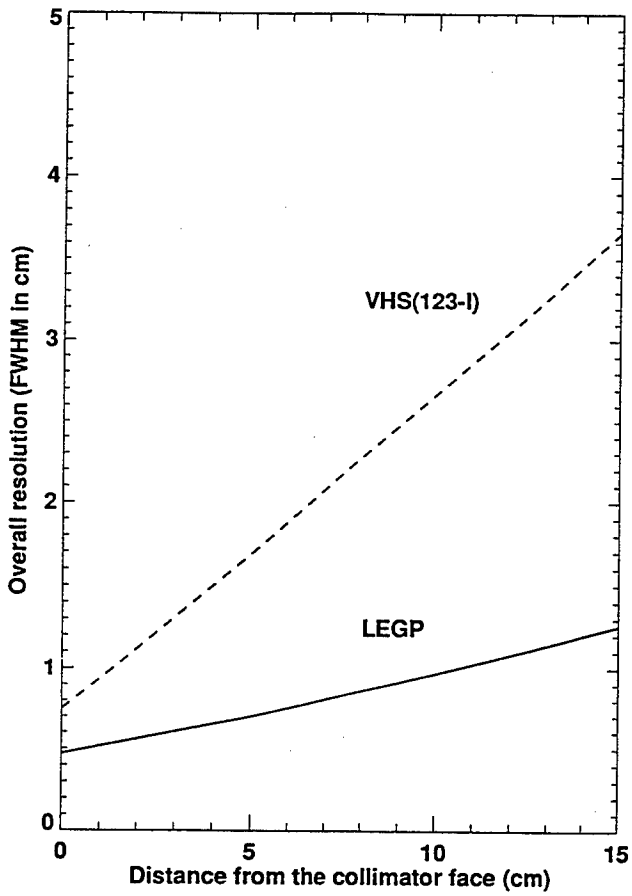

Figure 1. Overall spatial resolution of the gamma camera as a function of the distance between the source and the collimator face.

The performance of the gamma camera with the new collimator in the shielded room is yet to be fully evaluated. Only preliminary tests have been conducted to date. Completion of planned tests was delayed because the collimator manufacturer encountered difficulties meeting the required safety standard. The results of the preliminary tests show that the collimator sensitivity is 2574 cpm/μCi, which is 10 times of the sensitivity of the LEGP collimator.

The intrinsic background of the gamma camera in the shielded room was found to be reduced by a factor of 9. This may enable us to use the gamma camera without any collimator for certain studies that require shallow organ imaging with very low spatial resolution. The spatial resolution in this application will be resulted from the $1/r^2$ dependence of the count-density efficiency on the distance between the source and the camera. The camera will be placed as close as possible to the subject's body.

LDRD FUNDING:

FY 1995	$109,736
FY 1996	$110,070
FY 1997	$4,809

Note: This project involves animal vertebrates or human subjects.

Positron Emission Magnetic Resonance Imaging (PEMRI)

Charles S. Springer, Jr. *96-06*
Manoj K. Samm
Jean Logan
Christoph A. Felder
Xin Li
Ildikó Pályka
Jing-Huei Lee
Nora D. Volkow
Alejandro V. Levy

PROJECT DESCRIPTION:

Three of the most powerful medical imaging techniques in use today are Positron Emission Tomography (PET), Single Photon Emission Computed Tomography (SPECT), and Magnetic Resonance Imaging (MRI). In a major new initiative, the Department of Energy and Brookhaven National Laboratory (BNL) have recently moved to incorporate SPECT and MRI Laboratories with the two-decade old, world-renowned, PET Laboratory at BNL. The entity encompassing these is called the *Brookhaven Center for Imaging and Neuroscience* (BCIN). Early last year, a new SPECT Laboratory was set up in the Medical Building. A new High-Field MRI Laboratory Building has been completed by BNL, housing an MRI instrument purchased by DOE and NIH, which features a magnet with a field strength of 4 Tesla. This is the largest field strength used for humans, and there are only eight such instruments in the world. The MRI Lab achieved its first human images in June 1996 and had studied approximately 75 subjects by October 1997. During this period, the complex NMR system has also undergone a number of significant upgrades. A next-generation PET instrument has been recently installed in the PET Lab. The PET Building is diagonally across an intersection from the MRI Building.

A charter mission of BCIN is to develop synergistic combinations of these imaging techniques. We are going about this in the most fundamental way possible, and this requires understanding exactly what information each kind of image contains. A significant fact is that the major strengths and weaknesses of PET and SPECT are rather complementary to those of MRI. We will illustrate this with PET, but similar comments can also be made with regard to SPECT.

The PET technique has the incomparable strength of being able to detect tiny (picomolar) concentrations of any of the vast array of bioactive compounds that clever chemists can label with the PET isotopes of nature. On the other hand, metabolic MRI is restricted to the detection of only a few of the handful of metabolic compounds that have concentrations greater than one millimolar. The spatial and temporal resolution of PET, however, is rather poor (no better than a few mm, and minutes, respectively). In sharp distinction, anatomical MR images made from the strong, ubiquitous ^1H_2O signal (the [^{1}H] in tissue water is *ca.* 100 molar) can have very favorable spatial and temporal resolution (sub-mm, and seconds). At a slight sacrifice of spatial resolution, ultra-fast MR images can even be obtained in less than 100 ms.

PREVIOUS TECHNICAL PROGRESS - Fiscal Year 1996

During Fiscal Year 1996, the creation of the *High-Field MRI Laboratory* was completed. The following lists some of the major milestones of its culmination.

November 1995: The two RF-shielded rooms were completed. *December 1995*: The magnetic field was passively shimmed to ±90 ppb over a 20 cm diameter spherical volume, which represents an extraordinarily high homogeneity. *January 1996*: The first NMR signal was obtained, as was the first image of a phantom sample. *April 1996*: The $1,250,000 building was completed. *May 1996*: Instrument installation was completed. *June 1996*: The first MR image of a human subject was obtained. *September 1996*: the first *functional* MRI of a human subject was obtained.

TECHNICAL PROGRESS AND RESULTS - Fiscal Year 1997:

We began experimental work on this project by learning to make MR images that are as compatible as possible with PET images of the same subject. Multiple image slices from either PET or MRI acquisitions can be mathematically combined, and then interpolated into three-dimensional data sets. In principle, these can then be re-sliced in any orientation desired, and analogous PET and MRI slices can be computationally *co-registered*. That is, the axes of the image data sets are centered and aligned, and the data set sizes are proportionally scaled until they are equal. However, one of the advantages of the MRI technique is that an image can be actually acquired for any slice orientation desired - simply by the appropriate adjustments of the three orthogonal magnetic field gradients used to obtain the image. Thus, error generated in the co-registration process can be minimized if the MR image slice acquired is as similar to the PET image slice as possible. Drs. Felder, Lee, and Levy have devoted effort to this goal.

We then proceeded to obtain both PET and MR images of several subjects. In some cases, PET images were obtained of the same subject using different tracers, on different occasions. This is important because different tracers are differently localized in the brain, and therefore produce different PET images.

It is just as important to understand the nature of the MR image to be utilized. As stated in the Project Description above, virtually all MR images are made from the relatively strong ^1H_2O MR signal. They thus, in some way, represent maps of water distribution in the body. However, simple quantitative maps of water distribution - called *spin density* images - are rarely exhibited. This is because, though they have the high resolution of MRI, they show little *contrast*. Water is rather uniformly distributed throughout most tissues.

Therefore, the exquisite contrast usually seen in MR images comes from a different source. To obtain this, appeal is made to different properties of the ^1H_2O MR signal - its relaxation times, T_1, T_2, or sometimes $T_{1\rho}$. These measure the rates at which the ^1H_2O magnetization returns to its equilibrium values (along different axes) after being perturbed by an RF pulse - or the rates at which the consequent MR signal disappears, when measured along different axes. It turns out that these properties differ for different tissues - mainly because of differential interactions of water molecules with macromolecules and macromolecular assemblies. By choosing a specific time during magnetization recovery, great contrast can be achieved because the signals from different tissues are recovering at different rates and they have different strengths at this time. However, the contrast comes at the cost of discarding some ^1H_2O signal from each of the tissues (because they are all recovering) in different amounts. The images

are no longer quantitative. Such images are called T_1-, or T_2-weighted MR images, and they comprise probably more than 90% of all MRIs used for clinical diagnosis. These principles are set out on the right side of the chart seen in Figure 1. Although there have been a number of reports of the combination of T_i - weighted MR images with PET images in the literature, these result in a contamination of the quantitative property of the PET (or SPECT) data with the non-quantitative MR image. We wish to avoid this problem.

In 1991, we introduced a third kind of fundamental MR image, the *relaxographic* image (RI).[1] This is an image made from a discrete portion of the distribution of T_i values that completely describes the recovery of the MR signal - the *relaxogram*. The sum of all of the RIs that can be made from the relaxogram equals the spin density image.[2] Thus, the RI is an elemental component of the spin density image, edited to display the loci of the spins enjoying a particular range of T_i values.[2] Since *all* of the MR signal is used to produce the relaxogram, all of the spins are represented. Given this, the RI is *quantitative*. It shows *all* of the spins - with those T_i values. But, it also exhibits high resolution, and the high contrast lacking in the spin density image.

An example of this is shown in Figure 2. At the top left is seen the recovery of longitudinal magnetization (Z axis), after inversion, in a single brain voxel. To the right of this is the formal inverse Laplace transform (ILT) of these data, the longitudinal relaxogram - the distribution of T_1 values for that voxel. A single peak is observed at ~1.6 s. The curve through the data points on the left is the Laplace transform of the relaxogram on the right. Near the bottom right is the sum of relaxograms - the *composite* relaxogram - for all of the voxels in the axial brain image slice studied. Just above this are three relaxographic images indicated with connecting lines. That (left) corresponding to the main peak in the composite relaxogram (T_1 ~0.83 s) displays white matter water of this slice. The RI (middle) arising from the main shoulder to high T_1 (~1.4 s) shows cortical grey matter water. The rightmost RI from the high T_1 (~2.6 s) foot of the relaxogram displays mostly CSF water from the subacrachnoid space. The image at the bottom left is a T_1-weighted image that is essentially a spin density image of this slice. It shows very poor contrast.

Investigators have also developed methods for combining spin density image data with T_i-weighted image data using post-acquisition processing to produce high-contrast, edited-quantitative images. This procedure is termed *segmentation* in the literature, and a recent example can be found in reference 3.[3] Thus, relaxographic images are *naturally segmented* images.[4] The segmentation process usually assumes that all the ^1H_2O signals from the spins in a segment - say white matter - have the same relaxation time. The results in Figure 2 suggest that this is not really true. Also, the extent to which relaxographic peak components (like white and grey matter) do actually overlap puts a natural constraint on the success that the segmentation procedure can achieve. Mr. Li has just begun work on ways to achieve curve resolution of relaxograms. Mr. Sammi and Dr. Levy are pursuing post-acquisition MR image segmentation.

In any case, as indicated in Figure 1, it is relaxographic (or segmented) MR image data that should be combined with PET data for the same slice. This maximizes the quantitative nature of the resulting image. Figure 1 shows that there are two general ways that the PET and MR image data can be combined: in the

real-space domain, to produce a PETAMR image, or in the *Fourier-space domain*, after which a Fourier transformation produces a PEMR image.

The first step in either of these procedures is the co-registration of the data from the two different imaging modalities. Real space data from analogous PET and MR image slices have been co-registered using the new GALAXY technique developed by Drs. Levy and Logan, along with other members of the BNL PET group.[5]

Mr. Sammi has been working with Drs. Felder and Levy to begin to produce PETAMR images. An initial effort is seen in Figure 3. The two images at the top are PET (right) and MR (left) maps of the same axial image slice of the same subject, and have already been co-registered. The PET image was made with the ^{18}F-labeled deoxyglucose (FDG) tracer. Since this is a metabolic substrate surrogate, the intensity of pixels in such an image is proportional to the metabolic activity of cells in the voxels represented by those pixels. It is known that FDG is trapped to a considerably greater degree in grey matter,[6] and this is evident in the contrast seen in the PET image at the top right of Figure 3. (The original of this Figure presents the PET intensity on the hot metal color scale - so that the redder the pixel color, the more FDG trapped.) However, because of the relatively poor resolution of the PET image [nominally $(6.5\ mm)^2$], the grey matter anatomy is not very evident. In comparison, the MR image at the top left [nominally $(0.78\ mm)^2$] displays grey matter water in considerable detail. This particular MR map is not a relaxographic (or segmented) image, but a T_1-weighted image chosen to emphasize grey matter water, along with some ventricular CSF conspicuities. However, for our present considerations, it serves as a stand-in for a grey matter RI.

Mr. Sammi combined the real-space data of these PET and MR images. The result is shown at the bottom of Figure 3, a PETAMR image. It beautifully combines the metabolic information of the PET image in its pixel color (the original is colored), and the high spatial definition of grey matter evident from the MR image. The approach employed by Sammi essentially uses the PET pixel color to "color" the underlying MRI pixels, which were originally rendered in grey-scale tones. This method is presumably somewhat similar to that of Pelizzari and co-workers;[7] though the latter is not described in detail.

It is obvious that, with this technique, if an MRI pixel is black the corresponding PETAMRI pixel is black, even if the overlying PET pixel had some color. The information contents are combined in a multiplicative manner. Thus, the PETAMR image seen in Figure 3 is a *"grey matter-edited" FDG image* - a map of only the grey matter FDG. PET intensity not arising from grey matter has been discarded. This is why Figure 1 refers to this kind of PETAMR image as "edited quantitative." There is some error generated to the extent that the point spread functions of the two image data sets are not the same. The particular example in Figure 3 also has some error due to the fact that the MR image used was not a pure relaxographic (or segmented) grey matter image. Nonetheless, the result seen is very encouraging.

Drs. Logan and Levy have also begun to implement the new method outlined in the original proposal - the PEMRI of the title. This involves combining the data from the two experiments at a fundamental stage of image representation. Specifically, the Fourier-space images are convolved. These are the Fourier

transforms of the real-space images, and this is indicated at the bottom of Figure 1. (The MR Fourier-space image is often called the k-space image.) The Fourier-space images are types of interferograms that exhibit only diffraction-type patterns, not the objects of real space. In the PET Fourier-space image, the PET inculcates metabolic information in the low spatial frequency components.[8] The MRI ^1H_2O intensity, however, supplies the high spatial frequency components not present in the PET data. The convolution is carried out following the general principles underlying the Constrained Reconstruction .Methods.[9] After the appropriate convolution of the PET and MRI Fourier-space images, a back Fourier transformation produces a *hybrid* real-space image that contains information from both basis images. We call it a *positron emission magnetic resonance image* (PEMRI) and, in principle, it also can present PET tracer mapping with a spatial resolution approaching that of MRI. As stated above, the latter is (generally speaking) about an order of magnitude greater than the spatial resolution of PET. If the MR image used is a relaxographic, or segmented, image, however, the PEMRI process concentrates all of the PET intensity into only the regions illuminated in the MR image, even if is not located there in reality. This is why we refer to this as "distorted quantitative" at the bottom of Figure 1. Dr. Logan is exploring the consequences of this aspect using data from a phantom sample.

Thus, PETAMRI and PEMRI represent the synergistic enhancement of *both* the PET and MRI images. A SPECT analog could be called SPEMRI (single photon emission magnetic resonance image). Of course, this approach can be applied to the combination of ultrasound, or x-ray (CAT scan) image information with MRI information (USOMRI, CAMRI). The analogous data from any pair of imaging techniques can be convolved according to these fundamental principles. This also includes data from MR spectroscopic (MRS) images as well. These often have spatial resolution similar to those of the nuclear medicine methods. The PEMRI method will also be useful for the data set pairs acquired from a combination PET/MRI instrument. Though we are not convinced of the wisdom of the latter approach, at least one group is involved in constructing and testing a prototype device for small animal models.

REFERENCES:

1. C. Labadie, T. M. Button, W. D. Rooney, J-H. Lee, and C. S. Springer *Proc. Soc. Magn. Reson. Med.* **10** 1218 (1991).

2. C. Labadie, J-H. Lee, G. Vetek, and C. S. Springer *J. Magn. Reson., B* **105** 99-112 (1994).

3. Y-H. Kao, J. A. Sorenson, and S. S. Winkler *Magn. Reson. Med.* **35** 114-125 (1996).

4. I. Palyka, J-H. Lee, K. Ugurbil, M. G. Garwood, and C. S. Springer *Proc. Int. Soc. Magn. Reson. Med.* **4** 1642 (1996).

5. A. V. Levy, D. L. Alexoff, F. Hode, M. Denis, D. Bertollo, A. P. Dhawan, J. Logan, A. B. Andrews, and N. D. Volkow *Proc. IEEE/EMBS*, **18** 452 (1996).

6. J. C. Mazziotta, and M. E. Phelps, Chapt. 11_in *Positron Emission Tomography and Autoradiography: Principles and Applications for the Brain and*

Heart, Ed. by M. Phelps, J. Mazziotta, and H. Schelbert, Raven Press, NY (1986), pp. 493-579.

7. C. A. Pelizzari, G. T. Y. Chen, D. R. Spelbring, R. R. Weichselbaum, and C-T. Chen *J. Comp. Asst. Tomog.* **13** 20-26 (1989).

8. A. V. Levy, F. Gomez-Mont, N. D. Volkow, J. F. Corona, J. D. Brodie, and R. Cancro *J. Nucl. Med.* **33** 287-295 (1991).

9. Z-P. Liang, F. E. Boada, R. T. Constable, E. M. Haacke, P. C. Lauterbur, and M. R. Smith *Rev. Magn. Reson. Med.* **4** 67-185 (1992).

PAPERS/JOURNALS/PUBLICATIONS:

We have described the relationship between relaxographic and segmented MR images.

- " 'Natural' Segmentation in Efficiently Computed Relaxographic Images" I. Palyka, J-H. Lee, K. Ugurbil, M. G. Garwood, and C. S. Springer *Proc. Int. Soc. Magn. Reson. Med.* **4** 1642 (1996).

Dr. Levy and his co-workers have described their registration approach.

- "The GALAXY Method for the 3-D Spatial Registration of PET Images to Talairach Brain Atlas" A. V. Levy, D. L. Alexoff, F. Hode, M. Denis, D. Bertollo, A. P. Dhawan, J. Logan, A. B. Andrews, and N. D. Volkow *Proc. IEEE/EMBS*, **18** 452 (1996).

We are preparing another conference proceedings describing our most recent results.

- "The Combination of Positron Emission and ^1H_2O Magnetic Resonance Images" M. K. Sammi, C. A. Felder, J-H. Lee, J. Logan, A. V. Levy, and C. S. Springer *Proc. XIIth Biol. Psychiatry Conf.*, in preparation.

LDRD FUNDING:

FY 1996	$100,208
FY 1997	$169,224
FY 1998(est.)	$175,000

Note: This project involves animal vertebrates or human subjects.

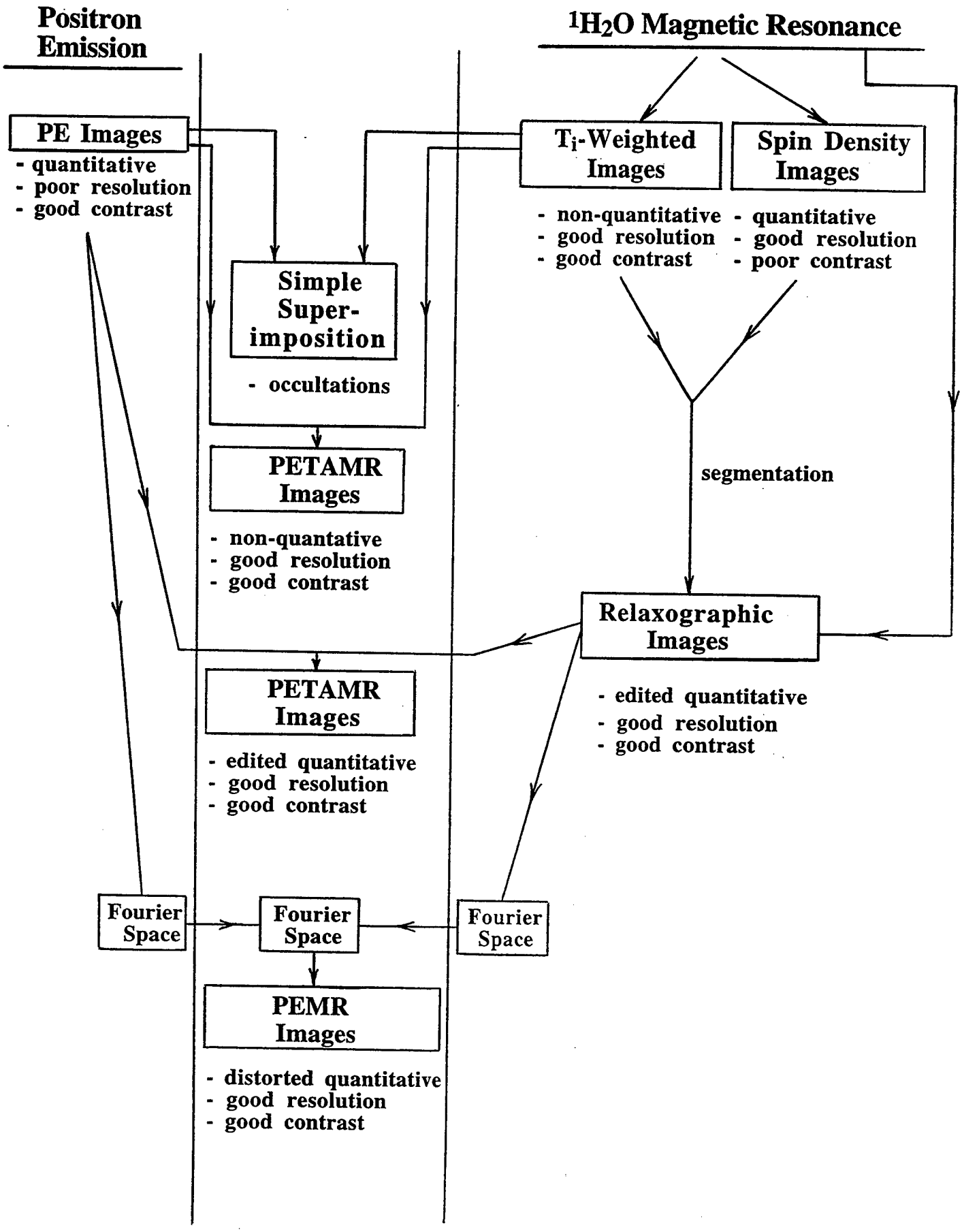
Positron Emission
^1H_2O Magnetic Resonance
PE Images
- quantitative
- poor resolution
- good contrast
T_i-Weighted Images
- non-quantitative
- good resolution
- good contrast
Spin Density Images
- quantitative
- good resolution
- poor contrast
Simple Super-imposition
- occultations
PETAMR Images
- non-quantative
- good resolution
- good contrast
segmentation
Relaxographic Images
- edited quantitative
- good resolution
- good contrast
PETAMR Images
- edited quantitative
- good resolution
- good contrast
Fourier Space
Fourier Space
Fourier Space
PEMR Images
- distorted quantitative
- good resolution
- good contrast

Figure 1.

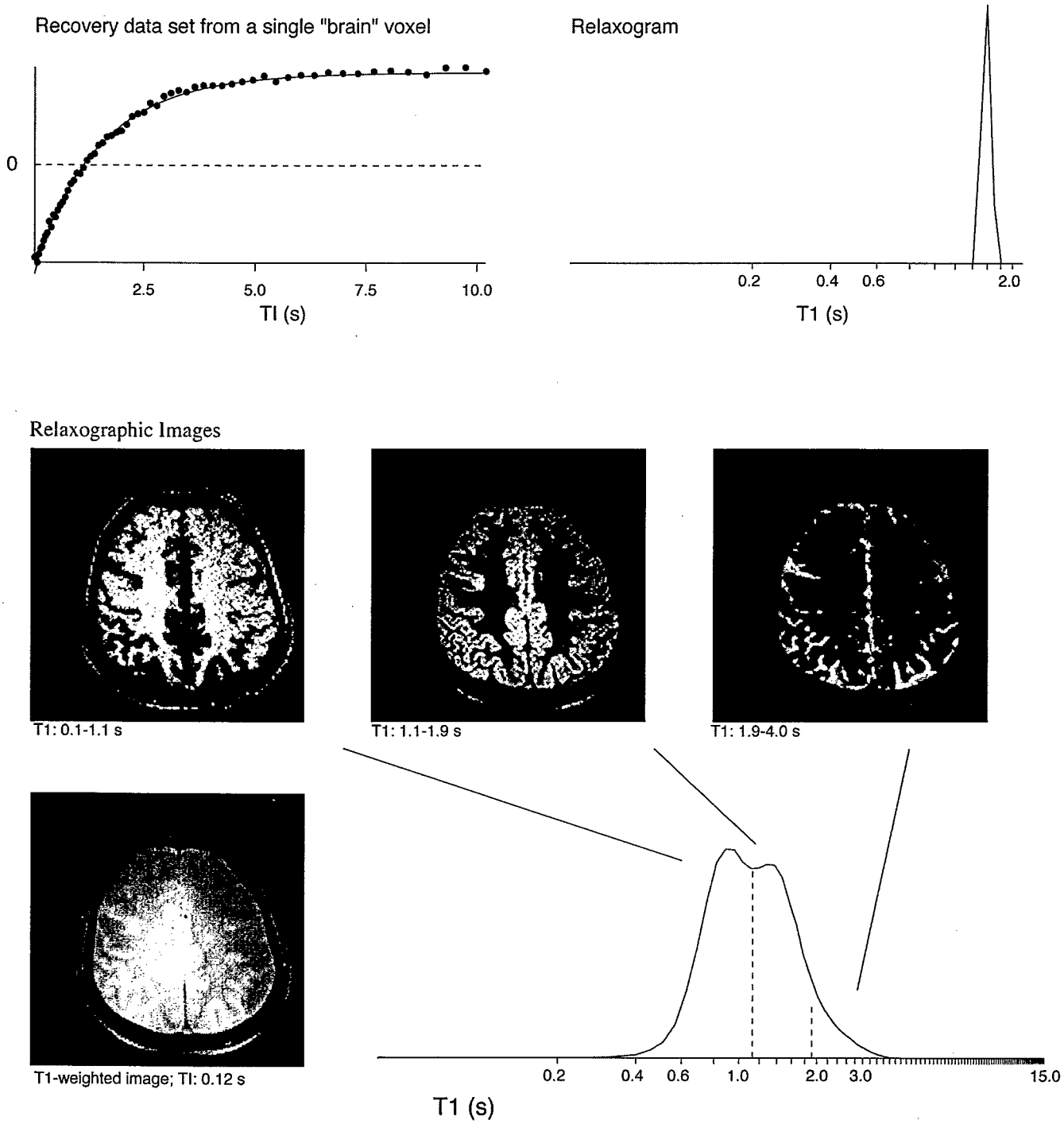

BROOKHAVEN CENTER FOR IMAGING AND NEUROSCIENCE
HIGH FIELD MRI LABORATORY/4 T

Figure 2.

MRI IMAGE

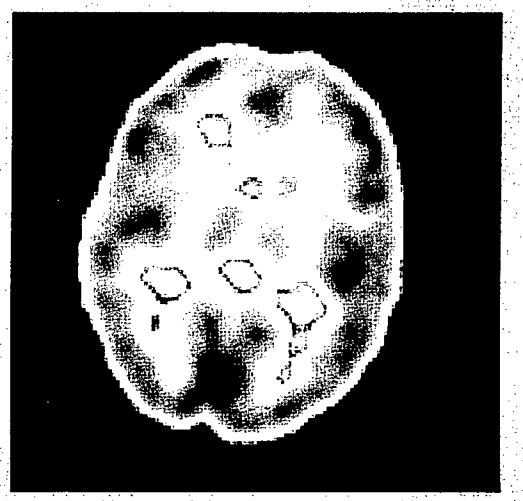

PET IMAGE

PETAMRI IMAGE

BROOKHAVEN CENTER FOR IMAGING AND NEUROSCIENCE

Figure 3.

In-Vacuum Undulator (IVUN) for the NSLS X-ray Ring

P.M. Stefan *96-11*
S. Krinsky
D.R. Lynch and
G. Rakowsky

PROJECT DESCRIPTION:

Statement of Work: The development of in-vacuum, short-period undulator insertion devices may be important to the future role of the NSLS within the synchrotron radiation community. In a number of experimental areas, such insertion devices would position the NSLS at the state-of-the-art as a radiation source, even against the third generation storage rings. Nevertheless, the realization of such a device requires an extension of existing technology. Preliminary studies addressing key issues for a prototype in-vacuum undulator (IVUN) for the X13 R&D insertion straight section are being conducted.

PREVIOUS TECHNICAL PROGRESS:

A portable de-ionized water heating system for carefully-controlled bakeout of in-vacuum undulator magnetic arrays was designed. A glow-discharge cleaning prototype was constructed to study the possibility of glow-discharge "obstruction", and the effects of the undulator magnetic fields. Setups for magnetic field mapping using the pulsed-wire technique and moving wire integration were constructed. Hall probe sensors suitable for mapping in a magnet gap of 3 mm or less were obtained. Mechanical and thermal finite element analyses for the IVUN designs were carried out. Vacuum/mechanical tests were conducted on prototypes of the main IVUN stainless-steel/aluminum flanged joint between the magnet arrays and the magnet drive system.

TECHNICAL PROGRESS AND RESULTS - Fiscal Year 1997:

Purpose: The NSLS Prototype Small-Gap Undulator (PSGU) project has successfully obtained small electron beam apertures (<4 mm) with long beam lifetimes in the X13 R&D insertion straight section, and produced intense synchrotron radiation with its 16 mm-period undulator. The PSGU incorporated a variable-aperture vacuum chamber, and a separate magnet drive with the undulator arrays, which operated in air. As a result of this construction, the undulator magnet gap was always at least 3 mm greater than the electron beam aperture. A logical extension beyond the PSGU is to eliminate the variable-aperture vacuum chamber and place the undulator magnet arrays directly in the accelerator vacuum: an in-vacuum undulator, IVUN. Challenges associated with the IVUN approach include: 1) undulator array construction adapted to ultra-high vacuum (UHV) requirements, 2) high sensitivity magnetic measurements for construction and verification of the small-gap magnet arrays, 3) radiation damage to essentially unshielded NdFeB magnets located near the stored electron beam, 4) mechanical systems to support, align, and drive the in-vacuum arrays. Proposing and testing technical solutions to these challenges is the purpose of this project.

Successful realization of a prototype IVUN device in the NSLS X-ray Ring would make possible the development of significant new x-ray sources for the NSLS Users. Each of the two NSLS X-ray Ring RF straight sections could be modified to accommodate in-vacuum undulators, which would bring

the total number of insertion device ports to 7 on the X-ray Ring.

Approach: For many of the challenges posed by an IVUN device, workable technical solutions can be evaluated through the construction and testing of simple mock-ups and prototypes, or in some cases, through analytical or finite-element models.

Technical Progress and Results: A prototype IVUN device, built in a collaboration between SPring-8 and the NSLS, was installed in May, 1997, in the X13 R&D straight section of the NSLS X-Ray Ring. Commissioning studies with IVUN began in the end of May, and by the middle of July, it had met all its major design goals: operation at a magnet gap of 3.3 mm with long beam lifetime, and production of 4.6 keV radiation in the fundamental, with usable fluxes in both the second and third harmonics. In no small measure, this accomplishment is due to the results of the present LDRD project. Work initiated in FY '96 was brought to a productive conclusion in almost all cases. An un-anticipated set of supporting studies was also taken up, and successfully concluded.

The de-ionized water heating system was not completed in time. When IVUN was installed, it was about 80% completed, consequently, a very slow, conventional bakeout was performed instead. The system will be completed this fiscal year, and probably used to perform a more thorough IVUN bakeout during a maintenance period.

Tests conducted with the in-situ glow discharge prototype chamber showed that "obstruction" of the glow could indeed be a problem. When the Ar gas pressure in the chamber was kept in the range typically used for other components (60 mTorr to 100 mTorr), the glow was excluded from the 10 mm high small-gap region, even though the cathode electrode was located in the center of the small-gap region.

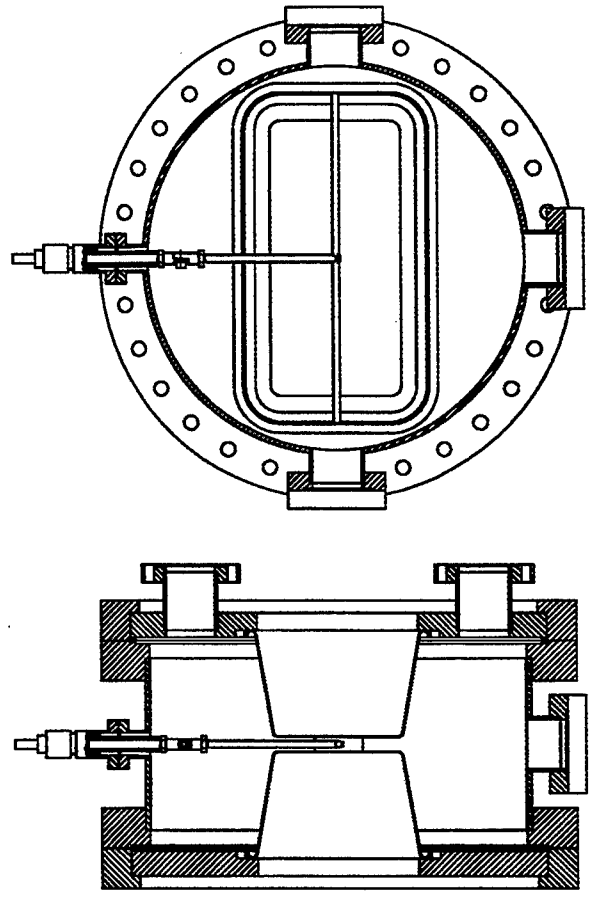

Figure 1. The in-situ glow-discharge test chamber.

However, when the Ar pressure was increased to 3 Torr, the situation reversed. The glow was then visibly confined to the small-gap region. Spare magnet modules from the PSGU were used to form a strong magnetic field in the gap. This did not have

a detrimental effect on the discharge. These results were applied to the conditioning of the actual IVUN device in May.

The three areas of magnetic measurement development, the pulsed wire technique, the moving wire integration method, and the use of small Hall probes, were all applied in measurements of the actual IVUN arrays. The small Hall probe with built-in temperature compensation was used to map the IVUN arrays. The results were in good agreement with those of our colleagues at SPring-8.

The small Hall probe was also used to measure the effect of 100 μm Ni foils applied to the surface of the magnet arrays. These foils serve as continuity sheets, to assure easy conduction of the image currents generated by the stored electron beam. Other labs have used stainless steel foils in the past, but the higher resistivity results in greater heat generation. In addition, our colleagues at SPring-8 had a bad experience when such a sheet *melted* in tests of one of their in-vacuum insertion devices at the ESRF. Ni is ferromagnetic, and is therefore strongly attracted to the magnet array surface, so that conduction cooling through the array itself is assured. Following vacuum anneal of the Ni foils at 1000 °C, measurements of the IVUN arrays, taken at a 3.3 mm magnet gap, showed a decrease in the 7000 gauss peak magnetic field by only 20 to 30 gauss. In addition, trajectory and phase-error plots showed no significant changes.

The pulsed-wire measurement technique was used to obtain the electron trajectory through the arrays. The results showed the same features seen in the Hall probe data. This technique was also able to measure the trajectory in the orthogonal plane, the Y trajectory. This was particularly valuable, since the Y trajectory revealed an un-expected problem in the way in which magnetic compensation was applied to optimize the X trajectory.

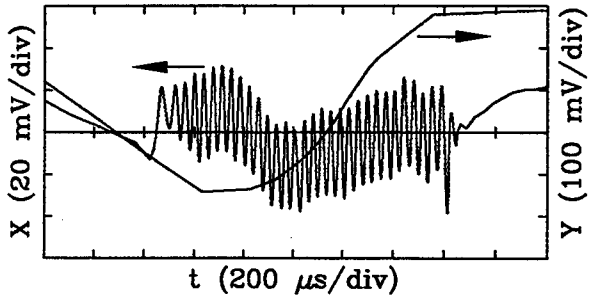

Figure 2. IVUN X and Y trajectories, taken using the pulsed-wire measurement technique.

The moving wire integration technique was applied to obtain the normal multipole fields of the IVUN arrays. This data was also obtained using Hall probe scans and pulsed-wire data. The results from all three methods were in good agreement.

Areas of the IVUN design previously examined using finite element analysis, both mechanical and thermal, have functioned well in the actual device. The main vacuum/mechanical connection between the magnet arrays and the magnet drive, which was tested with prototypes, has not caused any problems.

Late in March, as the IVUN magnet arrays were being installed on the drive system for magnetic measurements, a magnet block was found to be broken, and protruding from the array. This initiated an investigation into the cause of the breakage, since a similar "un-provoked" breakage occurred in Japan, just as the arrays were about to be shipped to BNL. The arrays are

basically constructed using magnet blocks of two different dimensions and magnetic orientations. The blocks which broke were both of the same type, and when broken, the pieces tend to be forced out of the array. When the pair of arrays is aligned to form an undulator, this type of broken block is attracted to the opposite array. The consequence of a block breaking when the IVUN arrays are installed in the NSLS X-Ray Ring would most likely be a movement of the block into the path of the stored electron beam. Opening or closing the magnet gap would not move it out of the electron beam path. Therefore, we had to determine why the blocks were breaking, and whether additional events could be expected. With assistance from the Materials Services Group in the DAS, the block broken at BNL was examined, and tests devised to measure various forces applied to the blocks in the actual arrays. Spare magnet blocks were intentionally broken, to measure the forces required. We determined that there was no flaw in the design of the blocks, or in the block material, but found that a block exchange procedure could cause the breakage. During the optimization of the magnetic field quality of the arrays in Japan, individual magnet blocks were removed from the array and interchanged with others. When this procedure was performed by hand, without special fixtures, it was possible to apply very large forces on one end of a magnet block as its retaining clamps are secured. As a result, we designed and fabricated special fixtures and worked through both arrays, loosening and removing the retaining clamps, inspecting the magnet block ends, and replacing and tightening the clamps to a prescribed torque. The arrays were then mounted in the drive system and cycled from a 9.5 mm to a 2.0 mm magnet gap, 137 times, to produce magnetic loading equivalent to the worst-case the undulator would ever experience. No further breakage occurred. Magnetic mapping conducted before and after all of these tests showed no change in the field quality.

PAPERS/JOURNALS/PUBLICATIONS:

G. Rakowsky, J.J. Aspenleiter, W.S. Graves, L. Solomon and P.M. Stefan, "Magnetic Measurements on an In-Vacuum Undulator for the NSLS X-Ray Ring," 1997 Particle Accelerator Conference, Vancouver, Canada, May 12-16, 1997 (poster presentation).

Toshiya Tanabe, Hideo Kitamura and Peter Stefan, "Development of an In-Vacuum Minipole Undulator," 1997 Particle Accelerator Conference, Vancouver, Canada, May 12-16, 1997 (poster presentation).

P.M. Stefan, T. Tanabe, S. Krinsky, G. Rakowsky, L. Solomon and H. Kitamura, "Initial Results from an In-Vacuum Undulator in the NSLS X-Ray Ring," 1997 Synchrotron Radiation Instrumentation Conference, Himeji, Japan, August 4-8, 1997 (oral presentation).

LDRD FUNDING:

FY 1996	$100,118
FY 1997	$98,466

Spin Polarized Coincidence Spectroscopies

Peter D. Johnson *96-16*

PROJECT DESCRIPTION:

*L*DRD funding was originally obtained to enable the development of a new Coincidence Spectroscopy between Spin Polarized Core Level Photoemission and Soft X-Ray Emission. Coincidences between the core levels and the photons emitted in the subsequent radiative decay would allow studies of the site specific spin polarized valence band structure. The facility to be established on Beamline X1B at the NSLS would, therefore, be available for the study of technologically important alloy systems.

TECHNICAL PROGRESS AND RESULTS - Fiscal Year 1997:

Purpose: Site specific valence band information is difficult to obtain in alloys and compounds. However, techniques that rely on the initial excitation of a core level offer the possibility of obtaining such information. The main goal of this project is the development of a coincident technique that will allow the measurement of site-specific and spin dependent valence band information. It is hoped that the techniques will be used to study thin film ferromagnetic alloys. Through the use of controlled epitaxial growth on different substrates, we hope to study unique phases of these materials not available in the bulk. By varying the growth conditions it will be possible to study not only ordered phases, but also the effects of order-disorder transitions. Indeed, growth on different substrates may be viewed as a way of applying pressure to the system so that a whole range of magneto-volume effects may be studied. Such information is difficult to come by using any existing methods. We also hope to study organic superconductors and oxide thin films displaying giant or colossal magneto-resistance.

Approach: Spin polarized core level photoemission does not in itself provide valence band information, but the radiative decay of the core hole does involve electrons from the valence band. Further, the electrons involved in the radiative decay must carry the same spin as the core hole. Thus, labeling the spin of the photoemitted core electron is equivalent to labeling the spin of the valence electron. By measuring the energy of the radiated photon in coincidence with the spin polarization of the photoemitted core electron, we hope to be able to measure the spin resolved valence bands on the site from which the initial core electron was emitted.

Technical Progress and Results: The new spin polarimeter commissioned as part of this program represents a modification of the retarding potential micro-Mott polarimeter developed by the Rice University group. In the present design the electron optics in the scattering channel has been modified to increase the solid angle of collection and associated Figure of Merit. The spin sensitivity was determined by examining the photoemission from the core and valence levels of iron films grown on Mo(011). The Figure below shows spin resolved spectra recorded from the valence bands of an Fe 110 film. On the basis of comparison with earlier published studies it was determined that the Sherman function of the polarimeter, a measure of its spin sensitivity, was equal to 0.16-0.17, the anticipated value.

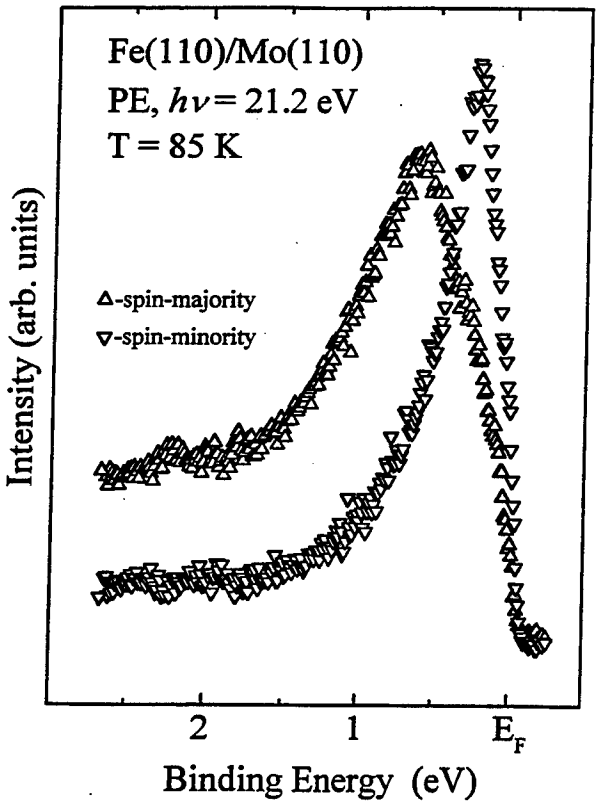

The design of the new polarimeter included a plane mirror deflector in the electron optics. This arrangement allows a measurement of both in-plane and out-of-plane polarization as defined by the crystal surface under investigation. This capability has been used in studies of the Gd(0001) surface. These preliminary experiments indicate that at liquid nitrogen temperatures the surface moments show a slight canting with respect to the surface plane.

This last year also saw the successful commissioning of the new soft x-ray emission (SX) spectrometer, funded by the Army Research Office and Boston University. This instrument is one of only three such spectrometers operational in the U.S. It allows the bulk electronic structure of novel and complex materials to be studied, measuring the atomic and chemically specific partial density of states (PDOS). A prerequisite for the optimal use of this spectroscopy is access to a high brightness soft x-ray beamline such as X1B. In two experimental runs this year three broad classes of materials were studied including organics superconductors, wide band gap nitride semiconductors and transition metal oxides. It is planned to continue the study of each of these classes of materials. However, to fully implement the coincidence program, some modifications are required. First beamline X1B still lacks refocusing optics. It is hoped that this will be rectified very soon. Secondly, some modifications are needed to the BNL Scienta chamber to allow the SXE spectrometer to be in its optimal position for maximum signal count rate. These modifications will hopefully be carried out in the near future.

PAPERS/JOURNALS/PUBLICATIONS:

"Conceptual Design of a High Efficiency Mott Spin Polarimeter," D.-J. Huang, P.D. Johnson and C.T. Chen (to be submitted).

"Spin Polarized Photoemission Studies of the Gd(0001) Surface," A.V. Fedorov, T. Valla, D.-J. Huang, G. Reisfeld, F. Loeb, F. Liu and P.D. Johnson (to be published in J. Elect. Spectros.).

LDRD FUNDING:

FY 1996	$78,999
FY 1997	$82,281

An Evaluation of the WSR-88D for the Remote Sensing of Cloud Properties

Mark Miller and Peter Daum *96-19*

PROJECT DESCRIPTION:

The National Weather Service WSR-88D radars, deployed at 161 sites in the United States and 19 abroad, provide unprecedented areal radar coverage. Each radar can perform volume scans measuring reflectivity, radial velocity, and spectral width over an area exceeding 280,000 km^2 every 5-10 minutes. Calculations suggest that it is possible to estimate the fractional coverage, geometry, and evolution of non-precipitating clouds over a significant subset of this measurement volume, which makes the WSR-88D a potentially cost effective tool for cloud research. Clouds are very difficult to represent in Global Climate Models (GCM), which are used to estimate the future consequences of fossil fuel consumption and to evaluate future energy use scenarios. Therefore, there is an opportunity to collect detailed information about cloud structure and coverage on an unprecedented scale, data that may ultimately be used to improve cloud parameterizations in GCMs.

TECHNICAL PROGRESS AND RESULTS - Fiscal Year 1997:

Purpose: Clouds cover a very large fraction of the earth's surface and have a large effect on the earth's shortwave radiation budget because of their high albedo. In contrast, clouds have varying effects on the longwave budget depending on their location in the troposphere; high clouds strongly influence the outgoing longwave flux, while low clouds have minimal influence since their cloud top temperatures are only slightly lower than the surface temperature. Because the characteristics of cloud fields are difficult to quantify, the impact of cloudiness variations on the earth's radiation budget is a major unsolved problem in atmospheric research. Moreover, the representations of clouds used in today's GCMs are generally crude despite the fact that changes in the quantity or distribution of clouds may strongly impact future climates. The critical problem in the development of the these representations is how to link the spatial radiative characteristics of a cloud field that exists over a large area (>100 km^2) to the average thermodynamic conditions in the volume that contains the cloud field. One approach to this problem is to measure the geometry, radiative characteristics, and thermodynamic environment of the cloud field over large areas for long periods, thereby producing a statistically- based representation that can be used in GCMs.

Approach: Cloud droplets present a relatively small backscattering cross-section to radars such as the WSR-88D, with its 10 cm wavelength. Even with advanced signal processing, clouds reside at the edge of detectability and are less likely to be detected as their distance from the radar increases. Moreover, scattering from targets such as insects, birds, ground clutter, and turbulent eddies (Bragg scattering) may be convolved with the cloud echoes from the WSR-88D under some circumstances. To test the capabilities of the WSR-88D to detect cloud droplet echoes from non- and weakly precipitating clouds, which are radiatively important and difficult to quantify spatially, the theoretical cloud sensing capabilities of the WSR-88D were determined and data comparisons were made with three accepted cloud sensors: a 94-GHz cloud radar,

satellites, and radiosondes.

The theoretical cloud sensing characteristics of the WSR-88D are shown in Figure 1 as a function of horizontal range, height, and permissible elevation angles for both the 4.7 (VCP 31) and 1.57 μs (VCP 21) pulse lengths. No beam refraction is considered in these calculations, δ_{syscal}=0, and beam attenuation by atmospheric gases is assumed to be negligible. The spatial characteristics of the minimum detectable reflectivity are complicated due to variations in the number of pulses averaged as a function of the elevation angle for VCPs 21 and 31. Using the 4.7 μs (VCP 31) pulse length, typical clouds (-25 dBZ) are theoretically detectable at a horizontal distance of 74 km for elevation angles less than or equal to 2.5° and to 80 km at elevations of 3.5 and 4.5°. Using the 1.57 μs pulse length (VCP 21), typical clouds (-25 dBZ) are detectable to 30 km at the two lowest elevation angles (1.45° and lower), to between 20 and 40 km at elevations angles 2.4° to 6.0°, and to 41 km at the highest two elevation angles. Beyond these distances, only the most reflective clouds will be detected, so cloud measurements in these regions may be subject to considerable error. Our work during fiscal year 1996 was primarily focused on quantifying the sensitivity of the WSR-88D radar and collecting data during a few cloudy periods to confirm our understanding of the nuances of the radar operation.

The calculations shown in Figure 1 represent the theoretical sensitivity of the WSR-88D radar, but do not quantify the nature of the radar target that produces the echo. Ideally, the only viable targets in the measurement volume would be cloud and small precipitation droplets, in which case it would be possible to directly interpret the radar reflectivity in the context of cloud

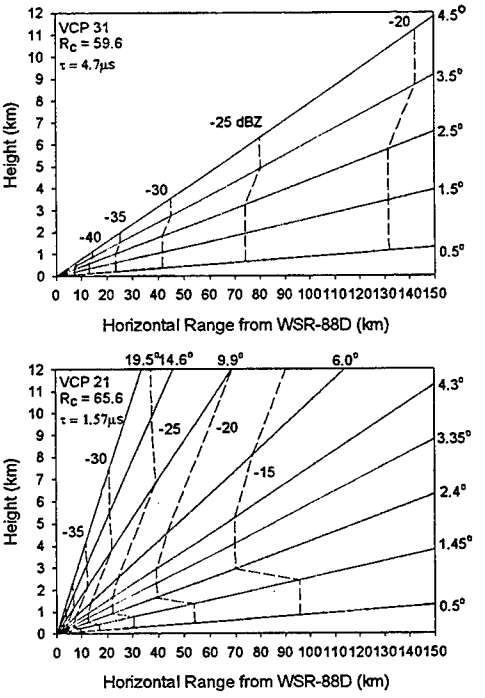

Figure 1. Range-height characteristics of the minimum detectable reflectivity when τ = 4.7μs and τ = 1.57μs. The angled solid lines are elevation angles (values are indicated) and the dashed lines are minimum detectable reflectivity contours in dBZ. These values represent the minimum value of reflectivity that a cloud must possess to be observable.

coverage and microphysical structure. If the sampling volume is sufficiently small and the transmitted wavelength short enough, such straightforward interpretation is probable, as demonstrated using specialized, non-scanning cloud radars. For the WSR-88D, the 10-cm wavelength introduces the possibility of echo contributions from moisture and temperature gradients (Bragg scatter), and its large sampling volume increases the probability of signal contributions from hard-targets such as insects and birds. Therefore, a critical issue is the magnitude and frequency of these undesired contributions. To address this issue, echoes from the WSR-88D were compared with coincident profiles from a short wavelength cloud radar and satellite data, as discussed below.

Technical Progress and Results: During fiscal 1997, the focus of this research was validation of the WSR-88D cloud sensing technique by comparisons with other cloud sensing technologies. One aspect of these comparisons was a series of experiments to determine if the echoes detected by a WSR-88D on cloudy days correlated with cloud measurements made by a 94-GHz cloud radar operated by the Pennsylvania State University (PSU). The PSU cloud radar was used to measure cloud properties in vertical column that was a subset of the WSR-88D measurement volume.

One example of the time-height cross-sections of the reflectivity profiles measured by the two independent radar systems in the column above the 94-GHz radar is shown in Figure 2. For comparison, the cloud boundaries computed from the reflectivity profiles of the PSU 94-GHz are overlaid with the WSR-88D profiles.

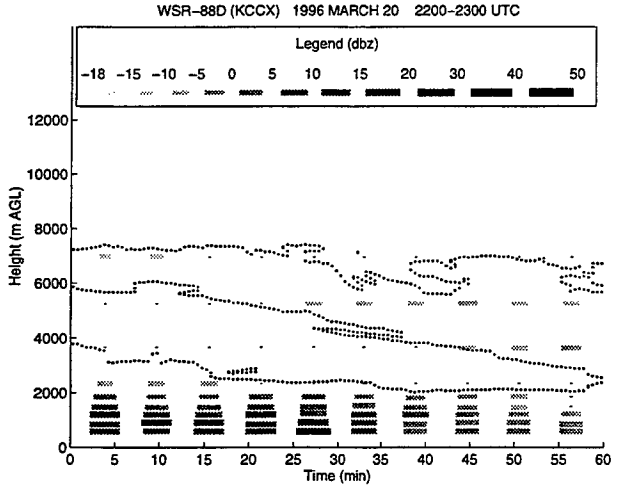

Figure 2. Observed reflectivities from the WSR-88D over the PSU 94-GHz radar located in State College, PA. The black dots indicate the reflectivity boundaries from the 94-GHz radar, and the small dashes indicate locations where the WSR-88D did not detect any return.

Data from 2200-2300 UTC 20 March 1996 (Figure 2) illustrate the detection of multiple cloud layers by the WSR-88D. Mid-level clouds with reflectivities in the range between 0 and -20 dBZ are detected above a more reflective stratus layer, which is producing light snow. Qualitative comparisons with the reflectivity from the PSU 94-GHz radar show good agreement, in this case.

These comparisons also demonstrated an important limitation of the WSR-88D for the remote sensing of clouds. During a few experiments, particularly during Autumn 1996, the WSR-88D received echoes from the vertical column above the 94-GHz when no cloud droplets were present. These non-cloud echoes were linked to strong temperature and moisture gradients in the measurement column (Gilbert, 1997), which suggests that the source of the WSR-88D echoes was Bragg scatter. Algorithms designed to infer cloud structure from these echoes would have produced erroneous results on these days.

To demonstrate spatial averaging techniques, data from a single clear air scan (VCP 31) collected on 21 November 1996 beginning at ~2300 UTC are shown in Figure 3 along with a GOES 8 IR satellite image and radiosonde data . Echo fractional coverage was defined as the ratio of target detections to the total number of observations, and the data were grouped into 200 m vertical bins. Height was computed from the elevation angle and slant range along the beam, and no refractive effects are considered.

Spatial variability in the echo field is quantified by computing the vertical distribution of echo fractional coverage in 200 m bins for the four quadrants surrounding the radar (90° segments; Figure 3). Data from the 3.5° and 4.5° elevation angles are combined for this analysis, and they show that there is less cloud cover south of the radar, particularly toward the southeast. Toward the northeast, which is in the upstream direction, there is

virtually complete overcast (>90%) and drizzle is observed in the subcloud layer. In contrast, in the downstream direction, toward the southeast, there is less cloud coverage (~80%) and less drizzle in the subcloud layer.

The infrared satellite image (Figure 3) also indicates less cloud to the south of the radar, and particularly to the southeast where a patch of clear sky is indicated. This analysis also suggests that the region to the southwest of the radar is characterized by a thin layer of clouds that have less drizzle in the subcloud layer than other quadrants, and that the clouds to the northeast of the radar have higher cloud tops (by as much as 400 m). Therefore, the WSR-88D at Upton, NY may be providing additional detail about the nature of the cloud structure and its spatial distribution, information that supplements the infrared satellite data from this period.

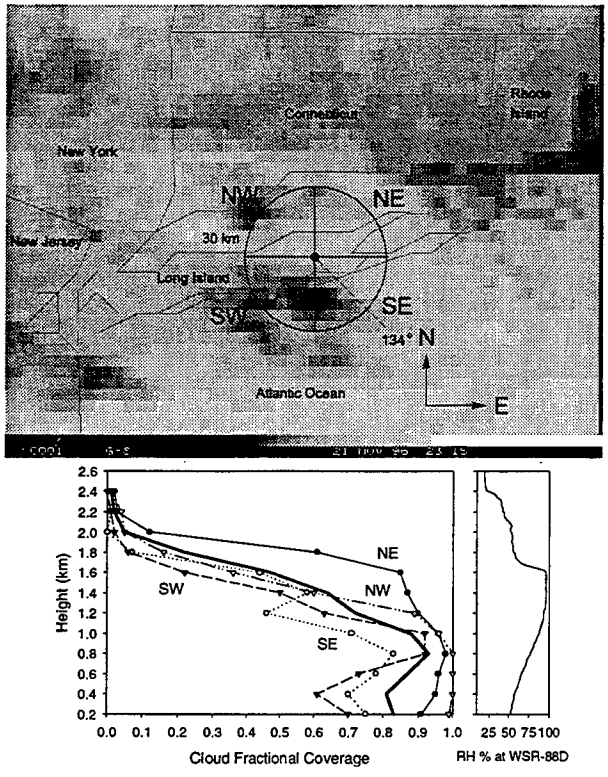

Figure 3. Spatially-averaged profiles of cloud fractional coverage sorted into 200 m bins and the domain average (heavy black line). The GOES 8 IR satellite photo and concurrent radiosonde data are also shown.

Other experiments performed in fiscal year 1997 showed that the WSR-88D could be used under some conditions to provide spatially-averaged estimates of the cloud reflectivity profile and maximum cloud top height in the domain, as well as information about the subcloud reflectivity structure. Most importantly, this technique was used to compute the vertical distribution of echo fractional coverage in the domain. Statistics of the reflectivity structure as a function of height were computed, which could be used in future algorithms to retrieve the microphysical structure of the cloud field.

While many of the results of this study are encouraging, others demonstrate that additional research will be required before the WSR-88D is generally accepted as a tool for cloud research. Quantifying the effects of Bragg scatter, biological echoes (insects and birds), and ground clutter will be necessary before reflectivities can be interpreted in the context of cloud microphysics on a routine basis. It may be possible to significantly increase the viability of this technique if it is used in concert with other cloud sensing technologies, rather than as a stand-alone cloud sensor.

PAPERS/JOURNALS/PUBLICATIONS:

A description of this work appears in *A Review of Research and Development Activity Related to WSR-88D Algorithms* (Brandes, 1996) and a manuscript has been submitted to a special issue of *Weather and Forecasting* devoted to the WSR-88D, and a future manuscript will be submitted on follow-up work in collaboration with the Pennsylvania State University. A paper detailing this work was presented at the 28th Conference on Radar Meteorology. Two masters degrees, one at the Pennsylvania State University (Gilbert, 1997) and one at the University of

Kansas (Lehenbauer, 1997), were conferred as a result of work on this project.

FOLLOW-UP FUNDING:

A proposal to the Department of Energy's Atmospheric Radiation Measurement Program in May, 1997 is pending.

LDRD FUNDING:

FY 1996	$77,893
FY 1997	$115,159

Studies of Nano-scale Structural Defects Using Advanced Electron Diffraction and Imaging Techniques

Yimei Zhu *96-22*

PROJECT DESCRIPTION:

The project was designated to study nano-scale structural defects in materials using advanced transmission electron microscopy that is complimentary to x-ray and neutron diffraction techniques. In fiscal year 1996, we successfully addressed the special distribution of electrons and holes on a nano-scale in $YBa_2Cu_3O_7$ and $Bi_2Sr_2CaCu_2O_8$ high temperature superconductors; in fiscal year 1997, we studied phase-transition-related structural defects in $SrTiO_3$, and revealed the possible origins of the two-length scale and the central peak observed in x-ray and neutron experiments.

TECHNICAL PROGRESS AND RESULTS - Fiscal Year 1997:

Purpose: The phenomena of the two-length scale and the central peak observed in $SrTiO_3$ and related materials by x-ray and neutron scattering have remained a mystery for more than a decade. Although it was speculated that nano-scale defects may play an important role in generating such phenomena, no detailed study was ever made, mainly because x-ray and neutron diffraction are not suitable for exploring local defects. In contrast, transmission electron microscopy (TEM) has a unique capability of probing small volumes of an area to study structural defects. With in-situ sample stages, we can cover a temperature range of 15-1300K, which allows us to directly observe the distribution and behavior of point-, line-, and planar-defects near phase-transition temperatures. Such studies will be of significant importance to materials science and to solid-state physics; they are expected to give new insights into the fundamental mechanism of structural phase-transitions.

Approach: In a three-step approach, we first carefully prepared TEM cross-section samples, using the same crystals employed in x-ray and neutron experiments to study the density of defects as a function of depth from the original cut surfaces of the crystals. Second, we used cooling stages and heating stages to study the change of crystal symmetry and the dynamic behavior of defects at various temperatures, especially near phase-transition temperatures. Third, we developed a theory to estimate the strain fields associated with the defects, and evaluated their contribution to the phase transition.

Technical Progress and Results: We investigated the overall structural defects in the $SrTiO_3$ single crystals. Figure 1(a) shows a typical morphology; B denotes the bubbles and D the dislocations. The bubbles, ranging from about 10 nm to 500 nm in diameter, are likely formed by supersaturated gas absorbed during crystal growth. When heated above 625K, they shrink, collapse, and eventually become nano-meter-size bubbles and dislocation loops, or simply disappear. Figure 1(b) shows the same area as Figure 1(a) after the sample had been heated in the microscope for 30 minutes at 650K. These nano-scale bubbles and associated dislocation loops were evenly distributed throughout the sample. We found that the local lattice distortion around bubbles and dislocation loops can give rise the central peak observed by neutron diffraction, similar to the origin of Huang diffuse scattering which appears near Bragg peaks.

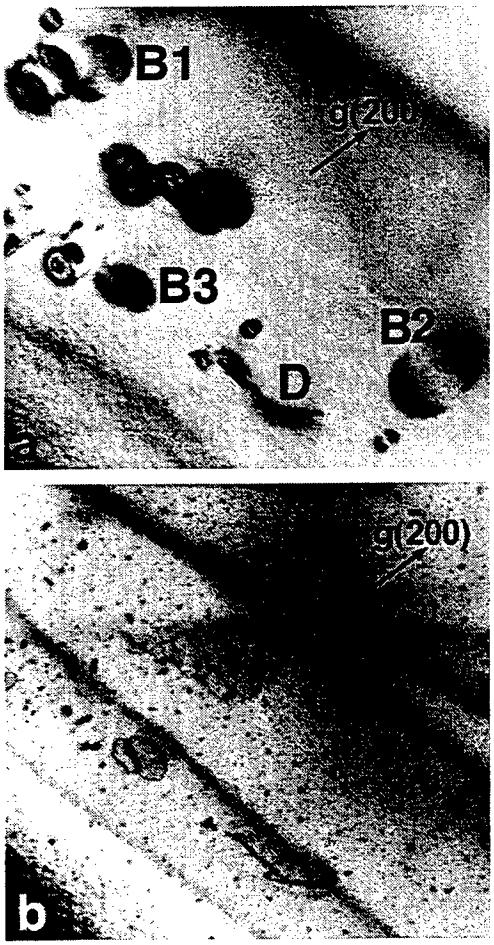

Figure 1: Bright-field images showing structural defects and the annealing effects on the $SrTiO_3$ crystal (**g**=-200). (a) before heating, (b) in-situ heated at 650K for 30 minutes and then cooled to room temperature. Note, the dot-contrast is nano-scale bubbles and dislocation loops.

In contrast, the dislocations, which are believed to be induced by the crystal□s manufacturer during mechanical cutting and polishing of its surface, were not distributed evenly. A high density of dislocations was observed only near the crystal surfaces. Figure 2 plots the density of dislocations which decreases drastically with increase of depth from the original cut surface of the crystal.

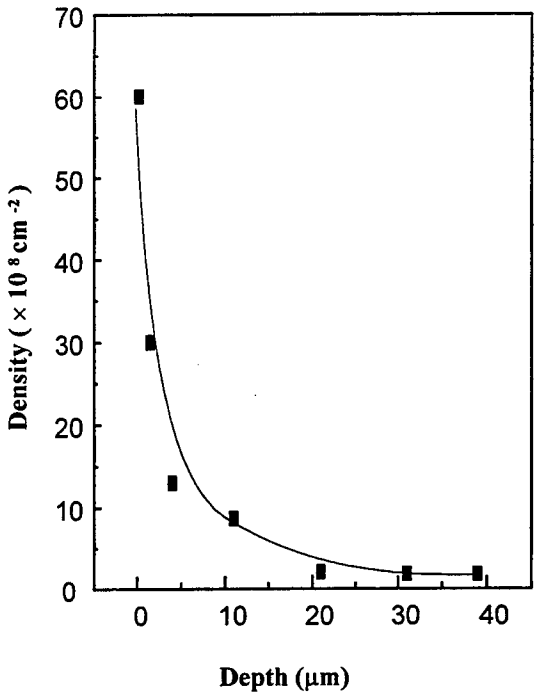

Figure 2: Dislocation density as a function of the depth from the cut surface.

Based on the linear elasticity theory for isotropic solids, we calculated the mean stress around the dislocations. Using the experimentally determined relationship between stress and transition temperature, we obtained the length scale, R, of the stressed region, which was assumed to have transformed into the low-temperature tetragonal phase at a given temperature T (T is larger than the phase transition temperature T_c), around a dislocation line. The values $\kappa=2\pi/R$ as a function of $T-T_c$ (Figure 3) coincide well with the temperature-dependence of κ for the long-length scale measured experimentally. Thus, we conclude that the stressed regions around dislocations are responsible for the so-called second-length scale observed in x-ray and neutron diffraction.

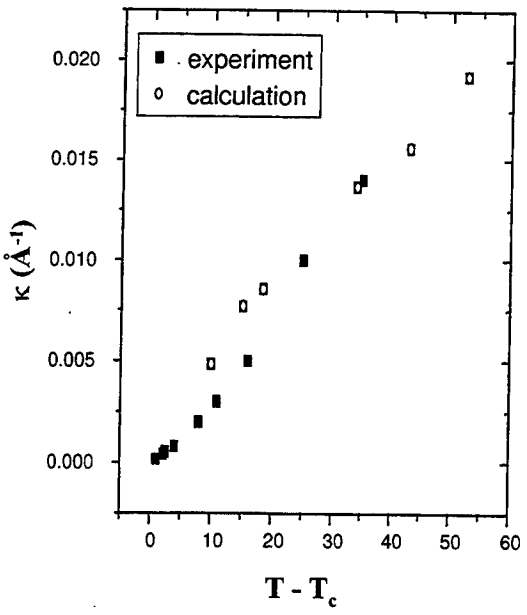

Figure 3: Temperature dependence of the inverse correlation length κ for the long-length scale. Solid squares are from experimental observations, while open circles represent theoretical calculations.

PAPERS/JOURNALS/PUBLICATIONS:

[1] Y. Zhu and J. Tafto
"Direct Imaging of Charge Modulation,"
Phys. Rev. Lett. **76** (1966) 443-446.

[2] Y. Zhu and J. Tafto
"Measurement of Charge Transfer in $YBa_2Cu_3O_7$ Using a Novel Electron Diffraction Method,"
Philo. Mag B, **75**, (1997) 785-791.

[3] L. Wu, Y. Zhu and J. Tafto
"Measurements of Valence Electron Distribution in Complex Crystals: A study of Oxide Superconductors,"
submitted to *Phys. Rev. Lett.*

[4] J. Tafto, Y. Zhu and L. Wu
"A New Approach Towards Measuring Structure Factors and Valence Electron Distribution in Large Unit Cell Crystals,"
submitted to *Acta Cryst. A*

[5] R. Wang, Y. Zhu and S.M. Shapiro,
"Structural Defects and the Origin of the Second-length-scale and Central Peak at Phase Transition of $SrTiO_3$,"
submitted to *Phys. Rev. Lett.*

LDRD FUNDING:

FY 1996	$102,697
FY 1997	$133,643

Research into New Database Methodology Based on the Object Protocol Model

Enrique E. Abola and *96-26*
Joel L. Sussman

PROJECT DESCRIPTION:

*R*apid development in structural and molecular biology has resulted in a dramatic increase in the size and complexity of data that must be captured in database systems. Researchers require immediate access to these data using query systems that are powerful, intuitive, and allow questions to be cast using natural language constructs. Specific objectives include construction of a database system that can access all data and knowledge inherent in PDB entries. It also includes development of tools and protocols that identify, access, and return data related to PDB objects which reside in other biological and chemical databases.

This project aims at addressing issues such as data representation and data access in structural biology using the contents of the Protein Data Bank. Results of the study will help us develop a deeper understanding of what is required to build systems that addresses user demands, expected to increase dramatically in the near future. The work will develop computational tools that enhances PDB's database and its query system.

TECHNICAL PROGRESS AND RESULTS - Fiscal Year 1997:

Purpose: Several areas are being addressed as part of this project that are expected to culminate in a database available on the Internet:

a) Development of tools for deposition of data in to the database.

b) Development of tools and auxiliary data resource for describing and managing chemical and structural information on biologically and medically important ligands that bind to proteins.

c) Development of a web-based query system with support for searches using ad-hoc queries.

d) Development of 3DB-Base, a structural database based on the contents of the Protein Data Bank.

The primary objective of this study is to build a database system capable of answering complex ad-hoc queries on biological systems. For example, researchers doing drug-design studies are interested in characterizing interactions between proteins and ligands. Questions such as "what residues in an HIV protease are directly involved in binding known inhibitors." Another interesting question is - "what is the affect of a specific mutation to the stability of the protein?," this question may be asked by one with sequences of a family of proteins along with mutants for which no structure have been reported. The database query system will require access to programs that do homology building, sequence threading, sequence comparison, structure comparison, molecular viewing, etc. before answers may be returned.

The system being built must be capable of answering these diverse questions. It must be highly flexible, easily extended or modified to reflect our changing understanding of biological processes. It must interconnected to other databases. It also must be capable of using new computational tools as they arise.

Approach: Data modeling work needed to support the activities described above are being done using the Object Protocol Model (OPM) developed by Dr. Victor Markowitz at Lawrence Berkeley Laboratory (LBL). OPM provides a complete database design and data management toolkit. The database itself is being implement on a SYBASE engine.

Programs for data deposition, *AutoDep ver. 2,* and for data browsing, *3DB-Browser*, are being developed for use on the Web. *AutoDep ver. 2* is a marked improvement from *AutoDep ver. 1* and is expected to improve the quality of the data being entered into the database. This deposition system is a crucial component of 3DB-Base as data loading tasks are facilitated by its use.

The web browser *3DB-Browser* is being developed in collaboration with Dr. Jaime Prilusky from the Weizmann Institute of Sciences. This form-based query system is capable of linking information stored in the PDB with those found in other relevant databases. It uses both the *Glimpse* text retrieval system and SYBASE SQL queries in answering questions entered through a form. The *fasta* program developed by Dr. William Pearson of the University of Virginia is used for searching sequence similarities between data stored in the PDB and those entered as a query string.

Finally, we are collaborating with Dr. Manfred Hendlich from University of Marburg, Germany to adopt his ligand database, RELIBASE, and his program, *Bali,* for use in this project. RELIBASE and Bali provide a powerful environment for describing and managing chemical and structural information on small organic molecules (e.g., inhibitors, cofactors, etc.) that bind to proteins.

There are three primary goals in developing resources for handling ligand information:

1. To generate, maintain, and distribute a data dictionary that contains complete description of PDB heterogen (ligand) groups. The data dictionary will be maintained as part of 3DB-Base.

2. To develop a mechanism that helps depositors (primarily through AutoDep) to submit a complete description of their heterogen groups.

3. To provide facilities that will allow users to query our databases for information on ligands and their interactions with macromolecules. Search mechanisms will include the use of smile strings or specifications based on a 2D-chemical diagram in much the same way as is done in most chemical search programs.

The following are needed to completely describe heterogen groups:

1. Description including name of the heterogen.

2. Complete formula including hydrogen counts.

3. Connectivity including the number of hydrogen atoms attached to heavy atoms.

4. Synonyms.

5. A 2D diagram of the molecule showing bond types.

6. SMILE string describing each group.

7. CAS number.

8. Chiral center specification.

9. List of other physical-chemical data such as binding constants, etc.

Items 1-4 are available in the current PDB Het (ligand) dictionary. Items 5-9 will extend this dictionary that will greatly enhance its utility and also significantly help in building new search mechanisms for het groups. In addition to completing het group definitions, we will also have this data available in the standard MOL2 format, thereby making the data directly accessible to a number of existing application programs. The database RELIBASE is being used in completing this dictionary.

Due to the large number of newly deposited structures the processing of HET-groups has to be automated as far as possible without complicating the submission procedure for the depositors. A solution lies in the automatic generation of bond and atom type information from the submitted coordinates with a subsequent check and, if necessary, manual correction by the depositors. This approach provides the advantage that the whole process of HET group procession can be automated completely as the knowledge about the chemistry of the HET group is supplied by the depositors. After having the exact information about bond and atom types HET groups can be processed further (unique numbering, comparisons with the HET dictionary, etc.). The necessary tools are already available or are currently in development:

- Automatic determination of bond and atom types - The program BALI (M. Hendlich, F. Rippmann, G. Barnickel. BALI: Automatic Assignment of Atom and Bond Types for Protein Ligands in the Brookhaven Protein Database. *J. Chem. Inf. Comput. Sci.*, in press), was recently developed to generate bond and atom types for small molecule ligands from the PDB for subsequent storage in the RELIBASE system. BALI derives bond and atom types according to the MOL2 specification from Tripos by analyzing structural features (e.g., bond distances, bond angles) and by an identification of functional groups. Using a test set of 120 compounds from the PDB, BALI generated completely correct assignments for 90% of all structures. Calculation times are in the range of 0.1 seconds per compound.

- Distortions in many structures primarily due to experimental uncertainties and/or the relatively low resolution of the data prevents BALI from achieving 100% accuracy. Therefore, there will be a need for depositors to manually check and possibly to correct assignments produced by BALI. This can be accomplished with the Moled3D program which is currently in development by Manfred Hendlich as a tool for 3D structure queries within the RELIBASE system. Moled3D allows the interactive manipulation (rotation, translation, changes of bond and atoms types) of 3D molecules within a World Wide Web (WWW) viewer such as Netscape. As Moled3D is written in Java it would be relatively easy to integrate into the AutoDep environment.

Technical Progress and Results:

Schema Development: We have completed a redesign of the 3DB-Base schema based on feedback from users and our collaborators. The current version of the schema is available at the following web address: **(http://www.pdb.bnl.gov/~abola/3DB/3DBbase.OPM)**

The new schema contains a richer description of the accessionable objects within the database allowing for the inclusion of user-supplied annotations. It also has a completely different description of the molecular contents of PDB entries. The redesign work will facilitate the adoption of new features being incorporated by Dr. Markowitz into OPM that enables us to call external programs (methods) from a query. Loading of this database is in progress.

AutoDep: The new version of the data deposition tool, *AutoDep2,* is now being released for general use. The new features include:

- A new method for navigating through the forms have been instituted. It is expected to simplify the processes of entering data which we hope will also help improve data quality.

- Uploading Files - Uploading files to the PDB has been simplified for users of Netscape version 2.0 or higher. An easier HTML forms-based file upload tool aids selection and transfer of files to the PDB. Standard UNIX compressed (*.Z) or GNU gzipped (*.gz) files may now be transferred.

- Validation Added - The program WHAT_CHECK by G. Vriend and R. Hooft has been added to AutoDep 2.0 (see the April 1997 PDB Quarterly Newsletter). Upon submission of data, processing and validation programs are run. An acknowledgment letter is sent by e-mail, with instructions for completing the submission process, when these programs are finished.

- A letter is sent automatically via e-mail with information that includes the ID codes issued for the submission and the entry enters the PDB processing flow.

- Depositor Information - Depositor information is now semi-automatic. After the e-mail address and/or family name is entered, AutoDep will complete the other fields if a unique match is found within the PDB database.

- Security - A tool has been added that allows changes to the AutoDep session password.

3DB-Browser: A new version of the browser was released this year. It included a number of features requested by our users. We are now using the Glimpse engine for text retrieval which provides a faster access to our entries. The number of fields that can be queried has been increased and we now include the capability of searching for entries in the PDB by specifying a sequence of amino acids. The results returned by the browser includes links to other data resources that are related to the results. Updating of the links are done through automatic links to these resources.

Ligands in PDB:. We have recently installed the database RELIBASE at PDB and are making it available to our users. Shortly, we will be building links between entries in this database and objects in 3DB-Base. This will then allow users to use the powerful query tool provided by RELIBASE to search for information stored in PDB. We are also tailoring RELIBASE for use in internal data processing tasks. A new PDB Het Dictionary will shortly be released that will contain complete description of ligands in the PDB.

The program BALI was installed and tested at PDB this summer. A new JAVA-based (*Mole3D*) interface is now being built

that will make it easier to enter new ligand information into the database. This program will be integrated with *AutoDep* and with 3DB-Base.

ACCOMPLISHMENTS:

Postdoc: D. Lin, Research Associate

LDRD FUNDING:

FY 1996	$14,394
FY 1997	$98,792
FY 1998(est.)	$95,000

Tailored Pulse UV/XUV Photon Source Development

Louis F. DiMauro and *96-27*
Erik D. Johnson

PROJECT DESCRIPTION:

The arbitrary shaping of temporal lasers pulses at visible and ultraviolet wavelengths is being studied. Applications include the design of an optimal pulse shaped for efficient photoemission from an ejector rf-electron gun for linear accelerators. Additional investigations are also proposed on the production of high harmonic radiation above 10 eV photon energies for use as a seed pulse in the UP-FEL project at the Source Development Laboratory.

TECHNICAL PROGRESS AND RESULTS - Fiscal Year 1997:

Purpose: BNL has launched several accelerator-based initiatives in recent years which rely upon the production and control of intense, short pulse, UV and VUV/XUV radiation. The 10 MeV Pulsed Radiolysis Facility (CRCR), the Accelerator Test Facility and the Source Development Laboratory (SDL) are all based on photocathode electron guns which require a short wavelength (UV) drive laser, with the latter having the additional requirement of a synchronized VUV/XUV injector beam for the UP-FEL project. Optimization of these experiments can be achieved in part by direct control over the temporal profile of the radiation pulse. One aim of this project is to develop strategies of efficient production and control of arbitrary pulse shaping in the UV-XUV range. Sources of this type will also be valuable tools for optimal control methods in atomic, optical, chemical and materials science. The second objective is directed at the development of a high harmonic source of coherent XUV radiation as a primary and sub-harmonic injector beam for the UP-FEL project. This development can be pivotal in extending the advantages of the seeded beam approach to FELs into the soft x-ray regime. The research proposed in this document remains a necessary and vital "missing" component for numerous BNL initiatives.

Approach: Rapid advances in optical engineering, such as the advent of chirped pulse amplification (CPA) to generate intense, ultra-short visible laser pulses and progress in the optical telecommunication sciences, has provided the tools necessary for the production of arbitrarily shaped pulses of coherent radiation. The experimental challenge is to synthesize these techniques and create intense, encoded UV-XUV coherent pulses. The fundamental principle is that an ultra-short laser pulse is governed by a simple transform relationship that connects the pulse duration with its bandwidth. The shorter the pulse is in time, the larger is the bandwidth associated with the laser's central frequency. Chirped pulse amplification makes use of this simple relationship for amplifying ultra-short pulses to gigawatt or greater peak powers while minimizing the potential for optical damage to critical amplifier components. The actual implementation of the CPA technique is accomplished by the use of dispersive optical elements, i.e., gratings, prisms, before and after amplification and is illustrated in Figure 1. A *weak*, ultra-short pulse first enters a stretcher apparatus which elongates the pulse in time by at least a factor of a thousand. This enables the efficient extraction of gain from the amplifier medium by lowering the peak power of the pulse by the same factor. Once the gain has been extracted the *amplified* pulse is ejected into

the compressor which reconstructs the temporal shape of the input pulse but with increased power (by a factor of 10^6). Thus, the stretcher and compressor provide the proper mathematical optical transform function for performing this operation.

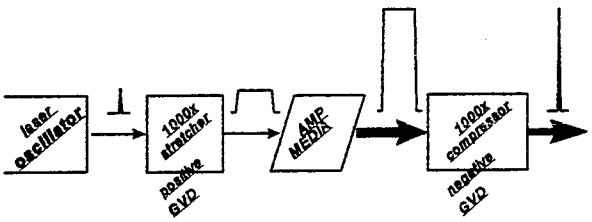

Figure 1. Chirped pulse amplification scheme.

The physical arrangement of the stretcher allows the incorporation of additional optical components which permits the controlled alteration of the input spectrum. The spectrum is altered in such a way that its transform after the compressor gives the desired pulse shape which differs from the original input pulse. For instance, proper modulation of the frequency spectrum of a temporal gaussian input pulse in the stretcher will transform it into a temporal square wave pulse following compression. It is easy to imagine that illumination of a photo-cathode with a square pulse will produce a more uniform electron beam as compared to a standard gaussian envelope. The technical development involves the extension of known shaping techniques and principles used for low powered visible beams into the high powered, UV range.

Technical Progress and Results: The direct technical progress linked to the SDL facility was slowed due to the delayed installation of a laser clean room in building 729. The 400 sq. ft., class-1000, clean room became an operational laser room in August 1997. A titanium sapphire laser system was installed shortly thereafter. The laser is a Spectra-Physics/Positive Light system purchased by the NSLS in FY1996. The laser has been tested and produces 28 mJ of 100 fs, 800 nm light at a 10 Hz repetition rate. Synchronization to the LINAC is accomplished by actively matching the laser oscillator's cavity length to a sub-harmonic of the LINAC's rf-source. By using nonlinear optics the laser system has a verified performance of 3 mJ pulse energy at the third harmonic wavelength of 267 nm. This output meets our initial requirements for illumination of the rf-gun photocathode. Our highest priority is the design and construction of an optical transport system for delivery of the 266 nm light to the gun hutch. The plan is to receive the gun assembly from Stanford in December 1997 and aim for a March 1998 commissioning of the LINAC. The designs for an arbitrary pulse shaper have been completed. The implementation on the SDL titanium sapphire laser will occur in parallel with the photocathode development. However, since the current unshaped 266 nm light is usable in the initial stages of commissioning, highest priority is given to operation of the LINAC.

A future requirement for the UP-FEL project is the need for a coherent VUV/XUV source of seed radiation in the 100-50 nm range. Generation of high harmonic radiation from high-density inert gas jets produced by intense field irradiation is one viable seed source. The major engineering issue is the effective coupling of the high harmonic radiation into the experimental target chamber, i.e., the UP-FEL wiggler. Optimization of the harmonic throughput onto a target depends upon a number of experimental parameters, i.e., optics, phase matching. However, one key factor is the

ability to efficiently separate the collinear harmonic radiation from the more intense, fundamental drive laser beam. Standard separation using dispersive techniques often results in hundred-fold losses. We have developed a novel excitation geometry for producing near gaussian spatial harmonic beams while making separation from the intense fundamental drive beam simple and efficient. Based on simple phase-matching considerations, a drive beam with a doughnut-like transverse spatial mode will produce *on-axis* harmonics in a near gaussian mode distribution due to conservation of momentum. Consequently, separation of the high harmonics from the drive laser is readily achieved by placement of a circular aperture. This efficiently passes the harmonics but blocks the fundamental beam. Our collaborator, Dr. Pierre Agostini (Saclay, France), has demonstrated the effectiveness of this technique. The experiments were performed in Saclay laser laboratory using an argon gas jet irradiated by a 100 fs, 800 nm (1.5 eV) fundamental beam with a doughnut-like mode. Argon gas exposed to an intensity of 0.3 PW/cm^2 produces up to the 35 th harmonic (53 eV). Figure 2 shows a CCD camera image of the 17th harmonic (25 eV photon energy) produced by this experimental geometry. The harmonic beam is circular and bright, containing approximately 10^9 photons per shot. A harmonic apparatus based on the Saclay design is near completion and will be moved into the P.I.'s laboratory in the Chemistry building (555A) in late October for characterization of the high harmonic output. Space has been designed into SDL laser room to accommodate this apparatus for VUV seeding of the NISUS wiggler.

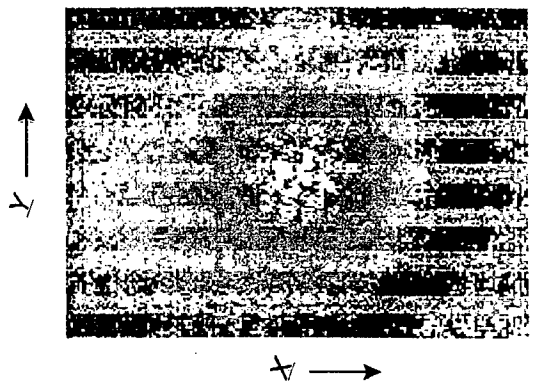

Figure 2. Spatial profile of the 17th harmonic beam produced by strong-field excitation.

LDRD FUNDING:

FY 1996	$71,570
FY 1997	$114,097
FY 1998(est.)	$120,000

Methods for Detecting Activation of the DNA-Activated Protein Kinase, DNA-PK, in Human Tissue Culture Cells

Carl W. Anderson *96-32*

PROJECT DESCRIPTION:

*D*NA-PK is a nuclear serine/threonine protein kinase composed of a large (>4000 amino acids) catalytic polypeptide, DNA-PK_{cs}, and Ku, a heterodimeric human autoantigen that binds DNA and targets DNA-PK_{cs} to it. *In vitro*, DNA-PK is activated by DNA ends and DNAs with single-to-double strand transitions (e.g., nicks, gaps, or breaks). DNA-PK phosphorylates several nuclear, DNA-binding proteins including the p53 tumor suppressor protein. These properties suggest that DNA-PK may function to detect DNA damage and initiate cellular responses. Recent studies have shown that DNA-PK is required for double-strand break repair and site-specific (V(D)J) recombination in mammalian cells.

Currently, it is not possible to measure DNA-PK activity in living cells; thus, it has not been possible to determine if DNA-PK is activated by DNA damage or by natural nuclear processes (e.g., DNA replication, transcription, recombination) that produce DNA structures similar to those that activated DNA-PK *in vitro*. To identify factors that activate DNA-PK in human tissue culture cells, we propose to develop methods to access the activity state of DNA-PK in living cells. We also will modify our current radioactive assay for DNA-PK to a fluorescence-based assay that will be suitable for screening potential inhibitors using a robotic assay.

PREVIOUS TECHNICAL PROGRESS:

Previously, we reported the sequence of a cDNA corresponding to the DNA-PK_{cs} polypeptide. Analysis of additional cDNA clones from a human T-cell library corresponding to the carboxy-terminal kinase domain revealed a 93 bp segment in four of five independent clones that was not present in the cDNA initially isolated from HeLa cells. The 93 bp segment appears to represent an exon that encodes 31 amino acids. RT-PCR showed that most DNA-PK_{cs} mRNAs in human cells have this exon. Thus, the nascent DNA-PK_{cs} polypeptide is composed of 4127 aa and has a predicted mol. wt. of 469,021 (470 kDa). A manuscript describing our analysis was published in (Connelly et al., 1996).

The carboxy-terminal segment of the human p53 tumor suppressor protein, containing the tetramerization domain and the single-stranded DNA binding domain, is phosphorylated at least two evolutionarily conserved sites, serines 312 and 392; a third site can be phosphorylated *in vitro* by protein kinase C. Another group has suggested that DNA-PK phosphorylates a site near the carboxy terminus of p53. To determine the biochemical consequences of phosphorylation at these sites, a segment condensation method that permits chemical synthesis of large (>90 amino acid) phosphopeptides was used to produce phosphorylated and non-phosphorylated derivatives of the carboxy-terminal tetramerization and regulatory domain of human p53 (residues 303 to 393). The five differentially phosphorylated, synthetic p53 peptides exhibited monomer-tetramer association as determined by analytical ultracentrifugation. Circular dichroism spectroscopy revealed that phosphorylation at Ser315 induced an increase in α-helical content that was abolished when Ser392 also was phosphorylated, suggesting

an interaction between N-terminal and C-terminal residues of the C-terminal domain of p53. Phosphorylation at serine 392 decreased the dissociation constant for tetramer formation 10-fold. Phosphorylation at serine 312 by itself had no effect on tetramer formation, but phosphorylation at this site negated the effect of phosphorylation at serine 392. The magnitude of the dissociation constant is consistent with a role for phosphorylation in controlling the formation of p53 tetramers in normal cells. Manuscripts describing these studies have been published.

To detect phosphorylation of p53 at serine 15, the site putatively phosphorylated by DNA-PK, we are attempting to produce antibodies that specifically recognize p53 only when phosphorylated at this site. Immunization of a rabbit with a phosphorylated peptide corresponding to the Ser15 site yielded polyclonal sera that was only marginally specific for the phosphorylated peptide. Immunization of mice with the same peptide yielded 49 hybridoma cell lines that reacted equally well with the phosphorylated and dephosphorylated peptide. These results suggest that the immunizing peptide is rapidly dephosphorylated after injection. Efforts to synthesize modified phosphopeptides that should be resistant to dephosphorylation currently are in progress.

TECHNICAL PROGRESS AND RESULTS - Fiscal Year 1997:

Purpose: The human genome is organized into 23 pairs of chromosomes. Each chromosome contains two very long DNA strands each of which consists of a linear chain of about 20,000,000 to 500,000,000 nucleotides. A critical problem in cell biology is maintaining the integrity of the DNA genome. Normal chemical and physiological processes cause tens of thousands of damage events per day, and external agents including X-rays and UV radiation also damage DNA. A single unrepaired double-strand DNA break may result in cell death, and unrepaired or improperly repaired DNA damage may lead to cancer. Human cells have several mechanisms for repairing DNA damage; they also have "checkpoint" mechanisms that prevent DNA replication and cell division (or that cause cell death) when DNA is damaged. One critical component in the DNA damage response mechanisms is the p53 tumor suppressor protein. p53 is a transcription factor that controls the expression of several genes that arrest cell cycle progression when DNA is damaged.

Although rapid progress has been made in characterizing DNA repair mechanisms and the cellular response to DNA damage, little is known about how damage is detected. Studies in yeasts have shown that protein kinases are important elements in the regulatory circuits that control cell cycle progression in response to DNA damage. A strong candidate for a human enzyme that detects DNA strand breaks is the DNA-activated protein kinase, DNA-PK. However, methods are need for determining the activity state of DNA-PK in cells so that the agents and conditions that activate DNA-PK can be identified and activation can be correlated with the biochemical mechanisms that govern the cellular response to genotoxic stress.

A major factor limiting the effectiveness of present cancer treatments is the relative resistance of cells to therapeutic treatments and the emergence of radio-resistant or drug-resistant tumor cells. Drugs that inhibit the repair of DNA strand breaks should increase the sensitivity of tumor cells to radiation and drug treatment. Thus, inhibitors of DNA-PK may be effective enhancers of genotoxic drugs for improved cancer therapy. In order to make

screening for DNA-PK inhibitors practical, a robust non-radioactive assay for DNA-PK activity is required.

Approach: First, we are characterizing the phosphorylation of human p53 and will determine whether specific sites are under-phosphorylated in p53 from human tumor cells that lack DNA-PK activity. These studies will show whether p53 (and, as resources permit, other putative substrates) are phosphorylated *in vivo* at sites that are phosphorylated by DNA-PK *in vitro*. Second, we will select and characterize human cell lines that express recombinant DNA-PK substrates. We hope to produce substrates that are expressed efficiently in human cells and that are phosphorylated specifically by DNA-PK. The phosphorylation state of these substrates then should reflect the intracellular activity state of DNA-PK. Third, we will develop polyclonal or monoclonal antisera that specifically recognizes p53 phosphorylated at the serine 15 site. This antisera will allow us to determine when p53 becomes phosphorylated at the DNA-PK site and to identify physiological factors that affect phosphorylation at this site. If serine 15 of p53 is phosphorylated primarily by DNA-PK *in vivo*, the antisera will provide a second method for determining the activity state of DNA-PK. Finally, we will design fluorescence-tagged peptide substrates that can be used in conjunction with our phosphopeptide-recognizing antisera to measure DNA-PK activity without a need for radioactive precursors.

Technical Progress and Results: As noted above, the carboxy-terminal segment of the human p53 tumor suppressor protein containing the tetramerization domain and the single-stranded DNA binding domain, is phosphorylated at two evolutionarily conserved sites, serines 312 and 392, and phosphorylation at these sites differentially affect the dissociation constant (K_d) for tetramer formation. The K_d for tetramer-monomer transition of the unphosphorylated segment was determined to be ~1-10 μM by equilibrium centrifugation. The magnitude of K_d is consistent with a role for phosphorylation in controlling the formation of p53 tetramers in normal cells. A detailed characterization of the effect of phosphorylation on tetramer formation was published (Sakaguchi et al., 1997)

Efforts to characterize the phosphorylation state of p53 in cells from DNA-PK proficient (e.g., M059K) and deficient (M059J) human cells by direct fingerprinting of $^{32}PO_4$ -labeled p53 was unsuccessful, at least in part because of low levels of p53. Recently, we obtained a limited amount of a purified rabbit polyclonal antibody specific for phosphorylated serine 15 of human p53. Western immunoblot analysis with this antibody showed that normal ML-1 and RKO cells, which express wild-type p53, were not phosphorylated at serine 15. This result suggests that phosphorylation of p53 serine 15 seen in previous studies was a consequence of kinase activation by damage caused by the labeling procedure. Surprisingly, p53 from M059J cells, which lack DNA-PK activity, were hyper-phosphorylated at serine 15, while serine 15 in p53 from M059K cells, which are DNA-PK proficient, was phosphorylated to a lesser extent. These results indicated that human cells contain a second kinase capable of phosphorylating serine 15 in human p53. One candidate kinase is ATM (the product of the gene disrupted in ataxia telangiectasia patients). Preliminary studies conducted by this investigator in the laboratory of Y. Shiloh, Tel Aviv University, indicate that ATM may phosphorylate p53 *in vitro*. Efforts currently are in progress to determine if ATM-deficient cells are capable of phosphorylating p53 serine 15 *in vivo*.

Efforts to develop hybridoma cell lines producing antibodies specific for p53 phosphorylated at serine 15 are in progress. A p53 specific peptide with a non-hydrolyzable phosphate derivative in place of serine 15 was synthesized and conjugated to KLH, and mice were immunized with the conjugate. Preliminary ELISA analyses indicate that sera from the immunized mice react with the p53 peptide and its chemically phosphorylated derivative. These efforts will be continued under the auspices of our NIH funded project Grant No. R01 GM52825-01A1, Function of the Human DNA-Activated Protein Kinase. The concept of using non-hydrolyzable phosphate derivatives to produce monoclonal antibodies that recognize specific phosphorylation sites led to development of a CRADA proposal with Oncogene Research Products, a major supplier of immunological reagents to the biomedical research community. The objective of this CRADA is to determine if the approach can be generalized to other phosphorylation sites, in particular ones associated with the cellular response to DNA damage, and eventually to other posttranslational modifications.

In an effort to develop non-radioactive methods for assaying DNA-PK, we determined that biotin could be attached to the amino terminus of a specific substrate peptide without significantly reducing the kinetic properties of the substrate. Unfortunately, with the commercial anti-phosphoserine antibodies available to us, we have not been able to detect phosphorylation of the biotinylated substrate peptide using the simple colorimetric detection methodologies available to us. However, a commercial company, Promega, recently developed a non-radioactive *in vitro* assay for DNA-PK that appears to be similar.

Previously we showed that DNA-PK activity is present at high levels in a variety of cultured human cells. In collaboration with researchers at the State University of New York at Stony Brook, we surveyed normal human tissues and cancers for DNA-PK_{cs} and Ku expression. Surprisingly, DNA-PK_{cs} expression is low or absent in several normal human tissues including breast, kidney, and mature lymphocytes. Most, but not all cancers expressed high levels of DNA-PK_{cs}. The significantly different expression levels for DNA-PK_{cs} seen in different tissues were unexpected because analysis of the DNA-PK_{cs} promoter structure suggests that DNA-PK_{cs} is a "housekeeping" gene with a rather simple promoter structure (Connelly et al., in press).

PAPERS/JOURNALS/PUBLICATIONS:

Anderson, C. W. and T. H. Carter. The DNA-activated protein kinase - DNA-PK. Curr. Topics Microbiol. Immunol. 217, 91-111 (1996).

Connelly, M. A., H. Zhang, J. Kieleczawa, and C. W. Anderson. Alternate splice-site utilization in the gene for the catalytic subunit of the DNA-activated protein kinase, DNA-PK_{cs}. Gene 175, 271-273 (1996).

Sakaguchi, K., H. Sakamoto, D. Xie, J. W. Erickson, M. S. Lewis, C. W. Anderson, and E. Appella. Effect of phosphorylation on tetramerization of the tumor suppressor protein p53. J. Protein Chem. 16, 553-556 (1996).

Sakamoto, H., H. Kodama, Y. Higashimoto, M. Kondo, M. S. Lewis, C. W. Anderson, E. Appella, and K. Sakaguchi. Chemical synthesis of phosphorylated peptides of the carboxy-terminal domain of human p53 by a segment condensation method. Int. J. Peptide Protein Res. 48, 429-442 (1996).

Sakaguchi, K., H. Sakamoto, M. S. Lewis, C. W. Anderson, J. W. Erickson, E. Appella, and D. Xie. Phosphorylation of serine 392 stabilizes the tetramer formation of tumor suppressor protein p53. Biochemistry 36, 10117-10124 (1997).

Connelly, M. A., H. Zhang, J. Kieleczawa, and C. W. Anderson. The promoters for human DNA-PK$_{cs}$ (*PRKDC*) and *MCM4*: Divergently transcribed genes located at chromosome 8 band q11. Genomics (in press).

Meetings:

C. W. Anderson, M. A. Connelly, H. Zhang, and J. Keileczawa, "The Promoters for Human DNA-PK$_{cs}$ (*PRKDC*) and *MCM4*: Divergently Transcribed Genes Located at Chromosome 8 Band q11." International Symposium on Ataxia Telangiectasia and ATM: Function, Genetic and Clinical Ramifications, Baltimore, MD, August 8-10, 1997, Invited Speaker.

Postdocs:
M. Connelly, Research Associate
M. Gupta, Research Associate
M. Sypes, Research Associate

FOLLOW-ON FUNDING:

NIH Grant R01 GM52825, 5/1/96-4/30/00, Function of the Human DNA-Activated Protein Kinase, P.I. C. W. Anderson, 5/1/97-4/30/98 $248,388.

Energy Research - Laboratory Technology Research Program Proposal for FY 1998 Multi-Year CRADA Project, "Development of Immunological Reagents for Analysis of DNA-Damage Responses in Human Cells," P.I. C. W. Anderson, 6/1/98-12/31/98 $202,800, submitted. This project, in partnership with Oncogene Research Products, seeks to evaluate a new method for deriving hydridomas that produce monoclonal antibodies capable of recognizing specific, critical target proteins only when they become posttranslationally modified (e.g., phosphorylated) at specific sites.

U.S. DOE Office of International Health Office, "The Effect of Low Dose Radiation and Dose Rate on Thyroid Disease: The Potential for Early Detection of Dysfunction by Tissue Markers and Molecular Methods for Assessing Radiation Damage," P.I. Ashok N. Vaswani (C. W. Anderson, Co-Investigator), submitted.

LDRD FUNDING:

FY 1996	$101,639
FY 1997	$107,565

Enzymatic and Regulatory Interactions of a Single Protein with Three Different Sites in Nucleic Acids

Sanford A. Lacks *96-34*

PROJECT DESCRIPTION:

The DpnM protein, a DNA methylase, was produced and crystallized in our laboratory, and its structure is being determined by x-ray crystallography at the NSLS in collaboration with crystallographers from the Biology Department. In addition to its enzymatic function, in which it binds to GATC sites in DNA and methylates the adenine residue, preliminary evidence suggested that the protein may have two regulatory functions in which it binds to two other sites in DNA and RNA, respectively. The aim of this project is to test whether this enzymatic protein does have regulatory functions in which it binds to nucleic acids and, if so, to identify the sequences of the regulatory binding sites in DNA and RNA, and to crystallize the DpnM protein with appropriate oligonucleotides. The DpnM protein will also be crystallized with a GATC-containing oligonucleotide, to which it has already been shown to bind, and the structures of the three different complexes will be determined by x-ray crystallography. In the event that one or both of the regulatory functions do not implicate the DpnM protein directly, the actual mechanisms of these regulatory processes, and others relating to gene expression in *Streptococcus pneumoniae*, will be explored and determined.

PREVIOUS TECHNICAL PROGRESS:

Construction of reporter vectors. Reporter vectors based on the streptococcal plasmid pLS1 were constructed by introducing the *cat* gene from the staphylococcal plasmid pC194, which encodes a chloramphenicol acetyltransferase (CAT). Restriction sites were strategically positioned upstream from the *cat* coding region to allow insertion of DNA segments containing putative promoters and ribosome-binding sites. Promoter activity was measured by the amount of CAT present in cultures containing the plasmid. The CAT activity was assayed photometrically in cell extracts after addition of chloramphenicol.

Test of P_0 promoter. With a demonstrated promoter, such as P_1, and a Shine-Dalgarno ribosome-binding sequence in the reporter vector, considerable activity, equal to 360 units, was observed. When a DNA segment from the *Dpn*II cassette that included the putative P_0 promoter substituted for P_1, no activity (<1 unit) was observed. Although this finding indicated an absence of promoter activity despite the presence of a consensus promoter sequence, closer examination of the segment cloned showed that an upstream transcription terminator could form a hairpin that included the -35 box of the putative promoter. It is possible that this hairpin formed in the supercoiled reporter plasmid and prevented the promoter from functioning.

Translational repression of *Dpn*I expression. To see whether DpnM could bind to *Dpn*I mRNA, we prepared a synthetic RNA (after cloning the *dpnC* gene and associated upstream DNA in the transcription vector pGEM3Z) that corresponded to the first 273 nucleotides of the natural mRNA. This segment was expressed from the SP6 RNA polymerase promoter in the cloning vector to give an RNA molecule corresponding to the leader portion and some of the coding region for *Dpn*I mRNA. The RNA, which was radioactively labeled, was subjected to gel

electrophoresis in the presence of various amounts of DpnM protein. No retardation of the RNA migration was observed in the presence of DpnM. To see whether the repression required the DpnM protein *in vivo*, we constructed a host strain of *S. pneumoniae* that carried the *Dpn*II cassette in its chromosome but with an insertion in the *dpnM* gene. This mutant host still methylated its DNA since it produced the DpnA methylase and the *Dpn*II endonuclease, presumably from a transcript starting at the P_2 promoter. The absence of DpnM did not prevent a *Dpn*I plasmid from establishment. Thus, neither approach taken to this question supports the hypothesis that the repression results from DpnM binding to the mRNA. The mechanism for this repression remains unknown.

Location and regulation of the P_2 promoter. In the above construction of a host strain with a *Dpn*II cassette in the chromosome that was defective in *dpnM*, we encountered an unusual behavior of the P_2 promoter. When cultures were grown maximally and held for several hours in stationary phase, the P_2 promoter lost its ability to function, as manifested by the cessation of DpnA methylase and DpnB endonuclease production. That the change was not in the promoter itself or in the downstream genes was shown by transferring the *Dpn*II chromosomal segment to a plasmid and demonstrating methylase activity when that plasmid was in a normal host able to support P_2 function. Furthermore, plasmids containing *Dpn*II cassettes identical to that originally in the chromosome did not express P_2 function when introduced into the altered host cells. We hypothesize that P_2 requires an unusual sigma factor, which is not available in the altered cells. Previous demonstration of the P_2 transcript start site showed no typical promoter consensus sequence in its vicinity.

Crystallographic analysis of *Dpn*II proteins. This year we succeeded in growing large crystals of DpnM complexed with its SAM cofactor. Using frozen crystals that had been soaked with mercury ions, we obtained good sets of data to 1.8 Å for multiple wavelengths at the NSLS stations X12B and X12C. With phases determined by the multiwavelength anomalous dispersion method, we obtained an electron density map showing α-helices and β-sheet structure typical of proteins and have begun fitting the polypeptide chain to the map.

TECHNICAL PROGRESS AND RESULTS - Fiscal Year 1997:

Purpose: The aim of this work is to elucidate several unusual mechanisms regulating gene expression in *S. pneumoniae*, which is a prominent bacterial pathogen. Cells of this species contain either the *Dpn*I or *Dpn*II restriction-modification systems encoded by interchangable genetic cassettes. The *Dpn*I endonuclease recognizes and cleaves methylated GmeATC, whereas the *Dpn*II system methylates GATC and cuts unmethylated GATC. Therefore, the two systems should be mutually exclusive. However, plasmids carrying the *Dpn*I cassette can be established in *S. pneumoniae* host cells carrying a functional *Dpn*II cassette, but the *Dpn*I genes are turned off. Also, under various circumstances, expression of *Dpn*II genes can be turned on or off. If, as suggested by preliminary evidence, one of the proteins produced by the *Dpn*II system, DpnM, which functions enzymatically to methylate the cell's own DNA and thereby prevent its cleavage by the *Dpn*II endonuclease, also participates in these regulatory processes, then this single protein may bind to nucleic acids in three different ways. If such binding is found, then the interaction of the protein with the nucleic acids will be investigated by x-ray

crystallography. At the very least, the enzymatic complex of DpnM and DNA could be examined. If DpnM does not function as proposed in regulating gene expression in this system, then the actual mechanisms of regulation of transcription and/or translation will be sought.

The *Dpn*II cassette contains three genes, *dpnM*, *dpnA*, and *dpnB*, which respectively encode two methylases, DpnM and DpnA, capable of methylating GATC, and the endonuclease, DpnB, in that order. Under steady-state production of the enzymes, a putative promoter (P_0) upstream from the *dpnM* gene is turned off, possibly by binding to DpnM; it may be turned on when DpnM is deficient, as when the system is introduced into a "naive" cell, to increase transcription of the *dpnM* gene. DpnM might block such transcription by directly binding to DNA at P_0. In the steady state, *dpnM* was shown to be transcribed from a promoter (P_1) immediately adjacent to it so that the mRNA contains no ribosome-binding site upstream of *dpnM*. A third promoter (P_2) transcribes only the downstream *dpnA* and *dpnB* genes. Another possible regulatory function for DpnM, involving the *Dpn*I cassette, may be in blocking translation from mRNA containing the *dpnC* gene, which encodes the endonuclease *Dpn*I that cleaves methylated (GmeATC) sites. When *dpnC* is introduced into a DpnM-containing cell, its mRNA is made, but no *Dpn*I protein is produced, which suggests that its translation is blocked, possibly by binding of DpnM to the mRNA.

Approach: Five aspects of this project are: (1) Crystallography of the *Dpn*II system proteins and their complexes with nucleic acids. (2) Recognition and regulation of *Dpn*II promoter P_2 and its putative sigma factor. (3) Analysis of promoter P_0 and the effect of DpnM on its function. (4) The effect of DpnM on expression of *Dpn*I in methylating strains. (5) Analysis of expression of another pneumococcal protein, RNase HII, which showed similarities to DpnM in its transcription and translation.

Crystallographic analysis of the complex of the DpnM protein and its cofactor, *S*-adenosylmethionine (SAM) will continue. Attempts will be made to crystallize the DpnM protein together with a GATC-containing DNA oligonucleotide. Gel retardation showed that the protein binds such oligonucleotides, and we shall vary the crystallization conditions and test a variety of oligonucleotides of different length, since other workers have shown crystallization of protein-oligonucleotide complexes to be dependent on oligonucleotide length. Similar approaches will be taken with the regulatory complexes, if they are established. Data from DpnM-oligonucleotide complexes should readily lead to determination of their structures by molecular replacement of the DpnM moiety. Crystals of the *Dpn*II endonuclease complexed to DNA will also be analyzed to see how this protein binds to the GATC site.

The reporter vector will be used to investigate the nature and expression of the P_2 promoter. First, the sequence that is recognized will be defined by removing parts of the DNA in that region and by substituting bases in the segment(s) necessary for promoter function. Second, the promoter in the reporter vector will be tested in strains that lost the ability to produce the DpnA methylase. If the promoter does not function in these strains, then an attempt will be made to demonstrate a sigma factor that is able to recognize the P_2 promoter in normal strains, but which is absent in the altered strains.

To continue the study of P_0, which may be blocked by an upstream hairpin element, a

segment of DNA carrying the promoter but lacking the hairpin will be tested in the reporter vector. If this configuration of P_0 is functional as a promoter in the absence of the *dpnM* gene, it will be tested also in its presence, to see if it is blocked. A caveat here is that the palindrome forming the hairpin may be necessary for the putative DpnM binding.

No evidence for an effect of DpnM on *Dpn*I expression was obtained previously, inasmuch as no interaction of *Dpn*I mRNA and the DpnM protein was observed in a gel retardation assay, and *Dpn*I plasmids still could be established in *Dpn*II host cells defective in the *dpnM* gene. A third approach, to delete part of the leader sequence between the *Dpn*I cassette mRNA start site and the ribosome binding site, showed some effects on *Dpn*I expression, and these effects will be examined to see if they can somehow explain the repression of *Dpn*I activity in methylating cells independently of DpnM.

Technical Progress and Results: **Crystallographic analysis of *Dpn*II proteins.** The structure of DpnM, a monomer protein bound to its cofactor SAM, was determined from x-ray diffraction data to 1.8 Å resolution. The R_{factor} for this structure is 0.23 and the R_{free} is 0.28. Of the 284 amino acid residues in the protein, only residues 1-10 at the N-terminus and in loops 201-205 and 260-271 were too flexible for their positions to be determined. The structure contains 178 fixed water molecules, and the bonding of protein to the cofactor is clearly defined. The structure consists of two domains, one predominantly β-sheet, with α-helices alternating with the β-strands, and the other domain completely α-helical. The first domain binds SAM and contains a fold similar to that seen in other SAM-binding proteins; the other domain from its position and sequence appears to contain the DNA recognition site. DNA methyltransferases can be divided into four classes based on the site in DNA methylated and protein sequence homology. During this investigation, structures of DNA methyltransferases corresponding to three classes other than that of DpnM were reported. Our results, therefore, should fill an important gap in understanding methyltransferases and how they function. We are currently analyzing the DpnM structure and comparing it to the others.

With respect to a complex of DpnM and its DNA substrate, we have succeeded in obtaining several large crystals grown from a mixture of the two, but we have not yet been able to examine their diffraction. The *Dpn*II endonuclease has been crystallized with its oligonucleotide substrate under a variety of conditions in a quest to consistently obtain crystals of good diffracting quality. Although we obtained good diffraction data from one type of crystal, we have not been able to obtain derivatives of that crystal suitable for phase determinations.

Location and regulation of the P_2 promoter. Using our reporter vector in *S. pneumoniae*, we were able to localize the P_2 promoter to a 36-base-pair sequence. We also introduced restriction sites within this region to enable us to readily and economically vary the sequence in order to identify the recognition sequence and further investigate its regulatory mechanism.

Test of P_0 promoter. We removed one arm of the hairpin that embraces part of this promoter, and found that the promoter is now active. We have not yet placed it in a DpnM-containing cell to see if its action is repressed.

Translational repression of *Dpn*I expression. We were unable to obtain positive evidence for DpnM binding to *Dpn*I

mRNA, and the mechanism of this repression remains unknown.

Expression of the gene encoding RNase HII. In another ongoing project in our laboratory, an operon containing the *rnhB* gene of *S. pneumoniae* was cloned. Analysis of its nucleotide sequence suggested the possibility of several parallels to the regulation of DpnM synthesis. Application of techniques used in the LDRD project to this operon revealed 1) the dependence of transcription on a promoter with an extended -10 site, and 2) identity of the mRNA and translation start sites. Comparison of the cases of RNase HII and DpnM showed that translation in both could depend on rRNA recognition of a downstream mRNA binding sequence.

PAPERS/JOURNALS/PUBLICATIONS:

Zhang, Y.-B., Ayalew, S., and Lacks, S. A. The *rnhB* gene encoding RNase HII of *Streptococcus pneumoniae* and evidence of conserved motifs in eucaryotic genes. J. Bacteriol. 179, 3828-3836 (1997).

Lacks, S. A. and Springhorn, S. S. Purification of the DpnM DNA methyltransferase of the *Dpn*II restriction system of *Streptococcus pneumoniae* and crystallization of the protein complexed with *S*-adenosylmethionine. In preparation.

Tran, P., Bewley, M., Korszun, Z. R., Cerritelli, S., and Lacks, S. A. Crystallographic structure of the DpnM DNA adenine methyltransferase from the *Dpn*II restriction system of *Streptococcus pneumoniae*. In preparation.

Meeting/Conference Presentations:

13th Lancefield International Symposium on Streptococci and Streptococcal Diseases, Paris, France. September 16-20, 1996. Invited talk entitled "Unusual Properties of Promoters and Gene Expression in *Streptococcus pneumoniae*."

17th International Congress of Biochemistry and Molecular Biology. San Francisco, CA. August 24-29, 1997. Poster entitled "An Operon in *Streptococcus pneumoniae* Containing Genes Encoding Ribonuclease HII and Signal Peptidase I."

Postdoc:

S. Ayalew, Research Associate

FOLLOW-ON FUNDING:

These LDRD accomplishments served as the basis of an Energy Research--Laboratory Technology Research Program proposal for an FY 1998 Multi-Year CRADA project entitled "Gene Expression and Identification of Gene Function in the Genome of *Streptococcus pneumoniae*." This project, in partnership with SmithKline Beecham Pharmaceuticals, seeks to understand transcription and its regulation in the genome of *S. pneumoniae*.

LDRD FUNDING:

FY 1996	$111,076
FY 1997	$117,516

Low Frequency Dynamics of Novel Materials

Myron Strongin 96-37
Victor J. Emery
Gwyn P. Williams
G. Lawrence Carr
Christopher C. Homes
Vangal N. Muthukumar

PROJECT DESCRIPTION:

This project uses synchrotron radiation from the National Synchrotron Light Source (NSLS) as a unique source of far infrared radiation for measurements of the properties of solids in a relatively unexplored regime. This far infrared regime is of crucial importance for understanding correlated phenomena of novel materials that have been called "bad metals." This important class of materials includes high T_c superconductors, fullerides and organic conductors.

TECHNICAL PROGRESS AND RESULTS - Fiscal Year 1997:

Organizational

Purpose: The purpose of this project has been, and remains, to develop the use of synchrotron radiation for the investigation of novel materials in the optical regime down to a few wave numbers. In this present fiscal year significant changes have been made in the staffing of the program.

Approach: The work in this program involves close interaction between theory and experiment. The experimental work will make use of the unique capability of the NSLS VUV ring as a source of very far infrared radiation.

Experimental

Technical Progress and Results: During this period experiments have been done on the NSLS Bruker 113 spectrometer. At the present time this instrument is being used with an internal source, but the actual connection to the synchrotron is only a short time away. Synchrotron light has been brought into the lamilar grating monochromator that has been brought to Brookhaven and initial tests are being performed.

In this period a serious scientific program has started on the optical properties of "bad metals." There has been some success in designing a vacuum system that is compatible with the restricted space available with the present cryostats and Bruker 113 optical bench. By using activated carbon cryopumps in the small vacuum system and/or the cryostat itself, pressures in the 10^{-9} Torr range can be obtained. With this system it has been possible to start transmission measurements on ultra thin films as well as work on both manganate and ruthenate systems as well as Pr-doped YBCO. The work on thin films, studies the metal/insulator (M/I) transition in this two dimensional system and how the Coulomb interaction affects the transition. This model system serves as a simple paradigm for understanding how Coulomb interactions affect more complex systems, such as those discussed below. Work on $La_{1-x}Ca_xMnO_3$, a highly correlated system which shows a large magnetoresistance, investigates the unusual frequency dependence of the conductivity. The effect of ^{18}O substitution, which is known to suppress the M/I transition in these materials, is studied through temperature dependence of the phonons through the transition. Infrared measurements on newly synthesized ruthenates study the lower dimensional electrical and phonon properties in these materials. Pr (or rare-earth) doping in YBCO provides a mechanism to strongly

suppressing T_c without disrupting the CuO_2 planes in these materials, which may provide some insight into the nature of the pseudogap.

Theory

The emphasis in the theory part of the program is to formulate a strategy for understanding charge transport in these materials where the quasiparticle picture does not apply. In the case of the high temperature superconductors, it appears that the physics is driven by the spin and charge collective modes, and superconductivity comes about in an entirely novel way. The traditional BCS route involves a Fermi surface instability and a pairing of quasiparticles. This cannot apply to a bad metal, in which there are no well-defined quasiparticles and no well defined Fermi surface. In our present view, superconductivity develops as follows: The coupling between the charge and spin degrees of freedom leads to the development of a gap in the spin degrees of freedom, which is the analog of pairing. Subsequently the charge degrees of freedom exhibit a competition between charge ordering and phase ordering (i.e., superconductivity), which has been observed by neutron scattering experiments on high temperature superconductors.

PAPERS/JOURNALS/PUBLICATIONS:

This program has led to funding of a new initiative entitled "Charge Transport in Complex Metals."

Emery, V.J., Kivelson, S.A. and Zachar, O. Phys. Rev. B56. 6120 (1997).

Puchkov, A.V., Basov, D.N. and Timusk, T. Pseudogap state in high-T_c superconductors: an infrared study. J. Phys.: Condens. Matter 8, 10049 (1996).

Basov, D.N., Timusk, T., Thomas, G.A., Rapkine, D.H., Volkov, P., Guo, Q. and Poon S.J. Lattice dynamics of icosahedral quasi-crystals: an infrared study. Phys. Rev. B (submitted).

Basov, D.N., Liang, R, Dabrowski, B., Bonn, D.A., Hardy, W.N. and Timusk, T. Pseudogap and charge dynamics in CuO_2 planes in YBCO. Phys. Rev. Lett. 77, 4090 (1996).

Basov, D.N., Poon, S.J. and Timusk, T. Anomalous lattice polarizability in intermetallic compounds: an infrared study. Phys. Rev. Lett. (submitted).

Huang, D.-J., Reisfeld, G. and Strongin,M. A photoemission study of the transition from the insulating to metallic state in ultra thin layers. Phys. Rev. B55, 1977 (1997).

Homes, C.C., Carr, G.L., Basov, D., Strongin, M., et al. The transmission coefficient of ultra thin films. To be submitted to PRB:Rapid Commun.

Homes, C.C., Kamal, S., Bonn, D.A., Liang, R., Hardy, W.N. and Clayman, B.P. Determination of the condensate from optical techniques in unconventional superconductors. Physica C (to be submitted).

Homes, C.C., Peng, J.L., Greene, R.L. and Clayman, B.P. Optical conductivity of $Nd_{1.85}Ce_{0.15}CuO_4$: strength of the condensate. J. Phys. Chem. Solids (to be published).

Presentations:

Spectroscopies in Novel Superconductors (SNS'97) Falmouth, Cape Cod, Massachusetts, September 14-18, 1997.

LDRD FUNDING:

FY 1996	$77,465
FY 1997	$84,693

BNCT for Leukemia Through *Ex Vivo* Purging of Bone Marrow

Jeffrey A. Coderre and *96-38*
John D. Glass

PROJECT DESCRIPTION:

The overall objective of this project is to experimentally determine the feasibility of using boron neutron capture therapy (BNCT) to purge bone marrow *ex vivo* prior to autologous bone marrow transplantation.

Previous Technical Progress: In the first year of the project, the principle metabolite analog being considered was 3-boronoalanine, an analog of asparagine. We showed that the compound delivered boron to mouse leukemia and lymphoma cells, particularly to an asparaginase-sensitive line of mouse lymphoma cells that requires exogenous asparagine.

TECHNICAL PROGRESS AND RESULTS - Fiscal Year 1997:

Purpose: Many leukemias and lymphomas respond, initially, to chemotherapy, then become resistant to the therapeutic drugs. At this point, the patient can be saved only by eradicating his hemopoietic tissue and replacing it with healthy, genetically compatible marrow through a transplant.

Genetic matching for a marrow transplant is exacting: a match with a high probability of compatibility is often not available. The transplant recipient is a perfect genetic match with himself, but his own marrow is the source of his disease. The concept of an autologous transplant is, 1) to remove some of the patient's own marrow from his body, 2) eradicate the remaining diseased marrow from his body, 3) selectively remove the malignant cells from the harvested marrow, then 4) return the purged marrow to the donor / recipient. So far, the third step in this process is not very well perfected: a high percentage of autologous transplants result in recurrence of the original disease. Our objective is to selectively remove malignant cells from bone marrow with BNCT.

Approach: Our approach to cleansing bone marrow of malignant cells is to selectively deliver boron-10 to the malignant cells using boron-containing analogs of metabolites. Irradiation of the bone marrow sample would then selectively kill the boron-loaded malignant cells while sparing the normal bone marrow stem cells.

In this second year of the project, we synthesized a new boron-containing amino acid analog. It is much easier to prepare than 3-boronoalanine and is avidly taken up by a number of malignant cell lines, including leukemias and lymphomas.

Synthesis: When melphalan (4-[bis(2-chloroethyl)amino]-L-phenylalanine) is stirred with a solution of disodium borocaptate in sodium bicarbonate, a soluble product is formed in which one of the 2-chlorethyl groups alkylates the thiol of a borocaptate ion and the other chlorethyl group is apparently hydrolyzed. Removal of insoluble by-products by filtration or centrifugation, followed by acidification of the clarified aqueous solution yields a white powder (BSMel). On thin-layer chromatography this material shows a single ninhydrin-positive band which is clearly different from melphalan and from the product of hydrolysis of melphalan in sodium bicarbonate solutions (4-[bis(2-hydroxyethyl)amino]-L-phenylalanine). A neutron-track etch radioautograph of the thin-

layer chromatogram shows boron at the same chromatographic position as the ninhydrin-reactive band. An NMR spectrum of this product in deuterated sodium bicarbonate solution is consistent with S-alkylation of a single borocaptate group. The compound is readily soluble in dilute sodium bicarbonate solutions: stock solutions at 10 mg / mL are routinely prepared in 0.5% sodium bicarbonate solution for dilution into biological assay medium.

Biological Studies: There is more complete data now on the uptake of 3-boronoalanine into mouse cancer cells, but the results are substantially as reported last year: 3-boronoalanine delivers boron more efficiently to asparaginase-sensitive (asparagine-requiring) cells than to asparaginase-resistant (asparagine-sufficient) cells (Figures 1 and 2). This is consistent with our understanding of 3-boronoalanine as an asparagine analog.

The most significant biological results relate to the uptake of BSMel into a number of malignant cell lines . Both the asparaginase-sensitive L5178Y mouse lymphoma cells and the asparaginase-resistant L1210 mouse leukemia cells, for example, readily accumulate high concentrations of boron in the presence of BSMel (Figures 3 and 4).

PAPERS/JOURNALS/PUBLICATIONS:

There have been no publications of this work. The synthesis of BSMel in the second year of this feasibility study and the biological results obtained with this new compound have convinced the laboratory to continue the feasibility study for a third year.

NIH GRANT APPLICATION:

An NIH grant proposal entitled "Purging of Leukemic Bone Marrow Using BNCT" was submitted 5/23/97. It requests $ 185,243 in direct costs for the first year and $ 570,807 in direct costs over a 3 year period of support.

LDRD FUNDING:

FY 1996	$82,116
FY 1997	$86,342
FY 1998(est.)	$100,000

Note: This project involves animal vertebrates or human subjects.

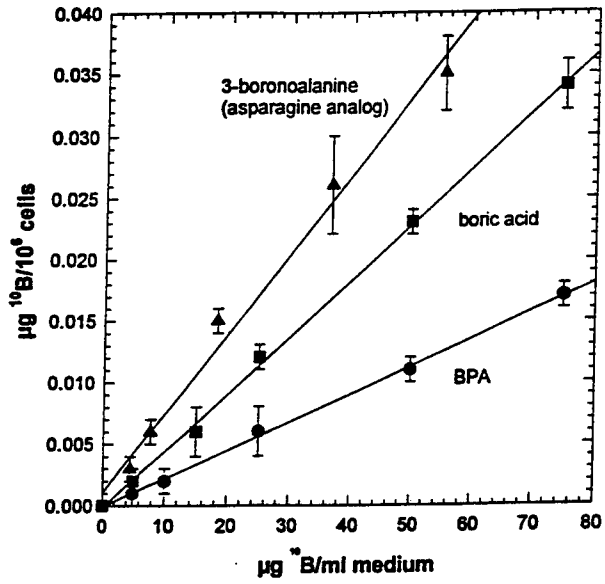

Figure 1. Asparaginase sensitive L5178Y murine leukemia cells concentrate the asparagine analog, 3-boronoalanine, compared to metabolically inactive boric acid which permeates tissues and cells at approximately its concentration in the medium. *p*-Boronophenylalanine (BPA), which is strongly concentrated in melanoma and glioma cells, is actually excluded by L5178Y cells, showing lower accumulations than the boric acid control.

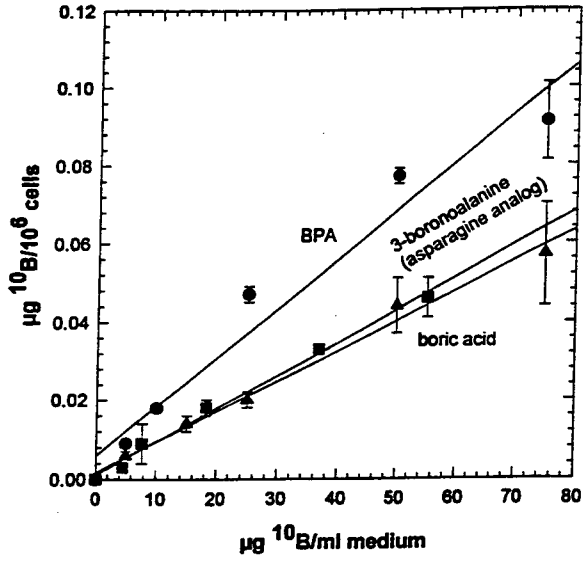

Figure 2. Asparaginase-insensitive L1210 murine leukemia cells do not accumulate the asparagine analog, 3-boronoalanine, compared to the boric acid control.

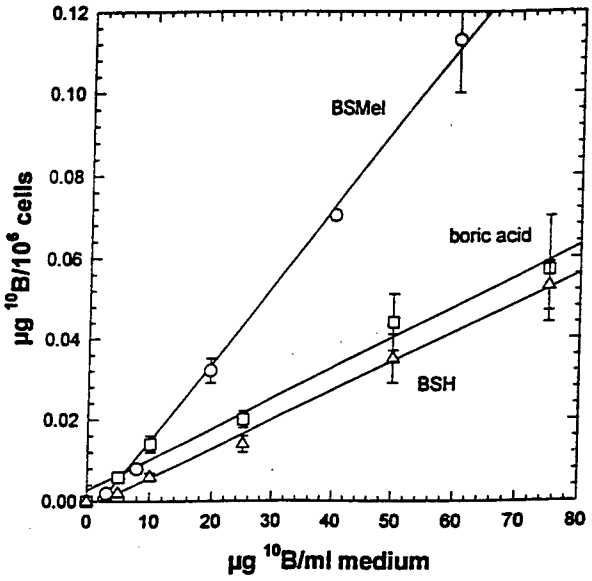

Figure 3. The melphalan-sensitive L1210 murine leukemia cells strongly accumulate the boron-containing melphalan derivative BSMel. Contrast this result with the failure of these asparaginase -insensitive cells to concentrate the boron containing asparagine analog, 3-boronoalanine, as shown in Figure 2. Note also that BSH is not accumulated by these cells: the uptake of BSMel can not be easily attributed to trivial mechanisms such as adsorption of the dodecaborane anion to cells or cellular components.

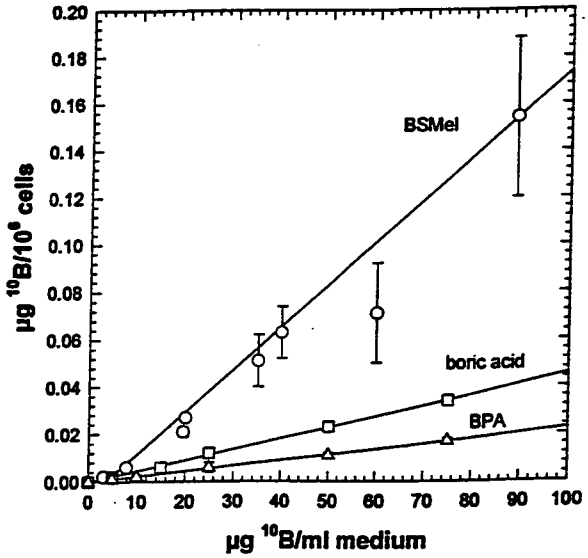

Figure 4. The melphalan-sensitive L5178Y murine lymphoma cells strongly accumulate the boron-containing melphalan derivative, BSMel. Note, again, that BPA is excluded by these cells, compared to the boric acid control.

Medical Physics Program Development

Elizabeth C. Selcow *96-46*

PROJECT DESCRIPTION:

The objective of this project is to develop an enhanced analytic capability in medical physics that will better enable the Laboratory to procure long-term outside funding. The results from this research will yield benefit to several of the ongoing medical projects at the Laboratory, including Boron Neutron Capture Therapy (BNCT) and nuclear medicine imaging. The specific areas of focus include integration of image information with the BNCT treatment planning software and the development of improved capabilities in the radiation transport analysis of diagnostic imaging and therapy systems. It is anticipated that this research will lead to projects in new technology areas that effectively integrate the multi-disciplinary expertise from the Department of Advanced Technology and the Medical Department at BNL.

PREVIOUS TECHNICAL PROGRESS:

During fiscal year 1996, we achieved several initial milestones for this project.

1. BNCT treatment planning

This work is a collaboration with Jacek Capala, BNL Medical Department scientist and Ballard Andrews, BNL Computing and Communications Division. Ballard Andrews developed the specific applications of the IBM Visualization Data Explorer Software package for the treatment planning of the BNCT clinical trials. BNCT is an experimental radiotherapy modality that is currently being used for the intractable brain carcinoma Glioblastoma Multiforme (GBM).

We initiated work on integrating information from Magnetic Resonance Imaging (MRI) scans together with the three-dimensional dosimetry distribution as predicted with the Monte Carlo analysis in the treatment planning software. The software, developed by Idaho National Engineering and Environmental Laboratory, includes the Monte Carlo program rtt_MC. This code has been tailored to provide the differential absorbed dose distributions for simulations of neutron irradiation in patient treatment for Neutron Capture Therapy. The two-dimensional radiation dose distributions are superimposed on the MRI scans after slicing the volumes along the axial, sagittal or coronal planes. Segmentation of the three-dimensional MRI data provides a rendered three-dimensional isosurface, onto which the three-dimensional dose isocontours can be mapped. This was accomplished using the commercially available IBM Visualization Data Explorer (DX) Software package, which provides an extensible modular programming environment for building visualization networks.

We developed a prototype for simultaneous visualization of the two-dimensional isodose contours superimposed on MRI image scans for transfer cuts representing sagittal, coronal, and transaxial views of the head. This prototype includes the display of the three-dimensional isodose surfaces superimposed on the three-dimensional reconstructed MRI image.

2. Radiation transport analysis of radio-biological systems

This work is a collaboration with Michael Todosow, Hans Ludewig, and Arnold Aronson, BNL Department of Advanced Technology.

We initiated a collaboration with the MIT Whitaker College of Biomedical Imaging and

Computation Laboratory on the radiation transport analysis of Single Photon Emission Computed Tomography (SPECT) imaging systems in order to become familiar with the science and technology of image analysis. This includes the relevant clinical concerns, the design and detection issues associated with imaging, the mathematical algorithms implemented for detection, image reconstruction, and processing, the factors contributing to image artifacts, and the specific radiation transport issues of particular concern to the simulation of imaging systems. We also collaborated with the BNL Medical Department in order to integrate our analysis with the Laboratory Directed Research and Development project (#94-37) : "Feasibility of SPECT in Imaging of ^{18}F FDG Accumulation in Tumors," with Gene-Jack Wang as BNL principal investigator and Peter Khan from the Department of Radiology at the State University of New York at Stony Brook.

Specifically, we began performing the Monte Carlo simulations of SPECT systems using the SimSPECT code, an MIT modification of the Los Alamos National Laboratory MCNP code for the specific application of SPECT systems. We simulated the projection data from several ^{99m}Tc and ^{18}F FDG (Fluorodeoxyglucose) SPECT experimental acquisitions obtained with the SPECT system in the BNL Medical Department. The simulations of the experiments for the ^{99m}Tc (140 keV photopeak) and ^{18}F (511 keV photopeak) point sources included representations of the source in air for variations in source to detector distance, and in varying thicknesses of water for a fixed distance. The results of the air calculations show the expected degradation with distance from the source in the FWHM (full-width-at-half-maximum) of the image profile at the photopeak.

TECHNICAL PROGRESS AND RESULTS - Fiscal Year 1997

Purpose:

1. BNCT treatment planning

The objective of the continued work is to further develop the capability to simultaneously visualize image and dosimetry information and adapt the software interfaces to the specific clinical requirements for routine treatment planning procedures. It is anticipated that this will facilitate more rapid responses to particular clinical concerns. One such requirement includes the ability to compute the total volume of the residual tumor region as seen on the MRI scans prior to BNCT irradiation. The clinical interest is to correlate the total residual tumor volume with the effective prognosis of the patient undergoing BNCT.

2. Radiation transport analysis of radiobiological systems

The specific focus is to develop improved capabilities in the radiation transport analysis of diagnostic and treatment systems. In order to accomplish this, we emphasized several aspects of the radiation transport analysis of radiobiological systems in our research. The first objective was to continue the work on the Monte Carlo simulation of SPECT systems and the collaboration with the MIT Whitaker College of Biomedical Imaging and Computation Laboratory and the BNL Medical Department. This involves performing additional simulations of additional ^{18}F SPECT phantom acquisitions. The overall goal is to use the Monte Carlo simulations to aide in the evaluation of images for patients. Other activities include the development of simulation techniques to facilitate the Monte Carlo modeling of complex anatomical regions and the application of additional radiation transport techniques in the analysis of specific imaging and therapy systems. These

techniques include the adjoint Monte Carlo and deterministic methods, which can provide valuable information to facilitate the analysis of radiobiological systems.

Approach:

1. BNCT treatment planning

The main components of the DX software application for BNCT involve visualization of the dose distribution, visualization of the diagnostic image scans, segmentation of the images, and co-registration of images from the imaging modality and the BNCT dose distributions. In particular, we have developed the following features. We can display the two- and three-dimensional visualization of the BNCT dose distribution, as computed with the rtt_MC Monte Carlo analysis in the BNCT treatment planning software. This includes the total dose and four primary dose components: boron capture (^{10}B), nitrogen capture, hydrogen recoil, and photons. In addition, the appropriate biological effectiveness factors and boron concentrations have been incorporated for each anatomical region. We can visualize the registered MRI image and BNCT dose planes along an arbitrary axis by slicing through the volumetric data set. The interior anatomical structures can also be displayed. The MRI images can be segmented to measure the volume of the tumor regions. This requires evaluation of the size of the contrast enhanced tumor volume and the ability to decipher between regions that are normal, tumerous, fibrous, or necrotic. Finally, we have effected an interactive numerical measurement of distance, volume and area with annotation features to facilitate archiving and retrieval of processed data sets.

2. Radiation transport analysis of radio-biological systems

There are several activities we pursued in the radiation transport analysis of imaging and therapy systems. The selection of specific areas to focus on was influenced by the potential benefit to ongoing medical projects at the Laboratory, the potential direct outside marketability of the individual research product, and the development of skills that could subsequently lead to the procurement of future funding. In order to maximize our leverage in obtaining funding in medical physics, we elected to apply our skills in radiation transport to a variety of timely problems in imaging and therapy systems. This serves to demonstrate to potential customers a comprehensive capability in the radiation analysis of radiobiological systems. To this end, research was conducted on the following specific activities.

The first activity is the Monte Carlo simulation of SPECT systems and the collaboration with the MIT Whitaker College of Biomedical Imaging and Computation Laboratory. This work was the basis of a subcontract to MIT, entitled "Simulation of ^{18}F-based Nuclear Medicine Imaging via the Monte Carlo Code SimSPECT," which supported a doctoral student for one semester. The activity was motivated by a growing clinical interest in the utilization of SPECT systems with PET radiopharmaceuticals. In fact, several researchers have recently demonstrated that, in cardiac FDG imaging, SPECT with 511 keV collimators can provide a diagnostic accuracy similar to PET. Monte Carlo radiation transport analysis can aid in the development and understanding of these systems and help improve the collimator and detector designs. In particular, Monte Carlo simulations of SPECT systems facilitate the evaluation of the effects of physical processes such as scatter and attenuation that degrade the quality of the acquired images. By isolating the regions contributing to the scattered components of the images, and subsequently removing the scattered

contributions, the resultant image is improved. The simulations can provide information to improve the existing scatter correction algorithms used in image processing and in particular to tailor the corrections to this specific system. The overall benefit of the analysis to an experimental/clinical project is to help in the final image evaluations, both for phantoms and patients. The analysis can further improve images by designing optimized collimator/detector systems.

As part of this activity, we have applied our methodology to the modeling and simulation of a sophisticated heart phantom and a gamma camera fitted with a 511 keV collimator. The resultant images can then be compared with typical clinical cardiac SPECT images.

A second activity involved the development of a methodology for the generation of a voxel-based Monte Carlo simulation database. The doctoral student supported under the MIT subcontract contributed to this effort. The motivation for this work was to address difficulties encountered in the modeling of complex anatomical regions, which are characterized by nonregular heterogenous volumes with multiple re-entrant surface features and are therefore difficult to represent analytically. The modeling in the Monte Carlo simulation code SimSPECT is restricted to analytic surface representations. In order to overcome these obstacles, we have developed a simulation system using data generated by the MCNP-based SimSPECT code that allows the rapid formation of projection images given a voxel-based specification of any arbitrary three-dimensional source distribution.

A third activity involves the application of an alternate methodology for the radiation transport analysis of SPECT systems, which could improve the efficiency of the analysis. The Monte Carlo simulations of SPECT systems are intrinsically computationally inefficient with long characteristic running times for simulations that adequately represent experimental/clinical detected counts. This alternate technique is the adjoint Monte Carlo method. We have already mentioned that as part of image analysis, it is of interest to identify the specific scatter and attenuation contributions to the detected image from differential regions within the source. In particular, it is significant to establish relationships between variations in a given patient's anatomy and the quality of the acquired images, such as those used for tumor detection. By determining the sensitivities of scatter and attenuation to the final images as a function of different source-detector configurations, the quality of tomographic images may be improved. In this regard, the adjoint method can provide additional information to an analysis. In addition to providing the scatter contributions in an efficient manner, the adjoint method is particularly well suited for SPECT systems, and, in some cases, is more efficient than the forward method.

A fourth activity involves the analysis of a radiotherapy facility, rather than a nuclear medicine system, and evolved from the collaboration with MIT in medical physics. This work consists of applying the discrete ordinates radiation transport methodology to the analysis of the conceptual design of the MIT reactor fission converter-based epithermal neutron beam for the MIT Boron Neutron Capture Therapy program.

TECHNICAL PROGRESS AND RESULTS:

1. BNCT treatment planning

Three applications have been developed for the treatment planning of the BNL BNCT clinical trials. The first handles MRI image data taken immediately prior to neutron irradiation but typically after neuro-surgery has removed the bulk of the tumor. After co-registration of the rtt_MC dose and MRI data, two-dimensional slices can be generated at user specified intervals along sagittal, coronal, transaxial planes, along the neutron beam direction as well as at any arbitrary direction. Biological effectiveness factors for various tissues are incorporated so that only one input file is required to calculate the different dose components. Dose information for any arbitrary point in the data set may be retrieved by pointing and clicking on the feature of interest. Files can be saved in a number of different formats, with patient name, slice direction and dose component recorded.

The second application is designed for post-treatment follow-up. Co-registration of the dosimetry data with an MRI taken several months after neutron irradiation shows the location of residual tumorous lesions and the existence of possible recurrences. The correlation of the dose profiles to the recurrent tumor position provides valuable information to develop improved treatment planning protocols. The post-treatment MRI data set is typically shifted relative to the pre-BNCT MRI, so the program performs the necessary transformations on the original scan and then to the rtt_MC dose values to permit viewing the dose delivered to regions where recurrence may have occurred. An example of this application is shown in Figure 1.

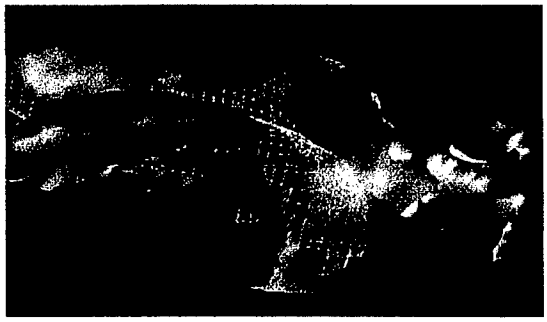

Figure 1. Superimposed MRI scans taken from a single GBM patient prior to BNCT therapy and four months afterward.

The third application performs three-dimensional segmentation and rendering of the MRI volume into multiple three-dimensional objects that can be selected, manipulated, measured and archived for future reference. Tumor volumes and distances between specified anatomical markers can be determined interactively. The rtt_MC dose can be mapped onto the tumor surface. Two-dimensional slices can also be displayed super-imposed. This application is of particular relevance in developing clinical prognoses. An example is displayed in Figure 2.

Figure 2. Cutaway of MRI head volume revealing GBM tumor. Color banding on tumor surface is the rtt_MC simulation of BNCT dose delivered to patient.

2. Radiation transport analysis of radio-biological systems

2.1 *Monte Carlo simulation of ^{18}F-based SPECT systems*

We have performed simulations of ^{18}F FDG SPECT acquisitions with the MCNP-based SimSPECT code developed at MIT, on several point source and phantom configurations measured with the BNL Picker 3-head PRISM 3000 XP SPECT camera/ 511 keV collimator. Results of the simulations for ^{18}F point sources show good agreement with the observed degradation with distance in the FWHM of the image profiles. Comparisons of the energy spectra show differences in the scattered lower energy regime presumed to be a result of incomplete modeling of the detector configuration. The additional modeling was not necessary when the lower energy photons of isotopes such as ^{99m}Tc are modeled. Other ^{18}F simulations include a water-filled cylindrical phantom, consisting of 5 hot spheres oriented around a central rod filled with ^{18}F. Reconstructed images of the projection data were performed using filtered back projection. Identification of the specific sources of scatter contributing to image degradation can be used to develop scatter corrections tailored to FDG SPECT systems.

In the SimSPECT methodology, each photon detected is tagged with information giving the location of the scattering collisions (source object, collimator, or detector if modeled), resulting in the identification of the specific geometric region contributing to the scattering at a specific energy. It is then possible to subtract the isolated scattered components from the final image, thereby resulting in a final image with fewer distortions. An example of quantifying the effect of collimator scatter on image distortion is shown in Figures 3 and 4, which display ^{18}F point source projections in air at a 10 cm source-to-detector distance both with and without the collimator scattering component. These s show the resultant improvement in the image quality.

Figures 3 and 4. Comparison of ^{18}F point source simulated projections. Images with and without collimator scatter components.

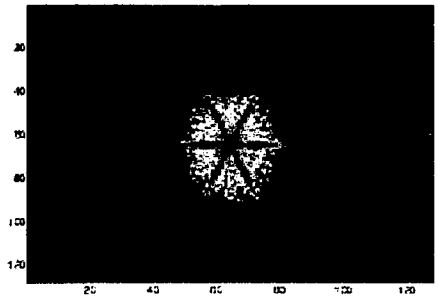

Figure 3. Total image.

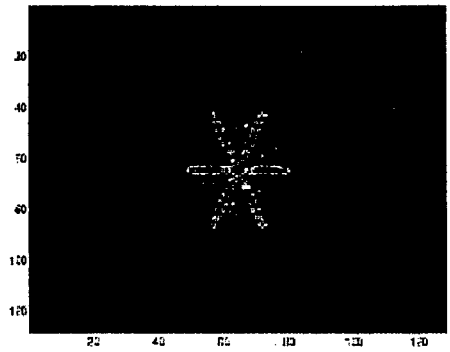

Figure 4. Image without scattered component.

We have also simulated cardiac FDG SPECT imaging, using a sophistocated heart phantom and a high energy high resolution collimator and gamma camera. The model is derived from medical atlases, Visible Man slices, ICRP's Report of the Task Group on Reference Man and MIRD phantoms. It includes a representation of the left and right atria and ventricles imbedded in a torso phantom. The 511 keV source was placed in the left atrium of the heart, with the probability of particle emission equal to the volume of the left atrium region. Both spectra

and images were generated. These images can then be compared with typical clinical cardiac SPECT images.

In summary, we have demonstrated the adaptation of the SimSPECT Monte Carlo simulation methodology to the analysis of SPECT systems using positron emitters. We have compared the simulations with experimental acquisitions, examined the effects of collimator and object scattering on image distortion, illustrated the impact of scatter corrections on improving the image quality, and applied the simulation methodology to generating images of an anatomically relevant model of a cardiac phantom. Given these results and the fact that ^{18}F SPECT is a developing technology, we can now investigate the commercial applications of this methodology which could be used to aide in the evaluation of images for patients.

Two possibilities have been envisaged for follow-on funding for this activity. The first is the investigation of commercial applications of the methodology that include the identification of scatter and attenuation corrections as well as collimator/detector optimization studies. Candidate recipients of generated proposals include detector manufacturers and pharmaceutical companies. The second possibility is a concept that involves the in-vivo generation of ^{18}F and ^{13}N with pulsed neutron generators followed by immediate imaging with SPECT gamma cameras. We have identified the Department of Energy, the National Science Foundation, and the National Institutes of Health as possible recipients of this proposal.

2.2 *Methodology for the generation of a voxel-based Monte Carlo simulation database*

The basis for this technique begins with the simulation of projection data from a uniform source distribution in conjunction with a realistic collimator model. For each detected photon in the projection data, the coordinates of the starting position within the source geometry are stored. Then, following a lengthy simulation of the uniform source, we use a three-dimensional voxel-based sampling matrix to specify the location and relative concentration of any arbitrary source distribution. The final projection images are created using only the photons originating from within the specified coordinates. This step takes place rapidly, within a few seconds, and allows any arbitrary image resolution and source distribution to be defined as per the specifications of the three-dimensional voxel-based matrix. It is possible to specify any source geometry, including those that are too complex or realistic to be modeled with the combinatorial geometry scheme of MCNP. The lengthy simulation must be repeated for the simulation of different collimators, source to detector distances, or the presence of non-uniform media in the source geometry. However, once a database of such simulations is completed, numerous acquisitions can be modeled from each set of projection data. We have completed some of the necessary database simulations based on a variety of source and collimator configurations. This can provide the foundations for generating anatomically relevant projection data with any degree of user-defined complexity.

The enhanced modeling capability that we have developed can be used to facilitate the Monte Carlo analysis of SPECT systems with complex patient source configurations. These include the representation of anatomical regions derived from MRI or CT scans. Current modeling capabilities with MCNP limit the fidelity of MRI based surface and region representations. We intend to explore the marketing potential of the application of this methodology to clinical systems.

2.3 *Use of adjoint Monte Carlo calculations in the simulation of SPECT systems*

In adjoint Monte Carlo calculations, the source densities are represented as response functions and the particles are transported backwards from the detector to the source. It is possible to tag any detector tally according to the region where the source originates. It provides information on the sensitivity of the detector image at one location and energy as a result of all possible source locations and energies from the patient or phantom. There are several distinct advantages to the utilization of the adjoint methods for SPECT systems. Adjoint calculations may be used to generate importance functions for variance reduction to reduce computational time requirements in lengthy SPECT simulations. Since the detectors in SPECT are characterized by having a small angle of acceptance from the originating source photons, adjoint calculations may be particularly well suited for these systems, and may be more efficient than forward calculations in certain cases. It is typically the small lesions on an acquired image that are of particular clinical relevance. Furthermore, a typical collimator for a SPECT gamma camera system attenuates the incident photon flux by a factor of 10,000. An increasing source-to-detector distance will result in further image degradation. The adjoint simulations can determine the relative contributions at the detector from different regions of the source with regard to different orders of scatter and spectra.

We have analyzed several cases with MCNP, including the simulation of projection data from a spherically shaped phantom source distribution in conjunction with a realistic collimator model. The collimator model represents a high energy high resolution parallel hole collimator, with hexagonally shaped and arranged holes. Cases representing forward and adjoint models were analyzed with the MENDF5 multigroup library and compared with the BUGLE-93 library. We have examined the effect of variations in source volume, source-to-detector distance, and choice of multigroup library on the computational time efficiency and the scattering contributions. We also compared adjoint multigroup simulations with forward SimSPECT simulations which use continuous energy cross sections. Further development of this application could lead to more rapid evaluations of the factors contributing to image degradation in nuclear medicine.

In summary, we have demonstrated, with the aide of the quantitative results obtained, the utility of the adjoint Monte Carlo technique for the analysis of SPECT systems. The specific benefits to the analysis methodology include the reduction in computational time requirements and the more efficient identification of the scattering and attenuation contributions to the detected photons as a function of differential regions within the source geometry. The applications of this technique will facilitate the development of more accurate scatter and attenuation correction factors for the evaluation of patient images. We plan to investigate marketing possibilities.

2.4 *Discrete ordinates analysis of the MIT reactor fission converter-based epithermal neutron beam design*

The methodology utilized the DORT/TORT two- and three-dimensional discrete ordinates code system, developed at Oak Ridge National Laboratory. The DORT simulations of the fission converter design utilized the MATXS12 cross section library in r-z geometry, with a P_3 Legendre expansion of the scattering cross sections. MATXS12 is based on ENDF/B-VI and has 69 neutron and 24 photon energy groups. Several models have been developed utilizing different

variable mesh grids, orders of approximation for the angular quadrature, and flux extrapolation models. The r-z models extend 2.93 m from the core reflector to the position of the patient or elliptical head phantom. Specific components of the models include sections of the heavy water and graphite reflectors for the core, the thermal column and fission plates, coolant pipes, filter design comprised of AlF_3/Al, Ti, Cd, and Bi, lead reflectors, collimator, and concrete shielding. The smallest model utilizes a total of 55,000 spatial mesh points and a symmetric S_8 angular quadrature. The in-air performance parameters at the target location include intensity, spectrum and dose rates, and the in-phantom figure-of-merit parameters include dose profiles, advantage depth, and advantage ratio. In addition to examining sensitivity to spatial mesh, angular quadrature, and flux modeling, the DORT analyses can be further used to collapse the cross sections into coarser-group structure for subsequent utilization in TORT analyses. The DORT and TORT results provide detailed information on the spatial dependence of the neutron and photon spectra, in addition to the performance parameters at the target location to be compared with MCNP simulation results. The results could also be used to design the medical therapy facility used for the BNCT irradiations at MIT.

We have demonstrated the application of the discrete ordinates radiation transport methodology to the analysis of a radiotherapy system. This analysis can be used to aide in treatment planning simulations and in the shielding design of a medical therapy facility.

SUMMARY AND CONCLUSIONS:

The goal of this research project was to develop enhanced analytic capabilities in medical physics. We have accomplished the development of improved methodologies for several areas of imaging and therapy systems.

The first area was the integration of image information with the BNCT treatment planning software. We have developed the capability to simultaneously visualize image and dosimetry information in a manner consistent with the clinical requirements for routine treatment planning. In particular, this provides valuable information to develop improved treatment planning protocols and clinical prognoses.

The second area was the development of improved capabilities in the analysis of SPECT systems with the use of Monte Carlo techniques. We have adapted a Monte Carlo simulation methodology to the analysis of SPECT systems with positron emitters, and used the results to improve the quality of the acquired image by correcting for the scattered contributions. Since 511 keV SPECT systems are emerging as a new technology field for clinical applications such as tumor detection, there exists very little work on the development of scatter and attenuation correction factors for these systems. We have provided two additional contributions to the Monte Carlo methodology. These include the development of an enhanced modeling capability for representing complex patient specific anatomical regions and the utilization of adjoint Monte Carlo to more efficiently derive the scatter and attenuation factors that degrade the quality of patient images.

PAPERS/JOURNALS/PUBLICATIONS:

"Discrete Ordinates Analysis of the MIT Reactor Fission Converter-Based Epithermal Neutron Beam Design," to be presented at the 1998 American Nuclear Society Radiation Protection and Shielding Topical Conference, Nashville, TN, April 19-23, 1998. E.C. Selcow (BNL) and A. Aronson (BNL).

"Use of Adjoint Monte Carlo Calculations in the Simulation of SPECT Systems," to be presented the American Nuclear Society 1997 Winter Meeting, Albuquerque, NM, November 16-20, 1997. E.C. Selcow (BNL) and J.C. Yanch (MIT).

"Monte Carlo Simulations of Positron Emitters in SPECT Systems," accepted for presentation at the 1997 IEEE Medical Imaging Conference, Albuquerque, NM, November 13-15, 1997. E.C. Selcow (BNL), A. Lu (MIT), J.C. Yanch (MIT), A.B. Dobrzeniecki (MIT), H.M. Khan (Stony Brook), G.-J. Wang (BNL), N.D. Volkow (BNL).

"Rapid Formation of Nuclear Medicine Images from a Generalized Voxel-Based Monte Carlo Simulation Database," Medical Physics, 24, 8, p. 1354, August 1997. A. Lu (MIT), J.C. Yanch (MIT), E.C. Selcow (BNL), A.B. Dobrzeniecki (MIT).

A couple of manuscripts describing the results of these projects are in preparation for peer reviewed journal publications.

Organization of special sessions at American Nuclear Society meetings on medical physics:

1997 American Nuclear Society Winter Meeting. Organized and chaired a special session on the application of reactor physics methods to medical physics. November 16-20, 1997, Albuquerque, NM. This session consists of eight papers. In addition, organized and chaired sessions on Neutron Capture Therapy, which consist of a total of twelve papers.

1998 Radiation Protection and Shielding Division Topical Meeting. Organized a special session on the application of radiation-transport methods to medical physics. April 19-23, 1998, Nashville, TN. (Co-organized with David W. Nigg from INEEL, with E.C. Selcow as the lead.) This session consists of ten invited papers.

1998 American Nuclear Society Annual Meeting. Organizing a special session on Imaging, Analysis, and Treatment Therapy. June 1998, Nashville, TN.

FOLLOW-ON FUNDING:

Submitted a proposal and successfully secured a contract funded under the auspices of the DOE Initiatives for Proliferation Prevention program. The objectives of this contract include investigating the medical applications of pulsed neutron generators produced by the All-Russian Research Institute of Automatics (VNIIA). The project is entitled, "Development of Pulsed Neutron Generators for Boron Neutron Capture Therapy."

LDRD FUNDING:

FY1996	$157,773
FY1997	$199,229

Autecology of the Peconic Bay Brown Tide Organism, *Aureococcus anophagefferens*

Julie La Roche *96-49*

PROJECT DESCRIPTION:

Brown tides, algal blooms of *Aureococcus anophagefferens*, have affected the living resources in many of the shallow bays on eastern Long Island. The brown tides first appeared in 1985 and they persisted for extended periods in 1986, 1987, and 1989. These blooms decimated scallop populations in Peconic Bay and Suffolk County began a brown tide monitoring program in 1986 to acquire hydrographic and biological data in Peconic Bay. The reoccurrence of brown tide blooms in 1995 sparked a renewed scientific interest. Based on an analysis of a time series data set collected by Suffolk County, several BNL researchers have recently proposed the "Groundwater hypothesis" to explain the bloom occurrence in the Peconic Bay. Our hypothesis postulates that brown tide blooms (>250,000 cells/ml) are caused by differences in the rate of supply of organic and inorganic nitrogen. This hypothesis has been widely endorsed by the broad scientific community but it remains to be tested experimentally in the laboratory and in the field. A combination of laboratory and field studies have been carried out to determine the role of macro-, micro-, and organic nutrients on the growth and photosynthesis of *A. anophagefferens*.

PREVIOUS TECHNICAL PROGRESS - Fiscal Year 1996:

The initial objectives were: 1) to examine retrospectively the oceanographic, meteorological and biological conditions that led to the development of the original 1985 brown tide in Peconic Bay; 2) to understand the photosynthetic and nutrient uptake physiology of the brown tide organisms found in Peconic Bay; and 3) to conduct nutrient-addition experiments with natural seawater samples from Peconic Bay that contain the brown tide organism in order to assess what nutrients limit primary productivity on a seasonal and interannual basis.

Of these three objectives, we concentrated initially on a retrospective analysis of historical data from the Suffolk County Department of Health Services, the U.S. Geological Survey and BNL's Meteorological Services. We developed an hypothesis which appears to explain the occurrence pattern of the brown tide algae over the last 12 years. This hypothesis suggests that the Peconic Estuary system now obtains inorganic nitrogen necessary for phytoplankton growth almost entirely from groundwater input that contains extremely high nitrate concentrations (>500 uM) as a result of prior and current agricultural practices and urbanization of the North and South Forks of Long Island. Brown tide blooms occur during years of low groundwater inflow and when dissolved organic nitrogen (DON) concentrations are high. We hypothesize that the Brown Tide algae are capable of utilizing DON, thus giving them a competitive advantage over other phytoplankton species which predominately utilize inorganic nitrogen species. The hypothesis is published in Global Change Biology, October 1997 issue.

This retrospective analysis represents significant progress towards understanding the factors controlling the Brown Tide occurrence. The hypothesis also explains an apparent Brown Tide requirement for high salinity. Many others have previously misinterpreted the relationship between rain, salinity and

Brown Tides in the Peconic Bay for two reasons: 1) it was not recognized that the salinity of the Peconic Bay is controlled by groundwater seepage, which is a lagged integrator of the local rainfall; and 2) the salinity/growth relationship for the brown tide algae was incorrectly determined in prior investigations. Our recently collected laboratory data, using both old and new isolates of the brown tide algae, indicate that the algae grow well at salinities as low as 21 PSU, but grow optimally between 24 and 31 PSU. Earlier studies suggested that the algae required relatively higher salinities (26 PSU), and this salinity requirement was used to explain why the blooms occurred when the salinity in Peconic Bay was high (average salinity in the Peconic Estuary is 28 PSU). We have demonstrated with our laboratory experiments that salinity itself does not play a central role in controlling brown tide, but rather is an indicator for the amount of groundwater (and thereby inorganic nitrogen) reaching the Peconic Estuary.

We began working on the third objective by conducting weekly bioassay experiments in Flanders Bay. This collaborative field effort with Suffolk County began in March 1996 and is designed to assess the role of various macro- and micro- nutrients in limiting the phytoplankton productivity in Flanders Bay. The nutrient addition bioassays conducted weekly with Flanders Bay water have demonstrated that iron, silicate and phosphate additions have little or no effect on phytoplankton growth. In contrast, nitrogen, provided either as ammonium, nitrate or urea, invariably results in an increase in phytoplankton biomass, confirming that the Peconic Estuary is nitrogen-limited, as are most other coastal marine systems. Phytoplankton samples from these experiments were analyzed to determine if any of the nitrogen sources preferentially enhanced the growth of *A. anophagefferens*, and in 1996 no significant enrichment was found, most likely because of the absence of a bloom in general.

TECHNICAL PROGRESS AND RESULTS - Fiscal Year 1997

Purpose: The purpose of this LDRD is to try to understand the physical and chemical factors that give *A. anophagefferens* a competitive advantage over other algal species present in the Peconic Estuary. The long-term objectives are to gain an understanding of the ecology of the brown tide organism, and the natural and anthropogenic factors controlling it. This information will be passed on to the Suffolk County Department of Health Services in the form of peer-reviewed publications, and may later be used by Suffolk County officials in efforts to manage the brown tides. In addition, the mechanism that we have identified is probably much more important in coastal areas than previously estimated.

Approach: A test of the groundwater hypothesis starts with the demonstration that growth of *A. anophagefferens* can be supported by DON compounds as a sole source of nitrogen and by demonstrating that DON from the Peconic Bay can be utilized by *A. anophagefferens*. This was done by adding selected organic nitrogenous compounds to 7 ml culture tubes that can be routinely measured in a fluorometer to monitor increase in chlorophyll fluorescence. I have begun identifying proteins that can be used as immunological probes to detect whether or not algae are utilizing DON in the field. This involves the characterization of specifically expressed proteins and measurements of enzyme activity, depending on the class of compounds being utilized. Several methods can be used to identify the specifically expressed proteins, ranging from coomassie blue or silver staining of total, soluble and

membrane proteins, to labeling of cell surface proteins using biotinylated reagents. The latter method has the advantage of selectively staining only cell surface proteins, thus eliminating the abundant intracellular proteins. Proteins identified as specific for a given source of nitrogen or for nitrogen limitation will be further isolated and characterized, with the goal of making immunological probes for field applications. This aspect of the work has just begun and will be continued in Fiscal Year 1998. The field study undertaken in March 1996 was continued throughout Fiscal Year 1997 and we expect to continue it through 1998. We have conducted an intercalibration exercise with the Suffolk County Department of Health Services to improve the quality of dissolved nutrient measurements.

Technical Progress and Results: Approximately 3 months were spent finishing the analysis of the time series data, and writing a manuscript for publication. A very significant achievement during 1997 has been the preparation of an axenic (bacteria-free) culture for *A. anophagefferens*, a task that has been undertaken without success by several group of researchers in the last 10 years. The expertise in phytoplankton culture at BNL made this task possible and we have succeeded in obtaining an axenic culture by subjecting the culture to sequential antibiotic treatments. During this process we have isolated several bacterial strains that may be either beneficial or detrimental to the alga. In general, this will benefit the entire scientific community working on the brown tide. Specifically, it allowed us to undertake physiological and biochemical studies of the nutrition of *A. anophagefferens* on DON and DOC, which were not possible to do with bacterized culture. Bacteria are considered to be more efficient than algae at utilizing dissolved organic matter, and bacterized cultures of algae are usually outcompeted by bacteria when fed dissolved organic matter. Figure 1 shows the growth of *A. anophagefferens* on glycine. Using the axenic culture, we have also begun searching for immunological probes against proteins and enzymes synthesized for the utilization of organic nitrogen substrate.

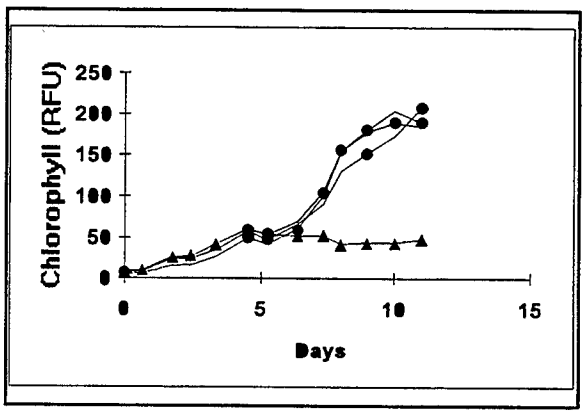

Figure 1. Growth recovery of nitrate-depleted *A. anophagefferens* after addition of 500 µM glycine on day 5 (●) relative to nitrate-depleted control (▲). Although the cultures were not axenic, bacterial biomass as determined by DAPI staining, was less then 10% of the algal biomass throughout the experiment. RFU=relative fluorescence units. Arrow indicates the addition of glycine on day 5.

PAPERS/JOURNALS/PUBLICATIONS:

La Roche J, Nuzzi, R. Waters R, Wyman K. Falkowski P. and Wallace DWR 1997. Brown Tide blooms in Long Island's coastal waters linked to interannual variability in groundwater flow. Global Change Biology 3:397-410.

Presentations:

Brown Tide Research Initiative, Westhampton Beach, April 97

14th Biennial Estuarine Research Federation International Conference October 97

Proposals: Submitted to NSF Biological Oceanography, pending

Students/Post-doctoral Fellow: One Master student (Helen Murray, part-time student at MSRC, Stony Brook) and 3 months of Dr. Mike McKay were supported by the LDRD.

LDRD FUNDING:

FY 1996	$98,405
FY 1997	$103,357
FY 1998 (est.)	$108,000

The Development and Demonstration of Accelerator Based BNCT Capability

D. Raparia *96-50*

PROJECT DESCRIPTION:

Statement of work: To study the feasibility of producing neutrons for Boron Neutron Capture Therapy, BNCT, with an accelerator rather than with a reactor. If a small commercial proton accelerator based system to produce neutrons is found to be feasible, then BNCT could become a readily available clinical procedure.

Previous Technical Progress: 3D Monte Carlo neutronics analysis was completed and it was found that of the total number of neutrons generated in a lithium target, ~ 5 to 10% would be available at the BNCT port. Test target beam tests were done using the BNL Van de Graaff . In preparation for an RFQ based system, an old 3 MeV Tandem Van de Graaff was removed from the Chemistry Department and a new beam transfer line was fabricated.

TECHNICAL PROGRESS AND RESULTS - Fiscal Year 1997:

Purpose: To study the yield and energy spectrum of neutrons produced using a proton beam (<2.5 MeV) from an accelerator, as an alternative source for Boron Neutron Capture Therapy (BNCT). The major emphasis is to study the feasibility of various production target designs to optimize the yield and energy spectrum.

Approach: The neutron generator for BNCT is based on a low energy (1.9 - 2.5 MeV) proton beam impacting a Lithium-7 target to produce neutrons by the (p,n) reaction. The resulting neutron flux is a function of both energy and angle, with a maximum energy of 800 keV in the forward direction when one use 2.5 MeV protons impinging on the target.

The filtering concept [1-4, 8] is based on slowing down of neutrons below 100 keV by inelastic scattering from fluorine. It is followed by an iron filter which takes advantage of minima in the scattering cross section at 25 keV, 70 keV, and 85 keV. Thus, there should be peaks in the neutron energy spectrum at these energies. In a real therapy source the spectrum will be further tuned by the addition of hydrogenous material. Calculations indicate that the resulting neutron yield per mA of proton current is high enough that the accelerator becomes relatively straight-forward.

The RFQ and Drift Tube Linac (DTL) for the beam tests will be provided by the Chemistry Department, coming from AccSys Technology Inc as part of a CRADA related to PET isotope production. The Department of Advanced Technology is responsible for the target design and construction aspects. The Medical Department is responsible for the installation of the detector instrumentation. The AGS Department is responsible for management of the effort, design and installation of the beam transport line, and to assist the installation and commissioning of the ion source, RFQ, DTL. Members from the Physics Department and the Department of Applied Science, in conjunction with other departments, will be involved in the experimental program.

Technical Progress and Results:

(1) A seven meter long beam line from the accelerator to the target, including quadru

poles, dipoles and beam diagnostics, was installed and individual components were tested.

(2) After long delay the accelerator arrived in March 97 and is now being commissioned.

(3) Proof of concept experiments were done at RARAF (Nevis Laboratories) for three different cases, namely:
(i) teflon and iron disks, (ii) teflon and iron disks with 1 cm polyethylene and (3) teflon and iron nested cylinders [6-7]. Analysis of data was completed. Figure 1 compares the the calculated and measured neutron spectra for nested cylinders, showing good agreement between the measured and calculated neutron spectra. Table 1 summarizes the measured and calculated parameters for the three cases. It should be noted that the experimentally determined beam current requirement of 5.3 mA using nested cylinders should be achievable in a commercially available accelerator.

(4) To evaluate the neutron output of an accelerator-based BNCT facility, studies were done at the medical reactor in which $^{10}BF_3$ detectors were used in phantoms. Benchmark curves [5] were produced which can used in testing the thermal and epithermal components of the neutron spectrum.

(5) An extensive 3D thermal analysis of the target design has been completed, and a mechanical design is underway[9].

	Disk	Disk + Poly	Nest. Cyl.
Gamma Factor[1]	6.4	18.2	28.5
Norm. Factor[2] (10^{-9})	2.26	2.32	2.32
Exp. Yield[3] n/mC(10^7)	2.03	1.09	5.25
Exp. Mean (100-200 keV)Energy keV	146	143	144
Calc. Mean (100-200 keV) Energy keV	147	147	148
Exp Mean (8.0-30 keV) Energy keV	19.2	16.7	18.9
Calc. Mean (0.0005-30 keV) Energy keV	16.9	10.1	15.5
Current[4] (mA)	13.7	25.5	5.3

[1] Gamma factors used to subtract the gamma background from the measured spectra, as determined iteratively from an exponential approximation.
[2] Normalization factor between measured and calculated spectra in the 100-200 keV region.
[3] Measured neutron yield per mC from 8 to 30 keV.
[4] Current required to deliver a fluence of 10^{12} n/cm^2 during 3600 sec, based on the experimental results.

Table 1. Summary of the measured and calculated parameters for proof of concept experiments.

PAPERS/JOURNALS/PUBLICATIONS:

[1] "NIFTI And DISCOS: New Concepts For A Compact Neutron Source for Boron Neutron Capture Therapy Application," J. Powell, H. Ludewig, M. Todosow, and M. Reich, BNL report 63605, June 1995.

[2] "New Concepts for the Compact Accelerator/target for Boron Neutron Capture Therapy," J. Powell, H. Ludewig, M. Todosow, and M. Reich, Proceedings of the 14th International Conference on the Application of Accelerators in Research and Industry, 1996, page 1309.

[3] "Target Studies for Accelerator-based Boron Neutron Capture Therapy," J. Powell, H. Ludewig, M. Todosow, and M. Reich, Proceedings of the 4th International Conference on Nuclear Engineering, 1996, page 493.

[4] "Target/Filter Concepts for the Accelerator Driven Boron Neutron Capture Therapy Applications," J. Powell, H. Ludewig, M. Todosow, and M. Reich, accepted for publication in Nuclear Technology.

[5] "Phantoms with $^{10}BF_3$ Detector for BNCT Application," D. E. Alburger, D. Raparia, and M. S. Zucker, submitted to Medical Physics.

[6] "Accelerator Based Neutron Spectra Analysis for the BNCT," L. Wielopolski, H. Ludewig, J. Powell, D. Raparia, J. Alessi, G. T. Danby. Y. Y. Lee, M. Zucker, D. I. Lowenstein, to be submitted to Medical Physics.

[7] "Estimation of the Gamma Component in the Proton Reconstructed Spectrum," L. Wielopolski and G. Han, to be submitted to Nuclear Instruments and Methods.

[8] "High Neutron Efficiency, Low Current Target for Accelerator Based BNCT Applications," J. Powell, H. Ludewig, M. Todosow, and M. Reich, submitted to Radiation and Shielding Topical Conference on Technologies for New Century, April 19-23, 1998, Nashville, Tenn.

[9] "Thermal-Hydraulic Target Test," H. Ludewig, J. Brodowski, and J. Powell, BNL Memorandum. October 22, 1997.

LDRD FUNDING:

FY 1996	$188,449
FY 1997	$412,137
FY 1998 (est.)	$200,000

Figure 1. Table Captions: Comparison of calculated (bar) and measured (line) neutron spectra for nested cylinders.

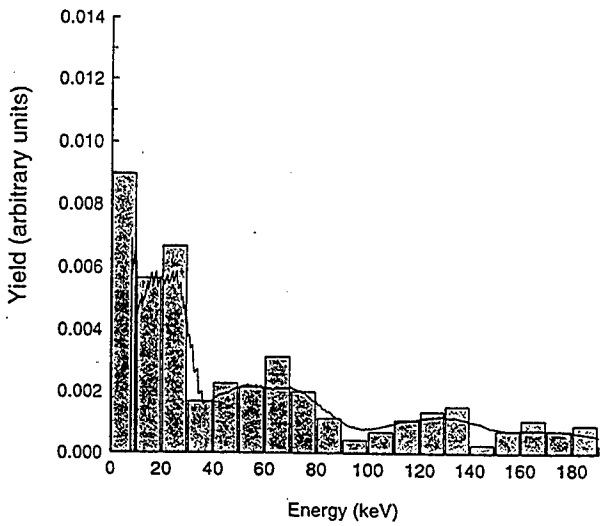

Physics Goals For a New Intense Muon Facility

William J. Marciano *97-02*

PROJECT DESCRIPTION:

The focus of this LDRD project remains largely the same as originally proposed: To identify and scrutinize the most compelling physics studies that could be carried out at a new very intense muon source capable of delivering 10^{11} ~ 10^{13} $\mu\pm$/sec, 4 to 6 orders of magnitude beyond current facilities available at TRIUMF and PSI. Such a source could be developed in the near term at Brookhaven's AGS or be part of the front end of a future muon collider complex.

The AGS is a particularly attractive muon source facility. It has been recently upgraded and has achieved record proton beam intensities, 6 X 10^{13} protons/pulse. Further intensity increases are also expected. Its utility as a muon (and antimuon) source for a future very high energy $\mu^+\mu^-$ collider has been investigated. In principle, it appears possible to produce a very clean secondary muon beam at the AGS with intensity approaching 10^{13}/sec. (The first effort would aim for 10^{11} μ/sec).

A very intense muon beam can have important applications well before the full muon collider dream is realized. Indeed, we have advocated* the possibility of a low energy physics program at the AGS which would take advantage of the unique opportunities available at such a facility. The envisioned program would include its own forefront physics research while helping to advance R&D for future muon collider technology.

In our effort to motivate the new intense muon source, we have outlined a program of low energy physics experiments that could be carried out there. The program would initially concentrate on fundamental physics studies, but later find applications in condensed matter via μSR and muon catalyzed fusion research. Some of the fundamental measurements envisioned include:

1. Precision Measurements of Muon Properties (τ_μ,g_μ-2,e.d.m.)

2. Muon Neutrino Studies (mass, oscillations...)

3. Searches for P and T violation in Muonic Atoms

4. Searches for Muon Number Non-Conservation

Each of these is undergoing close scrutiny in an effort to assess how far such studies could be pushed and to determine their potential importance and likelihood for uncovering "New Physics."

TECHNICAL PROGRESS AND RESULTS – Fiscal Year 1997:

So far, most of the LDRD effort has been directed at studies of the muon-number violating reaction μ^-+ Nucleus → e^- + Nucleus. The basic concept is simple, a stopped μ^- will quickly cascade into a 1*s* atomic obit and reside in close contact with the nucleus. There it lives of order 10^{-6} sec before either undergoing capture $\mu^- p \to \nu_\mu n$ or decay $\mu^- \to e^- \nu_\mu \bar{\nu}_e$. If, however, muon-number is not exactly conserved, the coherent reaction

$\mu^- N \rightarrow e^- N$ becomes possible. Its signature, a monoenergetic e^- with $E_e \approx 105$ MeV is very distinct and relatively easy to identify. Already, experiments have searched for that rare reaction and set an upper bound of 7 X 10^{-13} on its occurrence. With an AGS source capable of delivering 10^{11} μ^-/ sec, one could probe the 10^{-16} level. Recognizing that fact, a recent proposal (P940, W. Molzon *et al.*) has been submitted to BNL with the goal of searching for $\mu^- Al \rightarrow e^- Al$ to better than 10^{-16}. Because such an experiment detects only one final state particle, it can take very high intensities without encountering accidentals. Hence, we believe it could ultimately be pushed to the $10^{-18} \sim 10^{-19}$ level.

Preliminary studies of coherent muon-electron conversion were initiated at the 1996 AGS 2000 workshop and at a small but dedicated workshop held in July 1996 at the Institute for Theoretical Physics in Santa Barbara, Following those meetings, collaborative theoretical work with A. Czarnecki and K. Melnikov (Postdocs at Univ. of Karlsruhe) began. During FY97, the transition rate for muon-electron conversion in atoms was carefully examined and detailed computer calculations were carried out for arbitrary muon-number violating interactions. Relativistic atomic effects, Coulomb wavefunction distortions, finite nuclear distributions, etc. were taken into account for a broad range of stopping targets. The results have been shown at various conferences and are currently in Draft form "Coherent Muon-Electron Conversion in Muonic Atoms." Follow-up studies currently in progress include studies of specific models and their predictions including supersymmetry, heavy neutrino mixing, multi-Higgs etc. Also, the background from $\mu^- \rightarrow -e\nu\bar{\nu}$ decay in orbit is being reexamined to see if 10^{-18} sensitivity is feasible. These efforts will be facilitated by the arrival of A. Czarnecki at BNL (starting Sept.30, 1997), supported by LDRD funding.

During FY97, A. Czarnecki, K. Melnikov, and W. Marciano met as PSI in Switzerland to discuss their $\mu - e$ conversion work and participate in a workshop on muon-number violation. Ideas for pushing $\mu^+ \rightarrow e^+\gamma$ searches beyond 10^{-14} sensitivity were also scrutinized and a study of exploring that rare decay using polarized muons from a surface muon beam at the AGS was initiated.

A second part of the LDRD effort has been studies of new sources of *P&T* the muon electric dipole moment (which violates *P&T*) were examined in a variety of models. That work was a joint effort of L. Reina (HET postdoc), Oscar Vives (graduate student) and W. Marciano. It was found that muon e.d.m.studies become compelling at about 10^{-24} *e-cm* sensitivity. A more in depth study will be undertaken in FY98. For that purpose, Oscar Vives (now a postdoc in Spain) is planning to visit BNL for 6 months, partly supported by the LDRD.

Effects of *P &T* violation in muonic atoms have also been examined. Discussions with M. Pospelov (and LDRD visitor during FY97) elucidated possible signatures of CP violation. With the help of A. Czarnecki, we hope to expand that effort during FY98.

Preliminary work on the two loop radiative corrections to muon decay and the leading three loop electroweak corrections to g_μ-2 was started during FY97. Those calculations are necessary if one is to fully exploit future high precision measurements of such quantities. That effort will intensify during FY98.

A related project carried out under some

LDRD support involves muon collider physics and machine design studies. W. Marciano incollaboration with B. Kamal (HET postdoc) and Z. Parsa (BNL CAP) has examined Higgs resonance signatures and backgrounds at a $\mu^+\mu^-$ collider. Effects due to muon polarization and forward-backward polarizations were scrutinized. Also, new ideas for intersecting $\mu^+\mu^-$ storage rings with large crossing angles were advanced as a means of reducing severe detector backgrounds and neutrino radiation. Those studies will be expanded during FY98.

ACCOMPLISHMENTS:

Associated with some of the work reported above, there have been several AGS developments. A full proposal for a μ-*e* conversion experiment with 10^{-16} sensitivity (P940) has been submitted to BNL by W. Molzon and collaborators. Members of the LDRD have been asked to provide theoretical support for the experiment, if approved. A Letter of Intent has also been submitted to BNL by the muon *g-2* collaboration for a dedicated muon e.d.m. search with 10^{-24} *e-cm* sensitivity.

Many seminars and conference presentations regarding muon physics were given during FY97. Included were seminars at U.C. Santa Barbara, U.C. Irvine, U.C. Riverside, BNL, and U. of Chicago. Conference talks were given at Santa Monica, Vanderbilt Univ., APS-Washington DC, and Norway. In addition 5 lectures on muon physics were given at a summer school in Vancouver, Canada (TRIUMF) during the summer of 1997.

* W. Marciano, "The First Muon Collider and Low Energy Physics", BNL CAP Seminar 11/7/95.

LDRD FUNDING:

FY 1997	$91,434
FY 1998	$115,000

A Novel Curved Proportional Counter for X-ray Powder Diffraction Studies at NSLS

D.P. Siddons *97-08*
P.J. Pietraski, NSLS
G.C. Smith, B. Yu, Instrumentation

PROJECT DESCRIPTION:

There exist many areas where X-ray diffraction studies can reveal structure information that is unobtainable by other techniques. X-ray powder diffraction, in particular, is most effective when very large scattering angles can be covered by a single detector. The only device presently available for such studies is a commercial detector, which uses large signal amplification in a gas. This detector covers an angle of 120°, but operates with both limited counting rate capability and about 1mm position resolution; it is does not make full use of intense synchrotron X-ray beams. This project involves the construction of a new, prototype gas-filled detector, operating in a lower signal amplification mode and equipped with a large number of electronic readout channels. These features significantly increase the counting rate capability and improve the position resolution to one tenth mm. The recent discovery in our laboratory of a new electrode on which controlled electron multiplication can be sustained, and which can easily be curved to cover 120°, formed the basis for the original proposal.

TECHNICAL PROGRESS AND RESULTS – Fiscal Year 1997

Purpose: It is the intention of the proposed work to investigate a range of anode-cathode geometries, using a new electrode structure based on electron multiplication along the sharp edge of a blade. This new technique was proven to work in earlier studies which sought a solution to the instability problem that exists in microstrip gas detectors. A geometry which permits high counting rates with utmost electrical stability will be found, and incorporated into a prototype position sensitive detector, covering just under 50°, and implemented with high resolution encoding electronics also developed specifically for the device. Proof of principle will be established by tests on existing NSLS beam-lines. The long-term objectives are to show significant improvements of this new detector and electronics over existing devices, in order to justify requests for additional funding from outside agencies for a full sized, fully implemented device. Such an instrument would be in demand at powder diffraction lines at all of the world's major synchrotron sources.

Approach: Our strategy focuses on the utilization of developmental radiation detector hardware already in existence in our laboratory, the purchase of machining time to fabricate specialist electrodes, and the investigation of the electrical characteristics of these electrodes with standard techniques developed with our previous gas-filled wire chambers. A parallel effort has been launched to develop hybrid multi-channel electronics for readout of a prototype detector; funding has permitted the hiring of an electronics engineer for this purpose. Consideration will be given at a later stage in the project to the possibility of converting to monolithic electronics, which will be appropriate for a full-size detector and would take advantage of similar work already being carried out in this laboratory for LHC and RHIC detectors.

Technical Progress and Results: In the first year of this program we have studied the

electron multiplying properties of the thin blade anode which is the basis of this development. Fabrication technologies have been investigated, and we find that both electric discharge machining (EDM) and laser-cutting can provide anodes which are usable without further processing. Thus, the detector should be easy to replicate, an important point for ease of fabrication. The gas-gain properties of the edge of a thin metal shim have not been previously studied in detail, and it was necessary to perform a series of tests and calculations to allow a workable electrode to be engineered. A small test chamber was constructed which contained the anode and cathode structures, together with an X-ray window. Figure 1(a) shows a cross-section of the typical geometry that has been used. The important parameters are *d*, the anode-cathode spacing; *t*, the thickness of the anode; *b*, the recess of the anode with respect to the cathodes; *z*, the window-cathode distance; and *h*, the depth of the insulating spacers below the anode tip.

Figure 1(b) shows a photograph of the chamber and test electrodes.

The test detector has permitted measurements of gain uniformity and stability as a function of position in two dimensions over a range of values of *d*, *t*, *b*, *z*, and *h*. These detector parameters have also been studied in the context of electron optics and useful detector aperture. In general, the deeper the anode is recessed between the cathodes, the narrower is the aperture of the detector in the transverse direction, but this also leads to a more stable electrical operation, a very crucial property for turn-key operation at a beam-line. For the limited aperture required for our application, about 1 cm, we have determined that $d \sim h \sim b/2 \sim 2$ mm is optimum. A gas depth, *z*, of 15 – 20 mm provides very good efficiency in the 8-12 keV energy range of interest. The window potential, V_w, provides the field which permits electrons to drift, from the point of X-ray absorption, to the multiplication region at the

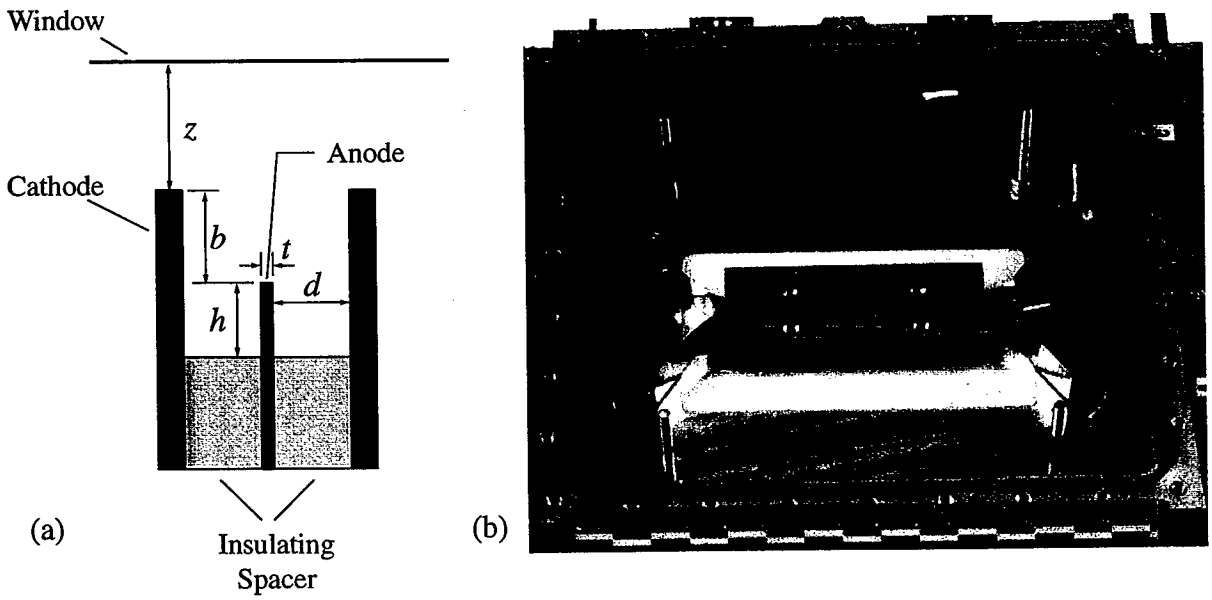

Figure 1 (a) Schematic diagram of new electron multiplying structure, indicating major electrodes and their spacings. (b) Photograph of test chamber, incorporating steel shims as anode and cathodes (sandwiched together in center of housing). X-ray window has been removed.

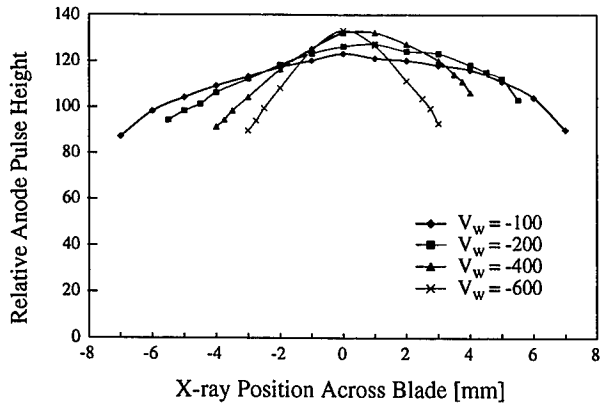

Figure 2. Anode pulse height (gain) vs position, from scan of a collimated X-ray beam across the direction of anode blade, for optimum electrode spacings.

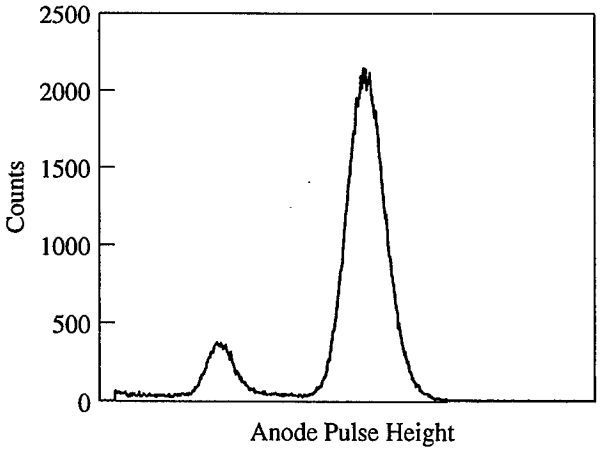

Figure 3. X-ray pulse-height spectrum, from detector with anode blade of t = 25 μm, for collimated beam incident directly above blade. Main (photo-) peak represents 5.4 keV, escape peak is at 2.4 keV.

tip of the anode. Figure 2 shows how gain at the anode varies as a narrow X-ray beam is traversed *across* the anode for several different values of V_W. It is important that the gain variation is small in relation to the intrinsic energy resolution, to prevent deterioration of the global resolution. V_W in the range 200-400V satisfies this condition. The intrinsic resolution is as good as the best wire chamber: Figure 3 shows a 5.4 keV X-ray energy spectrum from a finely collimated beam, with an argon-based gas mixture; the photo-peak and escape peak are extremely well-resolved.

Some interesting, and subtle, differences have been found in comparison with wire chambers. The blade has, to some degree, a flat top with right-angle corners. The electric field lines, in the region around the upper edge of the anode, end preferentially on the corners rather than the flat top. The major consequence of this is that the charge induced on the near (relative to the avalanche position) cathode is slightly greater than that on the far cathode, but their sum, of course, is constant. Figure 4 shows measured values of charge on the two cathodes when the entire detector is uniformly illuminated. It is clear that unequal

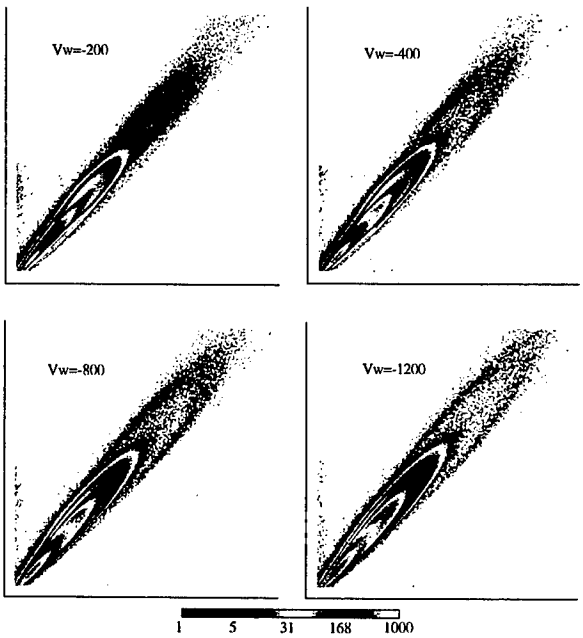

Figure 4. Plot of pulse height of one cathode (ordinate) vs pulse of other cathode (abscissa) for uniform irradiation of detector, for four different window voltages. This illustrates the inequality of induced charge on each cathode.

charge sharing is the rule rather than the exception. The primary consequence of this feature is that we will not be able to use staggered cathode readout strips to enhance the position resolution of the final detector, since such schemes rely on equal charge being induced in the cathodes for each event. This minor problem, however, is countered by the fact that this technique can utilize the full cathode charge, compared with only a half in standard wire chambers.

Based on the above measurements, we have arrived at an optimal geometry for the design of the prototype detector, which is shown in Figure 5. An exploded view, showing the curvature along the position-sensing axis, is shown in Figure 6. The electrode assembly is contained in a gas-tight enclosure having a curved X-ray entrance window. This window will initially be fabricated from metallized Mylar, since this material is easy to work. The final design will use a beryllium window, thick enough to withstand pressure of a few atmospheres of xenon to extend the energy sensitivity of the detector to higher X-ray energies. The position of the avalanche along the anode blade will be sensed by conventional means, using the induced charge on cathode strips along the length of the blade. There will be

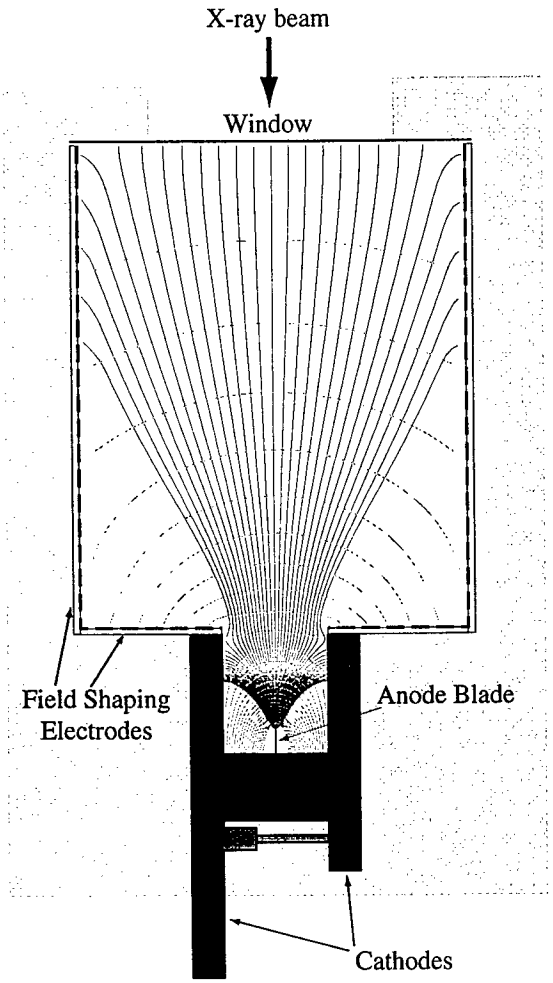

Figure 5. Cross-sectional diagram showing scaled design of prototype one-dimensional detector. Field lines (vertical) and equipotential lines indicate that, with the aperture defined by this window, ionization from nearly all X-rays absorbed in the active volume will drift to the anode.

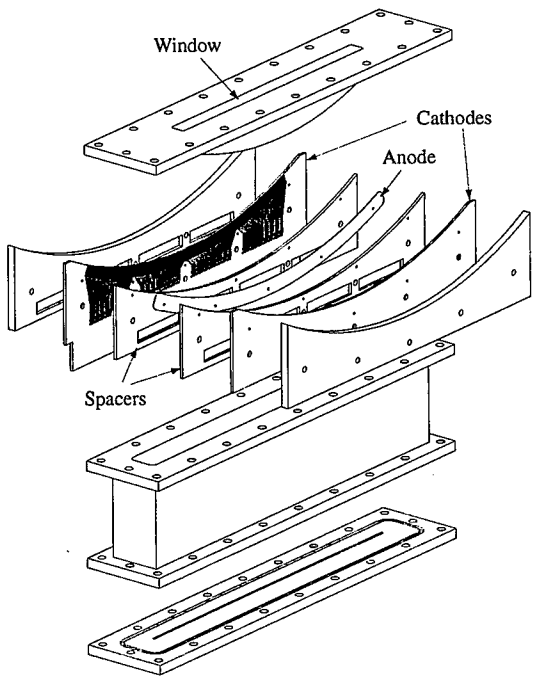

Figure 6. Exploded view of detector shown in figure 5.

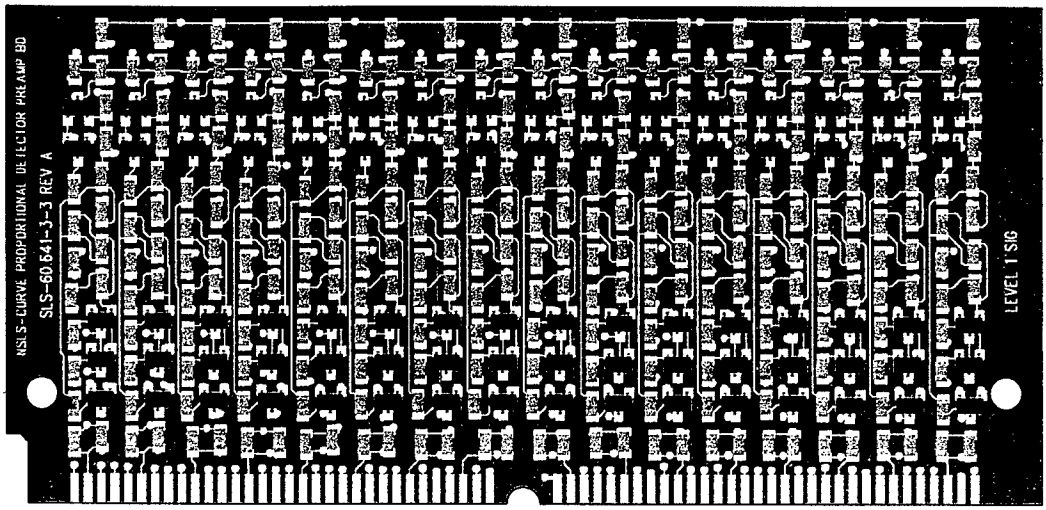

Figure 7. Layout of hybrid circuit board containing 32 preamplifier channels. This board will satisfy the front-end, readout requirement of ¼ of the cathode strips shown in figure 6.

128 strips on each of the cathodes, forming a radially symmetric pattern with radius of 25cm, equal to that of the anode, with a total angular range of detection of 45°. The cathodes will be fabricated using conventional printed circuit technology. Every cathode strip will feed its own pulse-shaping amplifier, whose outputs are digitized and analyzed. The centroid of the avalanche is determined in real-time with a precision greater than the intrinsic gas resolution, which is about 100 μm. Fabrication of a prototype detector head has been started. We have designed a high-density module which contains 32 preamplifier circuits on a board 3" by 1.5" (see Figure 7), a significantly higher density than used previously in similar detectors. Surface mount technology is well understood, allowing us to focus most of our electronic development efforts on the interpolation and histograming logic in the coming year. While a fully implemented 120° detector may well use CMOS integrated circuits (we have begun discussions with the Instrumentation Division, regarding this approach) the present prototype will be a formidable detector in its own right.

PAPERS/JOURNALS/PUBLICATIONS:

A paper describing this work will be submitted to the 1998 Vienna Wire Chamber Conference.

LDRD FUNDING:

FY 1997	$96,666
FY 1998 (est.)	$100,000

Extraction Kicker R&D for Target Shock Testing

A. J. McNerny *97-13*

PROJECT DESCRIPTION:

To develop a design for a full-turn fast kicker magnet and power supply system for the AGS and to test some aspects of the Pulse Forming Technology. This new system will greatly enhance the AGS fast extraction capability to accommodate almost entire energy range of the machine, as well as a large range in intensities.

TECHNICAL PROGRESS AND RESULTS – Fiscal Year 1997:

Purpose: The goal of this research and development is to produce a design of a fast kicker magnet and power supply system for the AGS. It will serve to provide beams for 1) target shock testing for the next generation pulsed spallation neutron sources, and 2) pion production target testing for muon colliders.

Approach: To carry out the research project, requires a comprehensive investigation of the various options in implementing a full-turn fast extraction system in the AGS. In order to accomplish this, we investigated the magnet design options, the magnet material options, types of power modulator design options, and overall system requirements. Based on these considerations, we proceeded to look into the detailed parameter choices. The techniques used were magnetic field simulations, electric circuit simulations, material and component availability, and the maturity of the technologies in implementing each option. Further efforts were spent in assessing some of the hardware and detailed high voltage layout. The final steps would be to perform prototype testing and to come up with detailed design, cost and manpower estimates for the construction and installation.

Technical Progress and Results: The present fast extraction system, or G10, has been designed exclusively for injecting into RHIC in that it extracts single bunches in a consecutive, periodic manner. Our investigation has shown that this system does not possess the flexibility of full-turn, high intensity, and variable energy from 2 Gev to 30 Gev. These are needed for SNS target shock testing and for muon collider experiments. Due to a variety of physical space constraints in the AGS, the choices come down to: 1) Upgrading the G10 extraction with a large aperture magnet and a variable length modulator to serve all FEB users, or 2) The addition of a parallel scheme, termed G20, which utilizes a full aperture magnet, and a variable length pulser. Together with a small thin septum at the H5 straight section, this system would provide a very efficient extraction system that would serve most needs of the AGS.

Naturally, the first option appears to be more attractive, and hence it was the first one to be investigated. The existing G10 kicker magnet is a C type magnet to extract beam in the 18 Gev to 30 Gev range. It has a vertical aperture of 22 mm and horizontal aperture of 33 mm. At lower beam energy (several Gev), the AGS beam size is relatively big. It requires a large vertical aperture of at least 70mm. The horizontal aperture requirement depends on a variety of factors, which is in the 50mm to 133mm range. In any case, a new magnet with a large or full aperture will be needed. Also, it requires a large deflection angle of 2 mrad.

For an ideal full aperture picture-frame magnet of 83mm in height and 127mm in width, the peak current is greater than 6000A.

Also, the resulting inductance of the full aperture magnet is much larger than the existing one. To reduce the load inductance, the magnet is often sectionalized. The ideal rise and fall time of the kicker magnetic field is to be less than 140 nS. This leads to a very high voltage requirement on the modulator. For a typical fast kicker modulator with moderate impedance of 15 to 25 ohms, the voltage is in the range of a few hundred kilovolts. High repetition rate is another crucial factor in this design, which means high burst mode power output and very high quality insulation of all high voltage devices and construction. In the study we considered the following options:

Power Modulator Design Options:

1. Lumped capacitor-inductor type Pulse Forming Network with matched resistor;
2. Coaxial cable Pulse Forming Line pulser with matched resistor;
3. Coaxial cable Blumlein pulser with matched resistor;
4. Multiple layer stacked coaxial cable pulser with matched resistor;
5. Flywheel circuit with solid state switching device.

Magnet Design Option:

1. Picture frame lumped magnet with central or side bus feed;
2. Longitudinal divided picture frame lumped magnet with central or side bus feed;
3. Picture frame traveling-wave magnet with input and output ports;
4. Longitudinal divided picture frame traveling wave magnet with input and output ports;
5. C shaped lumped magnet.

Magnet Material:

1) Lumped magnet: Ferrite magnet;
2) Traveling wave magnet:
   a) Ferrite magnet interleaved with metal plates air dielectric capacitor inside vacuum chamber;
   b) Ferrite magnet interleaved with ceramic capacitor inside vacuum chamber;
   c) Ferrite magnet interleaved with printed circuit board capacitor;
   d) Ferrite magnet interleaved with high permittivity ceramic block capacitor.

Switching Device Options:

1. Thyratron -- 70 kV to 100 kV;
2. Thyratron -- 40 kV to 60 kV;
3. High voltage and high current solid state switching devices.

All the above options have pros and cons. However, the conclusion is that to build a full aperture picture frame magnet kicker in G10 section is extremely difficult in many aspects, and is at the limit of available devices and components in today's industrial market.

We have run through two design exercises of C shaped lumped magnet with conventional coaxial cable line pulser. The first one

assumes that the vertical gap clearance is 50 mm, and the width is 60 mm, with a good field region of less than or equal to 2% for the beam aperture of 40 mm. This magnet aperture seems to be too small. The second one assumes that the vertical gap clearance is 70 mm, and the width is 85 mm, with a good field region of less than or equal to 2% for a circular area of 60 mm in diameter. Besides the difficulties of the very high voltage and high current design, the pulse forming line type modulator with high inductive load also causes some technical difficulties. With detailed analysis and circuit simulations, we found the following problems associated with the pulse parameters:

1) With a low impedance of 12.5 ohm, the rise and fall time is slower than 140 nS;

2) The cable attenuation might cause significant pulse droop;

3) There is pulse shape distortion for single pulse extraction, and

4) The pulse reflection after the pulse end is high.

Since the system reliability and the pulsed field quality for single bunch extraction is very important for RHIC and the G-2 experiment, it raises issues as to whether the large gap C magnet meets the required field iniformity; it seems necessary to consider another option.

The second system plan is to install a new large aperature fast kicker in the G20 straight section. With the help of a thin septum at H5, the deflection angle requirement of the kicker decreases to about 1.2 mrad. The kicker system being considered is a full aperture, picture frame, ferrite magnet powered by a set of distributed transmission cable constituing the pulse forming line modulator. By segmenting the magnet into a number of sections, the implementation might be accomplishable with modern high voltage components.

The areas that need further development are: the high power fast switching devices and their auxiliary driving systems; the high voltage cable for dc and high repetition rate pulsed applications; the high voltage primary power source; the insulation materials; and the low inductance, high peak current feed-through between the vacuum and the external fluid insulated circuitry. A disadvantage in this scheme is that several devices in the two straight sections have to be relocated.

An added advantage of this scheme is that the existing G10 system can continue to be used for RHIC injection and for the g-2 experiment while the G20 system is being developed for full-turn target shock extraction or for single bunch-multiple extraction schemes.

LRDR FUNDING:

FY 1997 $99,401

Plasma Window for Transmission of Synchrotron Radiation

A. Hershcovitch *97-16*
E.D. Johnson and
P.M. Stefan

PROJECT DESCRIPTION:

Prior to the initiation of this project it was demonstrated that the presence of an atmospheric arc plasma in a device increased the effectiveness of differential pumping structures by a factor of nearly 230 [A. Hershcovitch, J. Appl. Phys. 78 (1995) p. 5283]. Hence, the plasma establishes a vacuum-atmosphere interface with out any intrusive solid structures, i.e., the plasma acts as a window which separates vacuum and atmosphere. Inherently, such a plasma window is also transparent to a wide range of the electromagnetic spectrum, from the ultraviolet out into the hard x-ray regime. The present project is designed to develop and test a prototype window system for use at synchrotron beamlines. It should extend the prior technology by utilizing, magnetic confinement, venturi, and plasma thrusters, to improve the pressure differential and reduce the size of the apparatus.

TECHNICAL PROGRESS AND RESULTS - Fiscal Year 1997:

Purpose: The development of the plasma window for synchrotron radiation applications could have an important impact on both the NSLS and other light source facilities around the world. Attenuation and spatial structure which attend the use of conventional window materials (e.g. beryllium or SiN) represent a significant problem for various applications in synchrotron radiation research. Plasma windows show promise as an alternative to traditional windows for the separation of the experimental environment from the storage ring vacuum which could significantly improve the productivity of instruments like soft x-ray microscopes. Plasma windows possess none of the structure that has hindered the development of photon correlation experiments at low energies (a few keV), and would be impervious to thermal damage. In addition, the plasma may contain noble gases which would provide efficient high-order rejection for UV experiments, such as threshold photo-ionization spectroscopies. Other applications of this technology are foreseen which may have significant benefit for many programs throughout the laboratory. For instance, as the project commenced, ATF personnel showed interest in utilizing plasma windows for the CO_2 laser amplifier and an electron beam plasma accelerator

Approach: Before proceeding with plasma window development, it was crucial to ensure that plasma windows do not generate electromagnetic interference, which would adversely affect any NSLS experiments. Therefore, a series of electromagnetic interference tests had to be conducted. A test stand was built using the previously developed plasma window to perform the various tests. No external magnetic fields were incorporated in the original window configuration, since it was designed for various applications like non-vacuum electron beam welding, electron beam melting, and non-vacuum ion material modification. For transmission of synchrotron radiation from a light source like the NSLS, magnetized plasma windows can be used. In principle, these plasma windows should out-perform the original window, since higher pressure plasmas with lower densities can be generated with confining magnetic fields. Therefore, experiments with magnetized plasmas will be conducted.

Until a plasma window which can operate in oxygen is developed (arc housing made of special material), external gas feed is required. By feeding the gas through a venturi, additional differential pumping can be realized. To further enhance the window performance, perpendicular (to the window axis and to each other) electric and magnetic fields can be added in such a way that the **ExB** drifts guide escaping ions and electrons back into the window. Early MHD plasma thrusters were based on this principle.

Technical Progress and Results: A small test stand was assembled in the basement of building 535. The original plasma window, which was damaged during an electron beam transmission experiment, was repaired and mounted on a vacuum system.

A series of Electro-Magnetic Interference (EMI) experiments revealed that rf emission from the arc is negligible. In these experiments, no EMI or electromagnetic noise was detected on: a radio, a "Walkman," or a computer (PC) operating adjacent to the plasma window. Quantitatively, an EMI probe in the range of 30 - 300 MHZ detected rf noise of up to 0.7 mW/cm^2 on the arc power supply, and up to 0.9 mW/cm^2 on the arc circuit. However, on the plasma window itself, only 0.05 mW/cm^2 could be measured. The reason may be due to the fact that plasma frequency is so high that only EM radiation with a frequency higher than IR can escape. Finally, the "acid" test for rf noise was passed; The proportional counter electronics (belonging to Kirz and Feser) functioned well while the plasma window operated. These electronics are from the X-1A beamline, which would be a good candidate for utilization of a plasma window.

The plasma window coupled to a venturi operated successfully. The addition of the venturi resulted in enhancement of window performance by a factor of about 3 (i.e., the enhancement of vacuum separation over differential pumping reached a factor of 600). Additionally, the venturi seems to reduce the required plasma arc power level by 25%. Since gas rushing out from a venturi may be objectionable to some users, experiments were performed to reduce axial gas flow with a funnel and by deflection. A combination of the two yielded a factor of 30 reduction in axial pressure.

Motivated by interest and assistance from ATF, the plasma window was also successfully used to provide separation between a high pressure (68 psi) chamber and atmosphere. A laser beam (5 mW with a 543 nm wavelength) was passed from that chamber through the plasma window to atmosphere.

ACCOMPLISHMENTS:

From our results to date we can anticipate several near term applications and longer-term potential areas for further development. Plasma windows can be used to greatly improve the performance of five NSLS beam lines. At U-11 & U-13, two plasma windows can be used for vacua interface to contain an argon gas filter to remove higher order diffracted light from their UV monochromators. With a plasma window at X-1A, microscopy can be greatly improved since absorption (in an inhomogeneous window) is eliminated. Finally, since plasma windows do not have scratches or other structure, spatial coherence effects would no longer be a problem in experiments conducted at X-13 & X-25.

In addition to the obvious benefits to NSLS, ATF and the sciences and technologies they foster, plasma windows can greatly enhance the laboratory capability to conduct research in nuclear and high-energy physics, as well as medical and life sciences. BNCT based

on recirculating proton beams can be realized with two plasma windows on either side of a lithium cell. Plasma windows offer the only viable scheme for maintaining a highly localized, high pressure, lithium vapor cell inside a high-energy proton storage ring. Additionally, high energy and nuclear research, would also benefit from various internal targets, plasma strippers and plasma lenses, e.g., a plasma stripper/lens could enhance the stripping of heavy ions between the Booster and AGS, as well as, between the tandem Van de Graaff and the Booster. A plasma stripper/lens or an internal gas target "sandwiched" between two plasma windows could achieve the desired vacua separation.

Finally, it is worth noting that this work has been accomplished in large part through the efforts of two undergraduate students, who have participated in this project as part of their education. They are Alexander Jeffers (Pamona College) and Chris Castle (California Polytechnic State University at San Luis Obispo).

LDRD FUNDING:

FY 1997	$60,475
FY 1998 (est.)	$60,000

Development of New Techniques in Picosecond Pulse Radiolysis

James F. Wishart *97-29*

PROJECT DESCRIPTION:

The Chemistry Department has constructed a novel, state-of-the-art picosecond 10 MeV electron pulse radiolysis facility based on the same radio-frequency photocathode electron gun technology developed at the BNL Accelerator Test Facility. The new accelerator is the first of its type to be dedicated to the study of radiation chemistry. Similar facilities are planned or proposed at other laboratories, however those facilities will not be ready for two years or more. The facility itself owes its existence to a proposal which resulted from an LDRD project in 1989 (#89-42).

The unique design of this accelerator offers several advantages over other existing accelerators for the study of physical and chemical processes on the picosecond and femtosecond timescale. In particular, the new system includes a picosecond-synchronized femtosecond laser source which can be used to probe radiolytically-generated transients by time-resolved spectroscopy. Even more unique is the ability to do femtosecond excitation of radiolytic transients to probe their excited state physics and chemistry, and to examine the reactions of radicals with excited states. These studies are important for understanding charge recombination processes and radiation damage phenomena, and they will help in trying to comprehend the reactions which occur in heterogeneous, highly energetic and radiation-filled environments such as the Hanford waste tanks.

This project supports one research associate, to assist in the building of time-resolved femto- and picosecond excitation and detection systems which unite the capabilities of pulse radiolysis with flash photolysis, and to use the system to investigate the chemistry of radical species, charge recombination in hydrocarbons, and reactions of highly excited species.

TECHNICAL PROGRESS AND RESULTS - Fiscal Year 1997:

Personnel. Dr. Sergei Lymar received a Senior Research Associate appointment on this project in January 1997. Upon arrival he was encouraged to submit a proposal to the Environmental Management Science Program (EMSP) based on his experience in peroxynitrite chemistry and the capabilities of the new facility. In August he and Dr. Wishart received the only EMSP award at BNL ($700,000 over three years). The proposed EMSP studies will utilize the capabilities of our unique facility, for example the availability of synchronized laser pulses for generation of organic radical species prior to the electron beam arrival and the high penetrating power of the 10 MeV electron beam for studies in high-pressure cells to obtain mechanistic information from activation volumes. Design of experimental equipment specifically for these studies is now in progress.

Accelerator performance. A wealth of experience has been acquired in steering the electron beam to the experimental stations, focusing it on the targets, and minimizing the undesired dark current. Optimal magnet settings have been identified for different experimental requirements. A system for temporal and spatial electron beam diagnostics has been designed and the key component, a customized streak camera, has been ordered. Operation of the laser system has been

improved through the installation of a single-shot autocorrelator for measurements of the amplified infrared pulse and a computer-controlled, remote laser beam steering system.

Construction of the experimental stations. A station for kinetic measurements on the nanosecond and longer timescales has been built. Substantial effort was invested in sample cell development to eliminate RF noise (inherent to the picosecond electron beam itself) so that clean signals can be obtained at the shortest timescales. The first transient conductivity data obtained with the new accelerator (in cooperation with Dr. Holroyd) demonstrated the benefits of the picosecond pulse. Electron capture by benzene in supercritical ethane, a process too fast to be seen with our older equipment, was observed for the first time. The equipment for transient absorption kinetic measurements has been successfully tested. An experimental station for ultrafast pulse-probe pico- and femtosecond detection is being assembled. This station will utilize the precise synchronization of the light and electron pulses which is the most unique capability of our facility.

FOLLOW-ON FUNDING:

As described above, a grant from the DOE Environmental Management Science Program (EMSP), totaling $700,000 over three years, has been awarded to the investigators to study the reactivity of peroxynitrite and related species relevant to Hanford waste tank chemistry using the new pulse radiolysis facility and other techniques.

This represents a new direction and divergent from the current LDRD project for use of the facility because of the new experimental equipment that must be designed and operated in the development of these techniques.

LDRD FUNDING:

FY 1997	$104,103
FY 1998 (est.)	$115,000

X-ray Circular Dichroism of Biological Macromolecules

John C. Sutherland 97-39
Erik D. Johnson
Chi-Chang Kao

PROJECT DESCRIPTION:

Conventional CD–MCD Spectroscopy: Circular dichroism in the ultraviolet, visible and infrared provides information on the structure of DNA, RNA, proteins, polysaccharides, and other molecules of biological interest in solution, hence complementing the structural information obtained from crystallography. Such measurements have been important in molecular biophysics, structural biology, drug design, and related fields for about 30 years. Magnetic circular dichroism in the same region has been used to study the electronic structure of absorbing species, particularly heme- and other metalloproteins. Synchrotron radiation has been the source-of-choice for circular dichroism experiments in the vacuum ultraviolet ($\approx 105 \leq \lambda \leq \approx 190$ nm) since 1980, but the technology used in these experiments **cannot** be extended to shorter wavelengths.

X-Ray CD/MCD with Synchrotron Radiation: Interest in using circularly polarized x-rays generated by synchrotrons to measure CD extends back to the mid 1970's, however, usable beamlines are just becoming available. The most sensitive experimental arrangement presently in sight involves an elliptically polarizing wiggler that can switch between producing left- and right elliptically polarized x-rays at a frequency > 1 Hz. Such a device has been installed on beamline X13 at the NSLS, and preliminary testing has been performed. We recently obtained funds for a new monochromator to serve the elliptically polarizing wiggler on X-13 as part of the DOE facilities initiative. While other synchrotron sources are developing circular dichroism capabilities, there is a window-of-opportunity for BNL to begin a program leading to an x-ray CD/MCD research program and structural biology user facility at the NSLS.

We are testing the hypothesis that large circular dichroism signals occur when the wavelength of the circularly polarized light matches the pitch of the helix of a polymer such as DNA, RNA or proteins. Thus, unlike conventional circular dichroism, molecules containing different types of helical secondary structures with different pitches should also give maximal signals at different wavelengths, and the sign of the x-ray CD may indicate directly the handedness of the helix of the biopolymer. In collaboration with SUNY-Binghamton, we will extend these observations to polysaccharides. In collaboration with University of Southern California, we will explore the MCD of the L-edge absorptions of metals in the active sites of metalloproteins. Such studies will be particularly important for proteins containing metals such as zinc, whose complexes do not absorb in the visible or near infrared and hence have not been subjected to analysis by conventional MCD. We shall also work with Florida Atlantic University in studies of x-ray MCD of atoms and CD/MCD of small molecules in the vapor phase. These experiments will improve our understanding of the fundamental mechanisms of x-ray CD and MCD and develop a strong user base, hence increasing the probability of obtaining extramural support.

TECHNICAL PROGRESS AND RESULTS – Fiscal Year 1997:

Purpose: Circular dichroism (CD) is the difference between the absorption of left- and right-circularly polarized light, or more generally "electromagnetic radiation." Following the introduction of sensitive scanning dichromators in the early 1960's, CD in the visible and ultraviolet ($\approx 200 \leq \lambda \leq \approx 800$ nm) became a widely used method for studying the conformation of biopolymers in solution, in additional to many other uses in chemistry and biology. CD is observed only when the absorbing species lacks a center of symmetry, which can either be inherent, such as in a steroid molecule, or induced, such as that resulting from the dipole coupling among the helically stacked bases of DNA and RNA, or the amide bonds linking the amino acids in an α-helical structure of a peptide or protein. In the UV-visible region, the wavelength of the light is much greater than the pitch of the helical structures typical of biological macromolecules, and the CD anisotropy (the ratio of the difference in the absorption of left- and right circularly polarized beams to the average value) is small, typically $< 10^{-3}$. The conventional CD spectra of different biopolymers frequently overlap in wavelength, hence limiting the utility of CD in studies of complex bimolecular systems such as protein-DNA complexes. X-ray CD may overcome this limitation.

The extension of CD spectroscopy into the x-ray region has been discussed over the past two decades, but experimental facilities are just becoming available. All of the proposals for measuring x-ray CD involve some form of synchrotron radiation.

A speculative, but fascinating, possibility is that molecules with helical symmetries will show large circular absorption or scattering anisotropies for wavelengths congruent with helical pitch. The observation of circular dichroism requires absorption of the radiation by the components of the helix, but circular differential scattering does not. For the A and B conformations of DNA, there will be strong absorption by carbon for wavelengths corresponding to the helical pitch, while for the Z form of DNA, there will be absorption due to the L edge of phosphorous. Presumably, and in contrast to the circular dichroism in the ultraviolet, visible and infrared, the sign of the circular dichroism should reflect the absolute chirality of the molecule. Another possible advantage of x-ray circular dichroism is that the signals associated with different conformations may be separated in wavelength. In the case of DNA, this would be in complete contrast to the overlapping spectra of the B and Z forms in the ultraviolet, vacuum ultraviolet, and infrared. Spectral separation would facilitate the determination of the net secondary structure of molecules containing more than one type of helix, *e.g.*, complexes containing B form DNA, RNA, and proteins. Though speculative, the potential advantages of circular dichroism using x-rays justify exploratory investigations, particularly as much of the required instrumentation is already available. Our immediate interests are in elucidation of the structures of protein-DNA complexes, but the range of applications of x-ray circular dichroism will be as varied as that of circular dichroism in the ultraviolet and visible.

Approach: An ellipsodially polarizing wiggler capable of producing x-rays of alternating elliptical polarization has been installed in on the x-rays ring on the NSLS on the straight section connected to beamline X13. A beamline for hard x-rays is available, but a vacuum beamline suitable for the more biologically interesting range was not available.

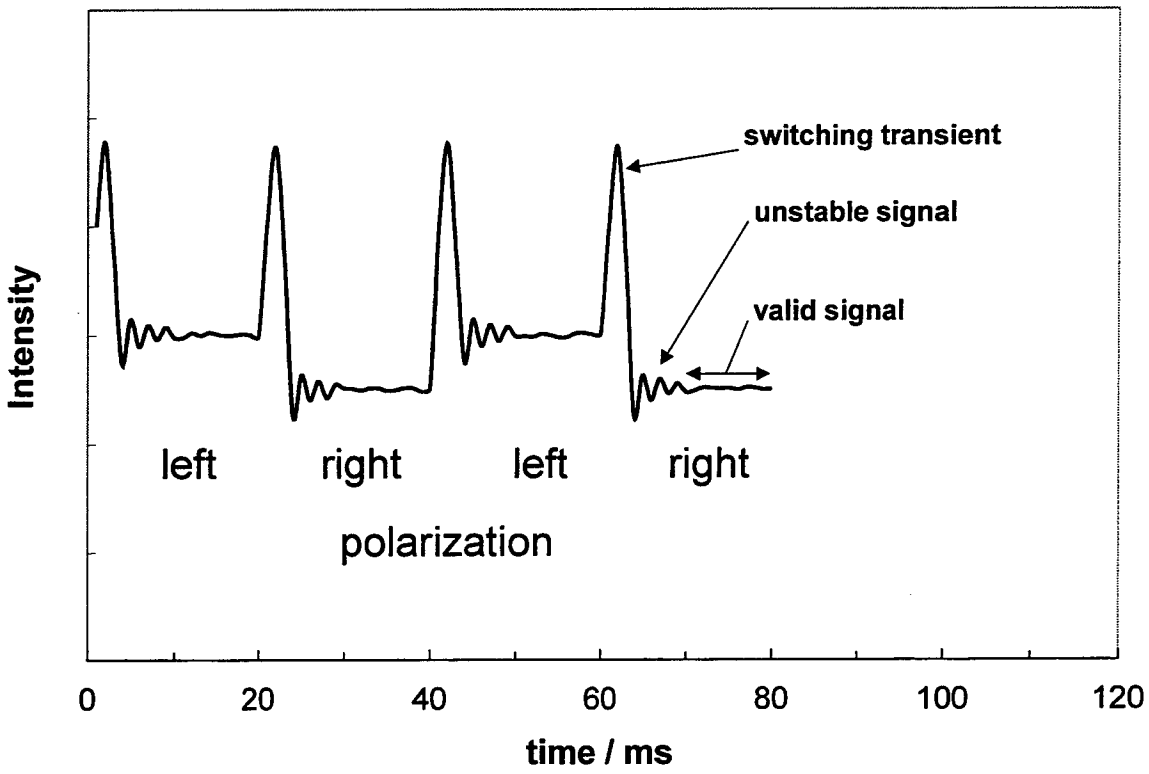

Figure 1 Schematic diagram showing the waveform generated by the beam from the elliptically polarizing wiggler that has been amplitude modulated by a sample that exhibits circular dichroism. The wiggler is shown operating at a frequency of 25 Hz, and hence a period of 40 ms. During each cycle, the polarization shifts from left to right and back to left, so there are two transient spikes per period; the first for the left-to-right transition and the second for the right-to-left transition. The transition spike is followed by a period of instability while the beams "settles." Circular dichroism is the difference between the absorption of left- and right-circularly polarized light. It is found by dividing the difference in intensity (for the stable data) for the two polarization states by their average value. The differences in intensity for the two polarization states shown in this Figure are greatly exaggerated compared to the differences that are detectable using our new "lock-in" method.

Funds for a suitable ultrahigh vacuum monochromator and other required components for use on this beamline were obtained from the 1996 synchrotron facility initiative. This beamline is designed to work in the spectral region from ≈ 300 eV (≈ 4.1 nm) to ≈ 900 eV (≈ 1.38 nm), which spans the range of the pitches of the helices of the various forms of DNA and RNA.

An important property of the intensity of the x-rays produced by the ellipsodially polarizing wiggler is that there is a large intensity spike produced during the transition between the two

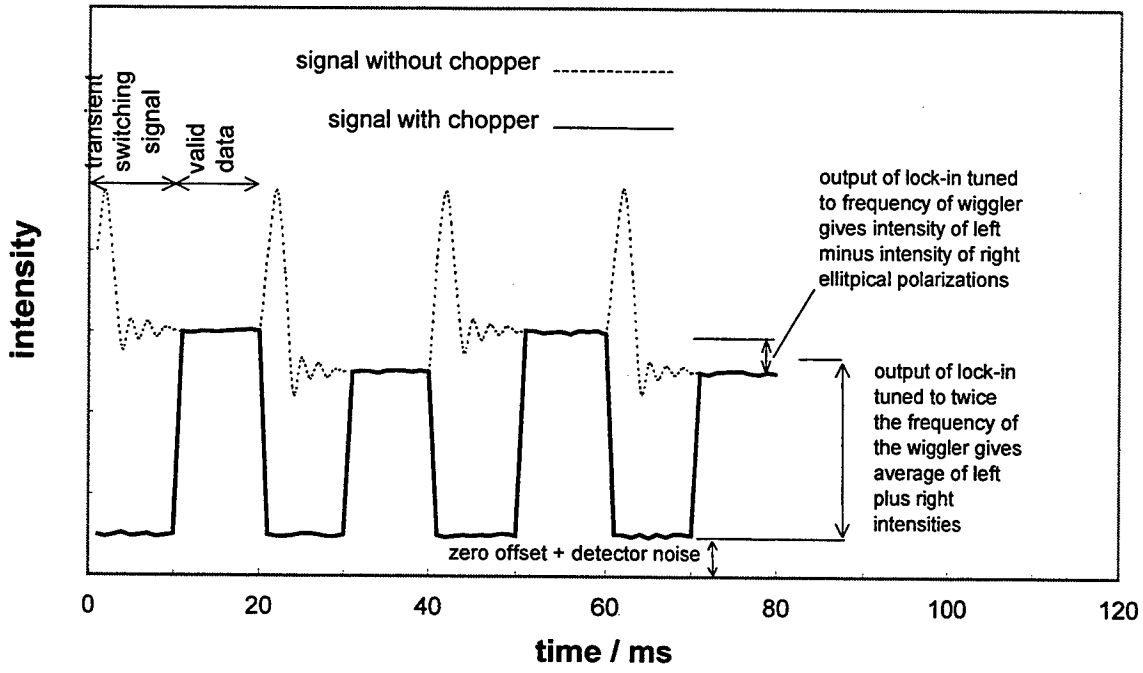

Figure 2 The waveform of the beam from the elliptically polarizing wiggler modulated by circular dichroism showing the effect of the beam "chopper" blocking the switching transients. The frequency of the open-closed cycle of the chopper is twice that of the wiggler. In our new method for detecting x-ray circular dichroism, a lock-in amplifier tuned to the frequency of the wiggler produces a signal proportional to the difference in intensity of the left- and right-intensities, while a second lock-in amplifier tuned to the frequency of the chopper (*i.e.*, twice the frequency of the wiggler) gives a signal proportional to the average value of the left- and right-intensities. The circular dichroism is the negative of the ratio of these signals. Note that the output of the 2f lock-in automatically corrects for any zero-offset or "dark signal," which is not the case when the selection of the polarization signals is done with simple digital gating

elliptically polarized states, as shown schematically in Figure 1. This results because the elliptically polarized light is obtained by alternately viewing the top- and bottom of the orbit of the circulating electron beam. Steering electromagnets tip the electrons alternately up and down as they pass through the alternating magnetic fields of the permanent (vertical) magnets of the ellipsodially polarizing wiggler. The intensity of the synchrotron radiation is greatest when the electrons are viewed head-on, and this happens mid way between the switch from top-to-bottom, and also from bottom-to-top viewing That is, the frequency of the intensity spikes is twice the frequency of the polarization switching of the polarization. In addition, there is a period of instability of the x-ray beam following each transition, as shown in Figure 1. In order to achieve maximum sensitivity in a circular dichroism

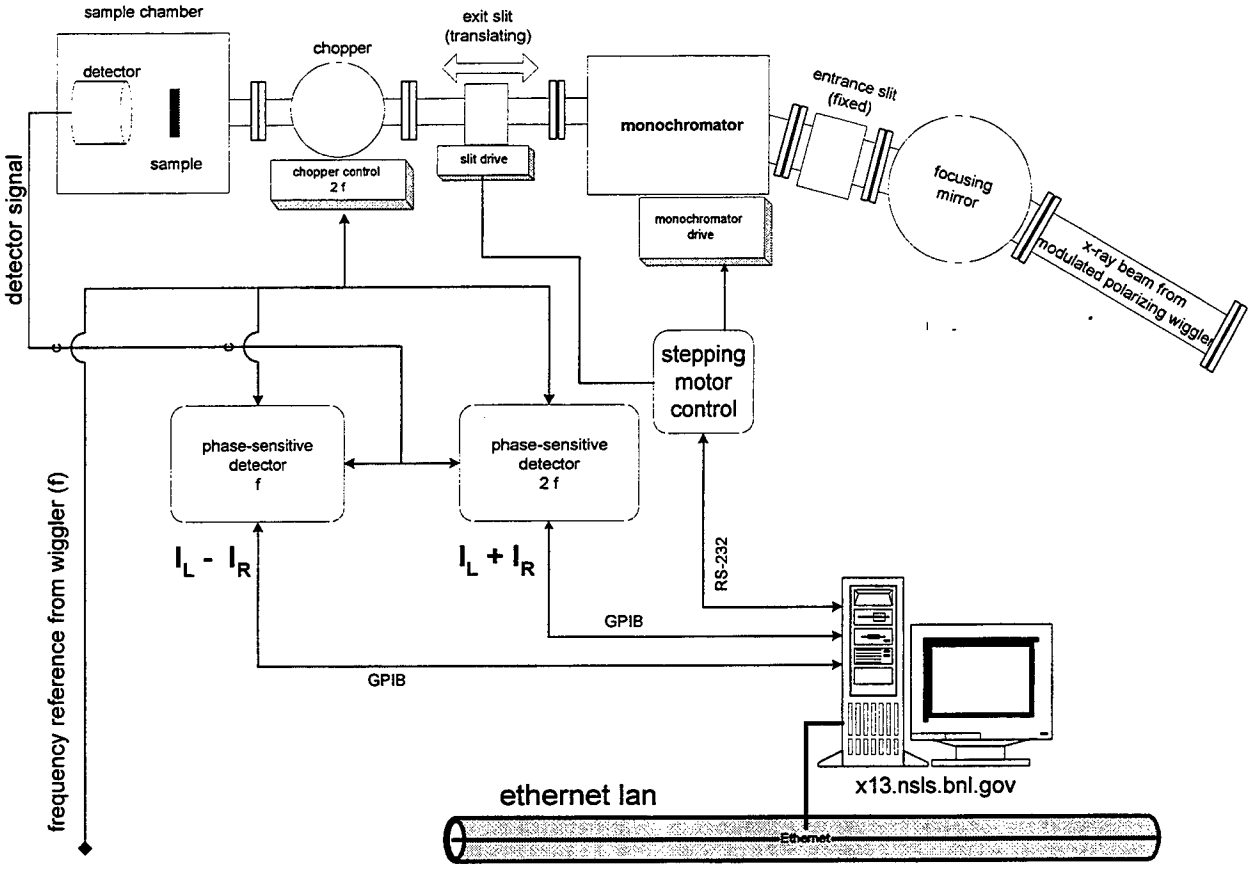

Figure 3 Schematic diagram of beamline X13A at the National Synchrotron Light Source showing the location of the mechanical chopper and the logical flow of data for the extraction of the circular dichroism signal The chopper is phase locked to twice the frequency of the ellipsodially polarizing wiggler so as to mask the switching transients as shown in the Figure. The output of the detector is applied to two lock-in amplifiers. One is tuned to the frequency and phase of the ellipsodially polarizing wiggler, and records the difference between the intensities of left and right circularly polarized light, $I_L - I_R$. The other lock-in amplifier, like the chopper, is tuned to twice the frequency of the ellipsodially polarizing wiggler.

experiment, we need to detect many-many photons, and hence analog detection is preferable to single photon counting. However, the switching transients interfere with analog signals, and cannot be easily gated out as can the pulses resulting from a photon counting experiment. Thus, we designed a system in which a rotating sector blade (a "chopper") blocks the switching spike and resulting period of unstable beam, as illustrated in Figure 2. This requires proper choice of the frequency of the ellipsodially polarizing wiggler and also that the chopper can be locked in both phase and frequency to the wiggler.

Technical Progress and Results: In view of the design considerations outlined above, we developed a new design for the signal processing electronics for use in the measurement of x-ray circular dichroism. This new method, which we call **Double Synchronous Detection of X-Ray Circular Dichroism**, is diagrammed schematically in Figure 3. Circular dichroism is proportional to the ratio of $(I_L-I_R)/(I_L-I_R)$, and these two signals are extracted by two phase-sensitive detectors ("lock-in" amplifiers) tuned to frequency f and 2f respectively, where f is the frequency at which the ellipsodially polarizing wiggler is operating.

As of 30 September 1997, all major components (entrance slit, monochromator body, exit slit, sample chamber, and mechanical "chopper" and its UHV housing, most signal processing electronics, and the beamline control and acquisition computer) are at the NSLS being assembled to become beamline X13A. In addition, the LDRD project has:

- Purchased, installed, and tested a beam "chopper," adapted it for x-ray and vacuum operation and installed it in a UHV chamber that will be inserted in the beamline between the monochromator and the sample chamber. (The chopper is critical for the high sensitivity "lock-in" method we have developed for measuring x-ray circular dichroism. Its function is discussed in greater detail below).
- Programmed the beamline computer to control the wavelength drive of the monochromator.
- Obtained access to signals from the elliptically polarizing wiggler phase reference signal and x-ray ring current signal which are required to measure x-ray circular dichroism.
- Obtained and tested the electronic components (lock-in amplifier and ratio circuit) required to measure x-ray circular dichroism.†

Thus all of the major components of X13A are at present. Readying the beamline for experimental studies requires:

- Completion of the alignment of the optical elements and assembly and testing of the vacuum chambers.
- Development of software to control the motion of the monochromator exit slit, which must be translated in synchrony with the scanning of the wavelength drive of the monochromator to maintain focus on the exit slit, and hence spectral resolution.
- Writing software to acquire x-ray circular dichroism data from the analog signal processing electronics and display, store and analyze these data. These programs are generally similar to those that we use on U9 and U11 for UV circular dichroism data but will be written to run under the more robust NT operating system.
- Acquisition of a second lock-in and other electronic components for permanent installation at X13A.
- The testing and trouble shooting inherent in the commissioning of a new beamline.

In parallel with the construction of beamline X13A, as noted above, we have developed a new, high sensitivity method for measuring x-ray circular dichroism with an elliptically polarizing wiggler. When this LDRD began, the NSLS elliptically polarizing wiggler had only been tested at 2 Hz, a frequency too low for optimum use of lock-in detection. We found that the

† A second permanent lock-in is required for the final design.

maximum switching frequency of the NSLS elliptically polarizing wiggler, which is 100 Hz, is unusable because the last switching transient has not died out before the next switch starts – *i.e.* the duty cycle for usable beam is zero. In our method for measuring circular dichroism with the elliptically polarizing wiggler, the optimum frequency for switching polarizations is the highest frequency that gives a duty cycle of usable beam of 50%, as explained in Figure 2. We found that for the NSLS elliptically polarizing wiggler, this optimum frequency is about 25 Hz, corresponding to a period of 40 ms. (The exact frequency is adjusted slightly to avoid interference from peaks in the noise spectrum of the x-ray ring signal.) This is the frequency/period illustrated in Figures 1 and 2. Note that the experiments to determine the operating frequency of the elliptically polarizing wiggler can only be conducted during times reserved for "studies" on the x-ray ring to prevent interference with the operation of other beamlines. Hence these experiments were painfully slow.

Our method for "lock-in" measurement of circular dichroism with the elliptically polarizing wiggler is shown in Figure 2. A rotating sector "chopper" operating at exactly twice the frequency of the wiggler blocks the switching transients and permits only valid data to reach the detector. The requirements for this chopper are unusual in that it must be locked in both frequency and phase to the switching of the wiggler. (Choppers are widely used in optical experiments, but in such applications it is the chopper that determines the frequency and phase and to which other components are referenced). A suitable device was identified and purchased, but thicker blades were fabricated to our specifications to insure that the x-ray beam was completely blocked. Additional modifications have been made to permit this chopper to operate in the evacuated X13A beamline.

Using both photon-counting techniques[‡] (where we selected the valid signal by electronic gating using a four-phase delay circuit previously employed in my laboratory for the simultaneous detection of fluorescence and phosphorescence), and the "lock-in" method described above, we measured the known magnetic field circular dichroism of Ni and Fe samples, hence validating the method.

To summarize our progress in the measurement of x-ray circular dichroism on beamline X13B:

- A method for high-sensitivity circular dichroism measurements using a two-lock-in technique was invented.
- The optimum (≈ 50% duty cycle) frequency for operation of the elliptically polarizing wiggler at the NSLS was determined to be ≈ 25 Hz.
- A rotating sector "chopper" that can be slaved to the frequency and phase of the elliptically polarizing wiggler was obtained and modified for use with x-rays. The chopper has been further modified for vacuum operation and moved to beamline X13A.
- Using films of Fe and Ni oriented by an external magnetic field as a test system, x-ray circular dichroism was measured.
- At both 2 and 25 Hz, the signal due to left and right elliptically polarized x-rays were separated by digital gating using a

[‡] While the extraction of circular dichroism by single-photon counting is easier to implement, restrictions on the maximum counting rate limit the precision to which data on each polarized absorption can be obtained, and hence the sensitivity of the circular dichroism experiment. The four-phase delay and gated counters we used in the initial measurements of large circular dichroism signals are available should they be needed.

four-phase gating circuit and gated counters.

- At 25 Hz, the test circular dichroism signals were detected both by single-photon counting and the more sensitive "lock-in" method. On the large signals presented by the Fe and Ni test samples, similar results were obtained with the two methods.

PAPERS/JOURNALS/PUBLICATIONS:

J. C. Sutherland, K. Polewski, D. C. Monteleone, J. G. Trunk, C.-C. Kao, and E. D. Johnson, "Soft X-ray circular dichroism using a modulated elliptically polarizing wiggler at the National Synchrotron Light Source," in *Advances in Optical Biophysics*, edited by J. Lakowicz and J.B.M. Ross (SPIE, 1998), (in press).

LDRD FUNDING:

FY 1997	$ 94,131
FY 1998 (est.)	$107,000

X-Ray Schlieren Computed Tomography

F. A. Dilmanian 97-44
L. D. Chapman
B. A. Dowd
D. P. Siddons
W. C. Thomlinson

PROJECT DESCRIPTION:

Ten (10%) to fifteen (15%) percent of clinically obvious breast cancers are not visible with conventional mammography [1]. Principally because the image contrast in conventional mammography is given by the x-ray attenuation of tissue, which varies only slightly from one tissue type to another. A new method of mammography was developed at the National Synchrotron Light Source in 1996, using monochromatic x-ray beams. The work was carried out within a wide collaboration that included BNL, the University of North Carolina and Carolina State University. The method originally was called X-ray Schlieren Imaging (XSI) [2]. The goal of the present proposal was to study the characteristics of X-ray Schlieren Imaging in the computed tomography (CT) mode. The basic method was later renamed to Diffraction Enhanced Imaging (DEI) [3]. This name change followed new experiments that were carried out in the past year at the NSLS, at the Advanced Photon Source (APS), Argonne National Laboratory (ANL), and at the European Synchrotron Research Facility (ESRF). A better understanding of the basic underlying physical phenomena seen in the images was obtained through this research [3].

The technique uses a perfect-crystal x-ray monochromator and an analyzer crystal positioned between the subject and the detector. This non-dispersive x-ray optic reflects the beam (and, therefore, produces a detector signal) at a constant yield only for a beam the angle of which has not been deflected by the subject. X-rays deviating in angle in the subject, either through the small-angle scattering mechanism or under the influence of the out-of-plane gradient of the x-ray index of refraction, land on an altered position on the reflection curve ("rocking curve") of the analyzer's crystal. The typical width of a narrow rocking curve (such as Si <333>) is about 3 μradian full-width-at-half-maximum (FWHM). The resulting modulation in the yield of the analyzer in turn modulates the image's gray scale, which is the basis for a new image contrast between two different tissue types. In other words, the monochromator-analyzer combination provides a detector signal that strongly depends on small variations (0.1 μradian) in the angle of x-rays being transmitted through the subject. This angular-dependence of the signal gives new, tissue-specific imaging information that is not available in conventional mammography. The information comes from two distinct interactions of x-rays with tissue : a) small-angle-scattering effect, which deflects x-ray photons out of their original direction, and b) out-of-plane gradient of x-ray index of refraction, which also deflects x-ray photons out of their original direction. The angular deflections of the x-ray photon in both these cases are extremely small, but they alter a photon's probability of detection. Hereafter, the former effect is called the "extinction effect" [3], and the latter is called "index-of-refraction effect"[2,3]. The extinction effect may vary much more strongly than the attenuation coefficient from one tissue type to another, leading to a tissue-dependent image contrast much larger than that in conventional mammography images; the index-of-refraction effect shows very sharp edges at the boundaries of different tissue

types, acting as a method of natural edge-enhancement method. Both effects are expected to have diagnostic value, as demonstrated in experiments with anatomical specimens [3].

The specific goal of this LDRD was to implement DEI in the tomography mode, and to comprehensively study DEI's tissue characterization by carrying out experiments with anatomical specimens and live animals. This tissue characterization cannot be done accurately in the radiography (planar-imaging) mode because of the effect of overlying tissues. DEI CT will give to DEI the same geometric-separation advantage that conventional CT gives to planar radiography. The subject will be rotated around a vertical axis.

The statement of the work for the present LDRD was changed slightly from our original plan as a result of the following events. First, the start of the program was postponed from October 1, 1996 to April 1, 1997, because we could not identify a suitably experienced postdoctoral research associate. At about the same time, around October 1, 1996, the beamline X27C, which we planned to use for most of this work, became unavailable to us, and is still so. Another beamline, X15A, will become available for this work in November 1997. Therefore, the statement of the work was changed to reflect the shifting of the work to X15A. However, the delay has worked to our advantage, as it allowed the group to study more thoroughly the basic underlying effects of the technique [3]. The measurements were carried out at the APS and ESRF. The new studies shed light on the small-angle scattering effect, and allowed us to separate this effect from the index-of-refraction effect. In particular, these studies showed that DEI of a standard mammography phantom with a tumor simulation has a 27-fold larger image contrast than a regular radiograph with a monochromatic beam. The radiation absorbed dose to the subject was less than 100 mrem, which is similar to the doses used in clinical mammography. The following is our revised statement of work.

a. To develop a computed tomography (CT) system for DEI at X15A
   The emphasis will be on the development of the monochromator/analyzer system. The monochromator will be a Bragg-Bragg device, while the analyzer will be a Laue crystal (see details below). The detector and the data acquisition system (DAS) will be borrowed from the Multiple Energy Computed Tomography (MECT) program [4].

b. To develop the basic algorithms for reconstructing DEI CT
   The CT projection data acquired at two or more data points over the entire width of the rocking-curve angles, and will be processed to produce at least three tomographic images: pure attenuation image, x-ray extinction image, and index-of-refraction image.

c. To undertake a comprehensive set of tissue-characterization studies
   Anatomical specimens, as well as normal rats and rats with 9L gliosarcoma brain and subcutaneous tumors will be studied. The studies will also include iodine contrast imaging, particularly around the I K-edge.

TECHNICAL PROGRESS AND RESULTS - Fiscal Year 1997:

Purpose: The objectives of this program are to develop a DEI CT system and to use it for quantitative characterization of several tissue

types *in vitro* (anatomical specimens) and *in vivo* (live animals). The following outlines the tasks in detail.

A. The following components of the DEI CT system will be modified or developed:

1. A Bragg-Bragg monochromator with 12 cm crystal width, using Si<333> (the existing system may be used as it is, or may be modified). An asymmetric CT scan with a 12 cm-wide beam will allow the imaging of subjects close to 20 cm in diameter.
2. A Laue analyzer crystal, and its tangent-arm positioning system.
3. An integral mechanical stand for both monochromator and analyzer.

B. The following components of the DEI CT system will be borrowed from the MECT program at X17B2:

1. A subject-positioning system for rats.
2. A modular CT detector with 0.9 mm element spacing. Images with a spatial resolution better that 0.9 mm can be obtained by slitting the detector to ½ or ¼ of the actual element-spacing of the detector, and using it in conjunction with a data acquisition method that employs sequential imaging with lateral shifts of the subject apparatus between different collections.
3. The data acquisition system.

C. The following image-reconstruction algorithms will be developed (producing three or four CT images from each set of data with Laue analyzer):

1. The apparent attenuation effect (i.e., simple transmission in the Laue analyzer) will be handled as in regular CT.
2. The effects of the two or three other parameters, i.e., the extinction coefficient, maybe the associated "radius of gyration"[3], and the "index of refraction" will be handled linearly, and then reconstructed.

D. The following tissue-characterization studies will be included:

1. Imaging anatomical specimens, including different tumor tissues.
2. Imaging normal live rats.
3. Imaging rats bearing intracerebral or subcutaneous 9L gliosarcoma tumors.

Approach:

a. Monochromator development

The monochromator will be a two-crystal Bragg-Bragg device. We will first use the system, developed earlier at the NSLS for planar DEI, as it is, and modify it later for additional requirements of the CT work. The analyzer, a flat Laue crystal, and the tangent-arm mechanical system that aligns it and unites it with the monochromator will be ready in early 1998 (the tangent-arm system will be fabricated in 1997). An Si<333> reflection will be used instead of Si<111> because it has much a narrower rocking curve, which is needed for angular sensitivity. The maximum beam width will be 12 cm, the maximum beam height will be 2 mm, and the energy range will be 20-50 keV.

b. Routine development

Two sets of CT projection data will be acquired, with the analyzer tuned at opposite sides of the rocking curve. The data then are combined to produce a three sets of CT projections for pure attenuation, extinction effect, and index-of-refraction effect. Routines appearing in References 3. will be used, and others will be developed. The extinction effect may be further processed to provide two separate images. CT reconstructions routines will be specially developed. In contrast to transmission CT in which the projections are

related to the logarithm of the signal, we note that, the projections in DEI CT (except those for pure attenuation) are linearly related to the different DEI image signals. Linearity stems from the fact that the rocking curve is a triangle to the first approximation, i.e., its two sides are straight lines; this produces a linear relationship between the angle on the x-axis and the yield on the y-axis.

c. System evaluation and tissue-characterization measurements

The system's general performance (i.e., spatial and contrast resolution, image noise, and contrast linearity) will be studied with standard and specialized phantoms, while the system's capability for tissue characterization will be studied with anatomical specimens, as well as normal rats and rats with 9L gliosarcoma tumors. Contrast imaging with iodine will also be explored. Three types of anatomical specimens will be used, those relevant to breast cancer, those relevant to normal tissue types, and those related to atherosclerotic plaques. Samples for the latter will be obtained from the clinical collaborators of the MECT program at SUNY Stony Brook. Rats bearing 9L gliosarcoma tumors, intracerebral or subcutaneous, will be inoculated at the BNL Medical Department. The work with the brain-tumor rats will include iodine-contrast imaging; in particular, images from near the iodine K-edge are expected to produce enhanced signals. Here, two factors affect the DEI images (i) the absorption differences above and below the absorption edge, and (ii) the large increase in the refractive index at the K edge.

Technical Progress and Results: The mounts for crystals and the components for the tangent arm for positioning the analyzer are being procured. In preparation for the start of the experimental program, at X15A (in place of X27C) the beamline is undergoing a significant upgrade. The X15A beamline became available in September 1997 for 50% of its operating time for white beam use (ideal for this program). Its present status is as follows: a new beryllium window is on order; the surface Standing Wave Apparatus belonging to Argonne National Laboratory has been repositioned in the experimental hutch; experimental hardware for the DEI and CT experiments is being assembled at the NSLS after being used in September at the APS; commissioning plans are being prepared in collaboration with the NSLS for the upgraded beamline to assure that it can operate at the higher energy of 2.8 GeV planned for next year (currently, operates at 2.5 GeV).

With these developments, we anticipate that the first experiments in X15A will be carried out in November 1997. By January 1998, about 10% of operating time will be dedicated to the DEI CT experiments funded by this LDRD. The time on the beamline will be shared by the CT program with the DEI work, the Argonne Surface Standing Wave experiments, and other NSLS and General User programs.

To proceed with the detailed planning and execution of the DEI CT experiments, we deemed it essential to understand the fundamental physics of the DEI process, as well as obtaining the use of, and modifying, X15A. The experiments which have allowed the detailed planning of the CT experiments were carried out in May and September at the APS at Argonne, and at the ESRF, Grenoble, France. Basically, these experiments were designed to accomplish the following:

a) develop the DEI imaging hardware to almost eliminate vibrations of the sample, monochromator and analyzer. This was a problem in the early experiments. By successfully reducing these effects to a

tolerable level, we now know the limits of resolution and stability that must be incorporated into the CT apparatus. The key was learning how to rigidly tie together the monochromator and analyzer, while still retaining the full motion of the sample and detector (image plate in these experiments). The result has been that the analyzer can be held stable to about 0.1 μradian, which is sufficient for DEI at energies as high as 30 keV.

b) fully develop quantitative calculations of the small-angle-scattering strengths, and compare them with the measured apparent absorption. This was achieved at 18 and 30 keV, and provides confidence in our understanding of the basic physics of the process. We can now begin the detailed development of the reconstruction algorithms for the CT images, as opposed to the planar imaging of DEI. Detailed understanding of the American College of Radiology phantoms and of human breast tissues (with tumor) has been accomplished, and images of refraction, absorption, and apparent absorption made. The results have clearly demonstrated dramatic improvements in image information, which should be present in the CT images.

c) demonstrate that the index of refraction and DEI images are independent of energy. Normal absorption coefficient and its atomic-number dependence rapidly decrease as the energy is increased, thereby reducing the conventional contrast. But the absorbed dose also will decrease. Thus, if the image information is constant (and greater than conventional absorption) at higher energies and at lower doses, then DEI will have significant advantages over the conventional imaging. In fact, the experiments confirm these expectations. DEI CT also should show the same dose/contrast advantages. We are confident that the experiment can be designed for higher energies for imaging of tissues and bones in anatomical specimens and in live animals.

PAPERS/JOURNALS/PUBLICATIONS:

Reference 3, below, describes work that was carried out after starting this program.

References:

1. Baker, L.H. Breast cancer detection demonstration project: five-year summary report. CA 32(4), 194-225, 1982.

2. Chapman, D., Thomlinson, W., Arfelli, F., Gmür, N., Zhong, Z., Menk, R., Johnston, R.E., Washburn, D., Pisano, E., and Sayers, D. Mammography imaging studies using a Laue crystal analyzer. Rev. Sci. Instrum. 67(9): CD-ROM, 1996.

3. Chapman D., Thomlinson, W., Johnston, R.E., Washburn, D., Pisano, E., Gmür, N., Zhong, Z., Menk, R., Arfelli, F. and Sayers D. Diffraction enhanced x-ray imaging. Phys. Med. Biol. (In press, Oct./Nov. 1997 issue).

4. Dilmanian, F.A., Wu, X.Y., Parsons, E.C., Ren, B., Kress, J., Button, T.M., Chapman, L.D., Coderre, J.A., Giron, F., Greenberg, D., Krus, D.J., Liang, Z., Marcovici, S., Petersen, M.J., Roque, C.T., Shleifer, M., Slatkin, D.N., Thomlinson, W.C., Yamamoto, K., and Z. Zhong. Single- and Dual-energy CT with monochromatic synchrotron x rays. Phys. Med. Biol. 42, 371-387, 1997.

LDRD FUNDING:

FY 1997	$59,792
FY 1998 (est.)	$97,000
FY 1999 (est.)	$44,000

Note: This project involves animal vertebrates or human subjects.

Biodistribution, Toxicity and Boron Neutron-Capture Therapy in Animals Using Metallotetracarboranyl-porphyrins

Michiko Miura *97-45*

PROJECT DESCRIPTION:

Statement of work:

1. To determine whether therapeutic tumor boron concentrations (>40 μg B/g) are achievable from boronated porphyrins in rats bearing 9L gliosarcomas as was shown in mice bearing mammary tumors. High tumor values should be attained with high tumor:blood and tumor:brain boron concentration ratios (each >5:1) and with minimal toxicity to improve boron neutron-capture therapy [BNCT].

2. To determine whether efficacy is possible by porphyrin-mediated BNCT using mice bearing leg tumors and rats bearing intracranial tumors using the optimal conditions determined in statement 1.

3. To determine whether imaging is feasible using single-photon-emission tomography [SPECT] of a copper-67 porphyrin or magnetic resonance imaging [MRI] of a manganese or gadolinium porphyrin.

4. To continue to synthesize boronated porphyrins, including analogues of NiTCP, and other boron-containing compounds and to continue to test them for their biodistribution and toxicity properties in tumor-bearing mice.

TECHNICAL PROGRESS AND RESULTS - Fiscal Year 1997:

Purpose: *p*-Boronophenylalanine [BPA] is currently being used as the ^{10}B carrier in BNCT clinical trials for the palliative treatment of malignant brain tumors (glioblastoma multiforme) at the Brookhaven National Laboratory Medical Department. Although there is no toxicity associated with BPA, the normal brain and blood accumulate about one-fourth the amount of boron found in tumor, which could potentially limit the tumor dose. The treatment window for neutron-irradiation is only one to two hours after infusion since BPA clears out of tumor rapidly. A residence time in tumor of days would permit efficient fractionation of BNCT without reinfusion of compound. Borocaptate sodium [BSH], a sulfydryl boron hydride cage compound is being used in Japan and is being planned for use in Europe for BNCT. However, its tumor:normal tissue ratios are less than 2:1, with similar pharmacokinetics to BPA. Therefore, the purpose of our work is to synthesize and test new compounds that could improve upon the efficacy of BPA- and BSH-based BNCT.

Background: BNCT is based on the production of high linear-energy-transfer ionizing radiation from the $^{10}B(n,^{4}He)^{7}Li$ reaction. It is therefore important that ^{10}B exist mainly in tumor tissue within the irradiation volume so that only tumor cells and their vasculature are selectively destroyed. For brain tumors, the critical tissues are blood and normal brain.

We have synthesized a series of carborane-containing porphyrins and tested them for biodistribution and toxicity in BALB/c mice bearing KHJJ mammary carcinomas. One porphyrin in particular, NiTCP (Figure 1), has been shown to be

nontoxic to mice at doses that delivered 40-50 μg B/g to tumor tissue with a tumor:blood boron concentration ratio >100:1 and tumor:brain boron concentration ratio >5:1. When the copper analogue, CuTCP, was given to rats at less than half the total dose given to mice, by intravenous [iv] infusion, 20-40 μg B/g was found in tumor with similar boron concentrations ratios to blood and brain and with little or no toxicity.

The lack of toxicity in these porphyrins was novel, since large total doses (>200 μg/g body weight) are required for BNCT. In contrast, photodynamic therapy [PDT], only requires <2 μg/g body weight of similar porphyrin or porphyrin-like compounds. PDT is another bimodal cancer treatment that involves administration of photosensitizers, e.g., porphyrins, to seek tumors, followed by visible light irradiation for production of cell-killing hydroxy radical and singlet oxygen species.

The distribution of BPA or BSH in all tissues within the neutron-irradiation volume is not entirely known. A compound that is imageable by SPECT or MRI would be advantageous for BNCT treatment planning so that boron concentrations can be determined in all critical tissues. Porphyrins have the ability to chelate a variety of metals. Copper is of particular interest as there exists a SPECT-imageable isotope, ^{67}Cu, and copper porphyrins are not expected to cause photodynamic side-effects in skin from ambient light as are other metalloporphyrins.

Objectives: The long-term objectives are to improve current BPA- and BSH-based BNCT by supplementing or replacing BPA (or BSH) with another boron-containing compound that has higher tumor:normal tissue boron concentration ratios so that higher tumor doses can be delivered. If the boron carrier can be imaged by SPECT or MRI, then boron concentrations in all tissues within the treatment volume can be estimated.

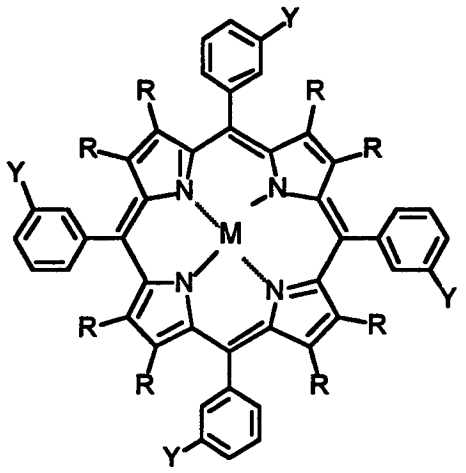

R = $CH_2CO_2CH_3$

Y =

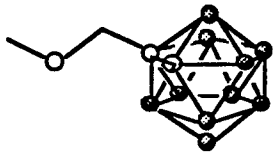

NiTCP, M = Ni

CuTCP, M = Cu

MnTCP, M = Mn(OAc)

Figure 1. Structures of tetraphenylcarborane-containing metalloporphyrins.

Approach: New carborane-containing porphyrins including analogues of NiTCP will be synthesized and tested in mice for biodistribution and toxicity. Toxicity determination is based on comparison with a control group of mice given solvent vehicle only. The observed parameters include: behavior, appearance, weight changes, and hematological, chemical, and enzymatic analyses of blood. In some experiments, histological examination of coded hematoxylin/eosin-stained liver sections are carried out. Boron concentrations are

determined by direct-current plasma atomic absorption spectroscopy [DCP-AES] and prompt-gamma spectroscopy.

Compound administration will be optimized for maximal tumor uptake with high tumor:blood and tumor:brain boron concentration ratios and minimal toxicity. The most promising candidates will be tested in mice bearing leg tumors for BNCT studies using ^{10}B-enriched compounds.

The same promising compounds will be given to rats bearing multiple subcutaneous 9L gliosarcomas for biodistribution and toxicity studies. When tumor and blood boron concentrations are optimized, BNCT will be carried out on rats bearing intracranial tumors.

MRI studies on rats using manganese derivatives and SPECT studies using copper derivatives will be carried out to determine whether imaging is feasible using these techniques.

Technical Progress & Results: CuTCP was given to Fisher rats bearing subcutaneous 9L gliosarcomas by intravenous [iv] infusion. Compared with intraperitoneal [ip] injection volumes, volumes that can be infused iv are much smaller. Although volumes of 0.095 mL/g body weight have been used, the resulting blood boron clearance half-times iv in rats was much greater than those when volumes less than 0.067 mL/g body weight were used. These doses and volumes require porphyrin concentrations of about 3.3 mg/mL, which are close to the limit of solubility.

Therapeutic levels of boron were attained in tumor when rats were given a total dose of 220 mg/kg body weight given over 48 hours. Boron concentrations of 54 μg B/g in tumor and 4 μg B/g in blood were achieved 2 days after the end of infusion (Figure 2). Shorter infusion times of 2 and 24 hours were tested but sufficient levels of boron could not be attained. It appears that porphyrins must be allowed to circulate in blood for a minimum period of time for penetration into tumor tissue to occur. Once porphyrins accumulate in tumor, they remain for days instead of hours, as is the case for BPA or BSH.

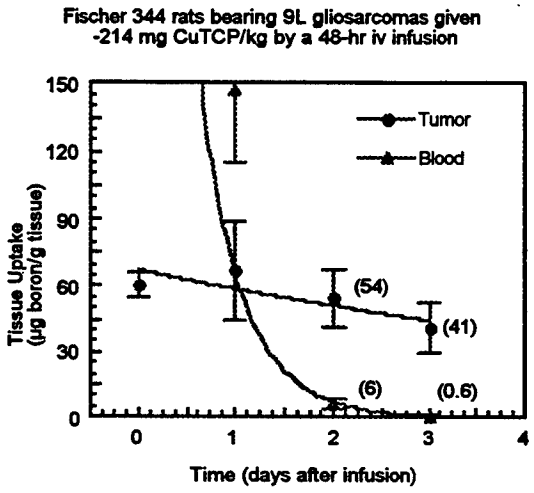

Figure 2. Boron concentrations in tumor and blood from rats bearing multiple subcutaneous gliomas at various times after the end of infusion.

Because supplies of ^{10}B-enriched decaborane, which is required for syntheses of carboranes, have been very limited, BNCT studies in rats have not been carried out. Demonstration of efficacy will therefore be shown first in mice, which require one-tenth the amount of compound. The use of murine breast tumor models seem pertinent as there appears to be correlation of porphyrin uptake with the rat glioma model.

The lack of toxicity from NiTCP was puzzling to us since porphyrins tested in the past have elicited abnormalities in weight change, physical appearance, behavior, platelet count, hepatic and renal enzyme levels.

Whether this can be attributed to the lipophilicity of NiTCP (requiring the use of solvating agents other than water), or to a structural feature of NiTCP is a question which was studied.

Before NiTCP, the porphyrin most thoroughly studied in our laboratory was VCDP, which is an analogue of heme, a natural porphyrin. Following a 4-day dosing period and a 4-day clearance period, 40-50 μg B/g were found in tumor tissue with 10:1 tumor:blood and 6:1 tumor:brain boron concentration ratios. Although toxic effects were observed in mice, most were reversible after 4 days. However, a particular side-effect, thrombocytopenia, could not be considered safe for patients with potentially hemorrhagic tumors such as glioblastoma multiforme. Before NiTCP, no porphyrin tested in rodents (VCDP, TPPS, BTPP, and BOPP) when given at potentially therapeutic doses, has been shown not to induce thrombocytopenia.

BTPP and TPPS are tetraphenyl-porphyrins, having a symmetric structure with phenyl substituents at the meso (methine) positions only (somewhat similar to NiTCP in Figure 1). VCDP and BOPP are natural porphyrin derivatives, having an asymmetric structure with substituents at the pyrrolic positions only (the R substituents in Figure 1). All four porphyrins are water-soluble.

We have synthesized two water-insoluble natural porphyrins, NiDPE and ZnDPE. They were each emulsified in CRM and PRG and tested in mice for any reduction in toxicities. Each was toxic at comparably low doses, and therapeutic levels of tumor boron were not attained.

In the KHJJ mammary carcinoma, NiTCP-H, an analogue of NiTCP (where Y = H in Figure 1) delivered as much boron to tumor as had NiTCP. While uptake of NiTCP-H in the B16 melanoma of C57Bl mice was only about 25 μg B/g in tumor, that in the EMT-6 mammary tumor was about 120 μg B/g, each 2 days after the last injection. Four days after the last injection, the EMT-6 tumor boron was still 114 μg B/g and the tumor:blood boron concentration ratio was greater than 500:1. In both types of tumors, NiTCP-H delivered twice as much boron as NiTCP and each are potentially therapeutic amounts. When CuTCP was tested, the boron biodistribution and toxicity were similar to those for NiTCP.

Unlike previous porphyrins tested, there was no serious toxicity, particularly thrombocytopenia, observed in mice given NiTCP-H, NiTCP or CuTCP.

^{10}B-enriched CuTCP-H has been synthesized and administered to BALB/c mice bearing EMT-6 leg tumors. Four groups of 7 mice each were irradiated with thermal neutrons at 5, 10, 15, and 20 MW-minutes at the Brookhaven Medical Research Reactor. A group of 3 mice which were given the porphyrin in a similar manner were euthanized at the time the previous 4 groups were irradiated for biodistribution. The 3 mice had tumor boron values of 79, 66, and 104 μg B/g and had blood boron values of 23, 0.2 and 2.3 μg B/g. One control group received no porphyrin nor any irradiation and another received neutron irradiation only. No information on efficacy is available at this time, since BNCT was carried out only one week ago.

Summary: Therapeutic concentrations of boron have been attained in both murine mammary tumor models and in a rat glioma model. NiTCP-H and CuTCP-H delivered robust concentrations of boron to the EMT-6 tumor, >100 μg B/g in mice, with >500:1 tumor:blood and >50:1 tumor:brain boron

concentration ratios. Neither compound appears to elicit toxicity in rodents even at the large doses given. These porphyrins have qualities that may substantially improve the therapeutic gain when combined with BPA for BNCT due to an increase in the radiation dose differential resulting from large tumor:normal tissue boron ratios. The long tumor retention time make these compounds particularly attractive for fractionation of BNCT, which may prove necessary for palliation of glioblastoma multiforme.

PAPERS/JOURNALS/PUBLICATIONS:

M. Miura, D.D. Joel, M.M. Nawrocky, P.L. Micca and D.N. Slatkin, *In vivo* studies of carborane-containing metalloporphyrins for boron neutron capture therapy. Proceedings for the 7th International Symposium on Neutron Capture Therapy for Cancer. Elsevier Science, NY in press.

M. Miura, P.L. Micca, C.D. Fisher, C.R. Gordon, J.C. Heinrichs and D.N Slatkin, Evaluation of carborane-containing porphyrins as tumour-targeting agents for boron neutron-capture therapy. Brit. J. Radiol., submitted.

M. Miura, D.N. Slatkin and J.A. Shelnutt, Boronated porphyrins and methods for their use. U.S. Patent pending.

LDRD FUNDING:

FY 1997	$86,157
FY 1998 (est.)	$111,000

Note: This project involves animal vertebrates or human subjects.

Development of Pump-and-Probe LIDAR for the In Situ Study of Fast Atmospheric Chemical Reactions

Arthur J. Sedlacek III *97-50*

PROJECT DESCRIPTION:

Since tropospheric ozone is central in the generation of the important oxidizing hydroxyl radical (·OH), there exists an important need to completely and thoroughly understand the factors that influence the atmospheric chemistry of ozone. However, although our understanding of ozone chemistry is quite mature, very little work has been conducted on examining the sensitivity of ozone's short-term chemistry on microenvironments, such as near-factory emission stacks, or over large bodies of water where the aerosol burden can be quite high.

In an effort to better understand and elucidate fast atmospheric photochemistry and the sensitivity of these reactions on microenvironments, the present LDRD was initiated to study the *in situ* reaction of $O(^1D)$, produced via the photolysis of tropospheric ozone, with ambient H_2O vapor, through the use of a novel pump-and-probe lidar technique. Specifically, the $O(^1D)/H_2O$ reaction shall be studied by using the output of a 266 nm Nd:YAG laser to generate the $O(^1D)$ (and $O(^3P)$) atoms via the photolysis of atmospheric ozone, and following the production and subsequent loss of the hydroxyl radical using a novel differential absorption lidar (DIAL)-like technique, referred to as RaDIAL, to monitor the species concentration on every laser pulse independent of interferences due to unknown, and typically varying, aerosol burden and laser energy pulse-to-pulse fluctuations.

TECHNICAL PROGRESS AND RESULTS - Fiscal Year 1997:

Background: The proposed experiments will examine the atmospheric chemical reaction of oxygen atoms with atmospheric water vapor to generate the oxidizing OH radical. The presence of the hydroxyl radical in the atmosphere is important in that it serves as the primary oxidizing species for the removal of the major pollutants as well as methane and carbon monoxide. Generally speaking, tropospheric ozone, O_3, can undergo solar-induced photolysis to generate atomic and molecular oxygen, viz.,

$$O_3 + h\nu \rightarrow O_2 + O(^1D) \quad 1a$$

$$O_3 + h\nu \rightarrow O_2 + O(^3P). \quad 1b$$

Depending upon the wavelength of light that photolyzes the ozone parent, either the metastable $O(^1D)$ or ground state $O(^3P)$ atoms can be generated. It should be noted that due to stratospheric ozone, a solar blind region exists just below 300 nm, therefore limiting the total amount of $O(^1D)$ atoms that are generated since only photodissociation in the Hartley band of ozone (2130-170 nm) can generate these excited atoms. It is well documented that the metastable $O(^1D)$ species undergo either energy-transferring collisions, generating $O(^3P)$,

$$O(^1D) + (N_2, O_2) \rightarrow O(^3P) + (N_2(v), O_2(v)) \quad 2$$

or can undergo a reaction with water vapor to produce the OH radical

$$O(^1D) + H_2O \rightarrow 2OH, \Delta H_f = -28.7 \text{ kcal/mol.} \quad 3$$

Typical daytime concentration levels of OH approach 10^6 molecules/cm^3 with a nominal chemical lifetime of about a second, and as a result, its chemical effects tend to be very localized. However, to follow the reaction of interest in various microenvironments requires a chemical sensing probe that is sensitive, provide volumetric mapping of the

area of interest and be easily transportable. One such tool that meets these requirements is LIDAR (Light Detection And Ranging).

In most atmospheric investigations that are designed to follow either the daily or seasonal variation of OH, the techniques of laser-induced fluorescence (LIF) or differential absorption LIDAR (DIAL) are most often used. These OH probes have achieved detection limits on the order of 10^5 - 10^6 molecules/cm^3. It is interesting to note that when an LIF laser is tuned to 282 nm, in order to access one of the ro-vibronic transitions of OH, low detection limits are often plagued by interferences from additional OH molecules that can be traced back to the photolysis of ambient ozone by the probe laser (see equation 3). [1] This observation provided the basis for the present proposed study: photolysis of ambient ozone in order to induce an *in situ* reaction of $O(^1D)$ with H_2O in order to better understand fast atmospheric photochemistry.

Of the physical phenomena exploited with open-path sensors (i.e., lidar), the differential absorption technique has routinely achieved detection sensitivities on the order of low ppm to ppb levels, depending on the absorption cross-section, albedo variation, atmospheric make-up (i.e., aerosol burden), laser pulse-to-pulse energy stability, and atmospheric turbulence. In a typical application of DIAL, two probing laser lines are directed to the area of interest and their elastic return signals are monitored: λ_1 located at a highly-absorbing wavelength for the chemical species of interest and λ_2 in a non-absorbing spectral region, as shown in Figure 1.

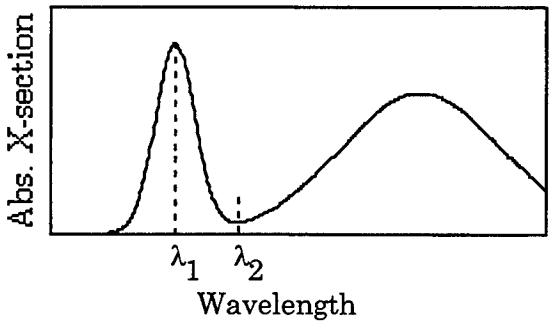

Figure 1: Schematic of the DIAL Technique

Elastic return of each outgoing laser line (λ_1 and λ_2) is provided through either a combination of Rayleigh scattering off of air molecules and the aerosol/ particulate-based Mie scattering or, if range-resolved mapping is not important, a retroflector [e.g., corner cube or sand-blasted aluminum as a back-drop].

In order to study the present reaction, for example, the probe laser would be tuned to the strong, narrow and well-resolved rotational lines of OH around 308 nm; specifically the $Q_1(2)$ and $Q_{21}(2)$ lines within the $A^2\Sigma^+$, $v' = 0$, <-- $X^2\Pi 3/2$, $v''=0$

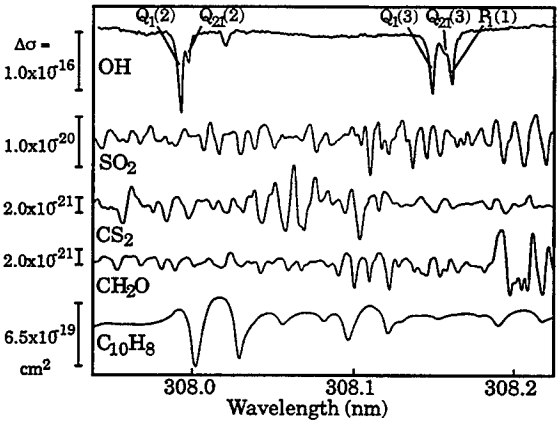

Figure 2: OH absorption spectrum (upper most trace) together with spectra from several other chemical species.

transition. These transitions are shown in Figure 2. However, despite the great sensitivity that the range-resolved DIAL platforms offer, they suffer from complex data reduction and error analysis complications due to real world complexities. This difficulty is a genetic one because the classical DIAL technique derives the molecule absorption information from the elastic-return channel mentioned above. Consequently, there is uncertainty in distinguishing variation in the return signal amplitude that is due to the presence or absence of the chemical species of interest from the spatial and temporal variations in the aerosol burden, or from laser power fluctuations. Although a variety of hardware and software techniques have been developed and implemented to confront these problems, the end result is typically an increase in the complexity of the DIAL platform. In an effort to address this significant short-coming, we have developed a novel lidar platform, referred to as RaDIAL, that combines the strengths of two existing lidar techniques to produce a system that can potentially achieve DIAL sensitivities without the complex data and error analysis thereby increasing the accuracy of the desired measurement. Work during this first year of funding focused on understanding this new open-path chemical sensing technique by conducting a series of proof-of-principle experiments.

Fiscal Year 1997 Activities: This RaDIAL technique utilizes the inelastic Raman scattering returns from atmospheric nitrogen and oxygen as the two *in situ* probing wavelengths for the DIAL-like measurement, where one of the Raman returns is tuned to the peak of the molecule absorption and the other to a non-absorbing region. In this way, the traditional concerns of atmospheric turbulence, aerosol burden and laser shot-to-shot energy variation in DIAL measurements completely disappear since the differential absorption measurement via RaDIAL takes place at *exactly* the *same time,* in the *same volume* of space and where the return signals propagate through the *same turbulence structure.* Consequently, the RaDIAL system potentially offers a superior chemical sensing technique when accuracy is critical.

One of the first species we investigated was atmospheric ozone. Shown in Figure 3 are ozone burden data collected using this technique along with data collected using a Dobson spectrometer. Although the scattering of the RaDIAL data is on the order of 15%, the agreement between the two independent techniques is excellent. It is also satisfying to note that these preliminary data represent the successful detection of a chemical species whose concentration is on the order of tens of ppb! It should be noted that the exploitation of the Raman returns from atmospheric nitrogen and oxygen as a method for estimating ozone burden has its origins in the work of Ranaut and co-workers [3] who in the early 1980s were developing a solar-blind Raman lidar platform for water vapor measurement and needed an in situ method for estimating the ozone burden. What we have done here is extend this idea beyond the measurement of atmospheric ozone and have successfully applied it to any chemical species possessing an absorption.

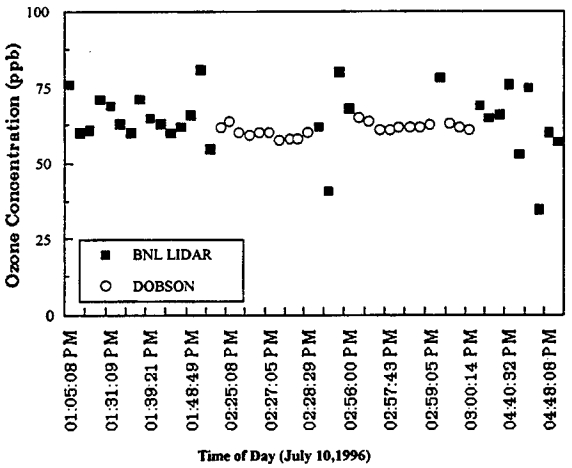

Figure 3: Ozone concentration measured as a function of time. Nominal stand-off distance is ~ 1.0 km.

In addition to probing for ozone, Brookhaven also received some seed money from DOE/NN-20 for a series of proof-of-

concept experiments which took place at the Remote Sensing Test Range (RSTR) on the grounds of the Nevada Test Site (NTS) and involved the detection of formal releases of acetone, nitrobenzene and sulfur dioxide at distances of 0.5, 1.4 and 3.3 kms. The present LDRD is leveraging off of research, experience and hardware obtained during BNL's participation in the DOE-funded CALIOPE program.

Shown in Figure 4 below is an example of some data collected from this summer's trip to NTS. In the present field experiment, acetone was poured into an open pan and allowed to evaporate. The laser operated at 266 nm thereby generating the probing RaDIAL wavelengths at 277.5 nm and 283.4 nm from atmospheric oxygen and nitrogen, respectively. At the beginning of the release, "baseline" data were collected at a distance of 1.05 km while the pan was loaded with the acetone. This was done so as to obtain an estimate of the tropospheric ozone loading. Once the pan was filled with the acetone, the range gating was changed to 1.37 km and the evolving acetone monitored as a function of time. Immediately following the commencement of the experiment, the measured nitrogen-to-oxygen ratio goes up to approximately 3.1. After approximately 5 minutes or so the measured ratio begins to decrease back to its expected "no-release" level of 2.6. This decrease is do to the extensive evaporative cooling that took place during this portion of the experiment. For example, at the beginning of the experiment the temperature of the acetone was ~ 38° C and, through evaporative cooling, went down to 3.7° C, which necessarily reduced the evaporation rate thus resulting in a reduction in the signal strength. A small "puff" is observed occurring at about 12:45 p.m., which is presumably due to re-heating of the now cooled acetone. At about 1:00 p.m., external heat was applied to the system thereby increasing the evaporation rate and causing the nitrogen-to-oxygen ratio to again go high. When all the acetone was used up (approximately 1:40 p.m.) the nitrogen-to-oxygen ratio returns to a new level dedicated by the 1.37 km range and 58 ppb loading of tropospheric ozone. Finally, it should be noted that in this spectral region, acetone is a very weak absorber owing to the fact that the absorption is based on a forbidden n -> π^* transition.

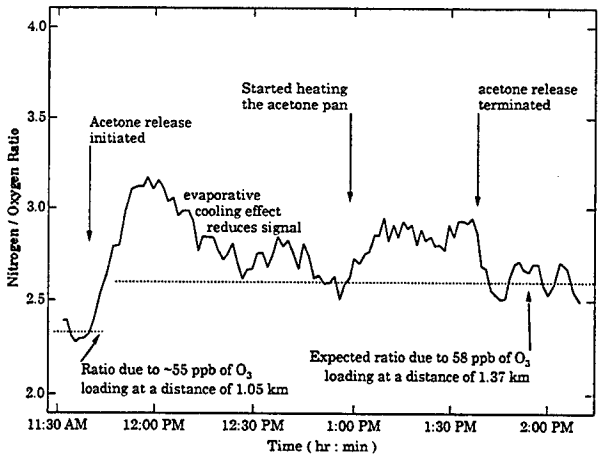

Figure 4: RaDIAL detection of an open-pan release of acetone at a distance of 1.37 kms.

This technique has also been successfully applied to the detection of SO_2, a precursor to acid rain, with a stand-off distance of 3.4 kms as well as nitrobenzene and the detection of emissions from a diesel generator.

With the successful development of this new, and highly sensitive technique, the study of the short-term ozone photochemistry will enter its second phase in fiscal year 1998; the detection of ambient levels of OH where the RaDIAL laser is set to 293.93 nm (34021.3 cm-1), therefore insuring that the Raman oxygen line will fall on the $Q_1(2)$ line of the OH ($A^2\Sigma^+$, $v' = 0$), <- - OH ($X^2\Pi^{3/2}$, $v''=0$) transition at 307.993 nm (32468.3 cm^{-1}) and the Raman nitrogen at 315.55 nm (31690.3 cm^{-1}). This will guarantee maximum sensitivity of the RaDIAL technique for OH detection. Although the laser wavelength could be set such that the Raman nitrogen line would fall on the $Q_1(2)$ line, this would require an excitation wavelength of 287.4 nm, thus potentially resulting in the creation of "probe" laser-generated $O(^1D)$ atoms from the photolysis of ozone in much the same

way as has plagued the LIF technique when using 282 nm excitation wavelengths.

Shown in Figure 5 is a schematic of the "probe" lidar platform that shall be used for the experiments. For the proposed experiments, the "pump laser" will be a 266 nm-based lidar system, and the "probe laser" will be a frequency-agile lidar system (both of which already exist at BNL). Each platform is composed of three main subsystems: (*i*) a laser system and beam transport optics, (*ii*) signal receiver telescope and spectral fingerprinting detection unit, and (*iii*) equipment control and data acquisition/processing subsystem. The laser source for the "pump" portion of the pump-and-probe lidar shall be Coherent's Infinity 266 nm Nd:YAG laser (beam width ~ 4-5 ns). Following expansion of the laser beam, to insure that the outgoing beam is eye safe before exiting the unit, the laser shall be directed to the area of interest. Using fast photodiodes and fiber optics, pump-laser firing information shall be forwarded to the "probe" lidar system for temporal synchronization. The laser system for the probe portion of the proposed experiments will be a Spectra-Physics GCR170 Nd:YAG-pumped dye laser system (Quanta Ray PDL-1) which will provide the required wavelength tunability. The RaDIAL return signals will be collected by a 16-inch Cassegrain telescope and focused onto the slits of a single-grating spectrometer (2400 grooves/mm) and then detected by Oriel's Intaspec V intensified CCD (charge-coupled device) camera for spectral fingerprinting. Temporal behavior of the hydroxyl radical shall be provided by changing the delay time between the time the "pump" laser (266 nm) generates the $O(^1D)$ atoms and the "probe" laser detects the OH radical through the RaDIAL technique. The collected probe lidar return signals will be immediately curve fit to a Voigt lineshape so that the N_2/O_2 ratio can be calculated in real time and will also be stored for off-line data analysis. All timing aspects for distance ranging a specific target is based on a single-master oscillator (clock) which provides triggering to the lasers and gate delay timing to the detector circuitry.

Upon the successful detection of the ambient levels of OH, the project will enter its third and final phase: the *in situ* creation of $O(^1D)$ atoms, through photolysis of ambient ozone, and following the insuing $O(^1D)$/water vapor reaction by monitoring

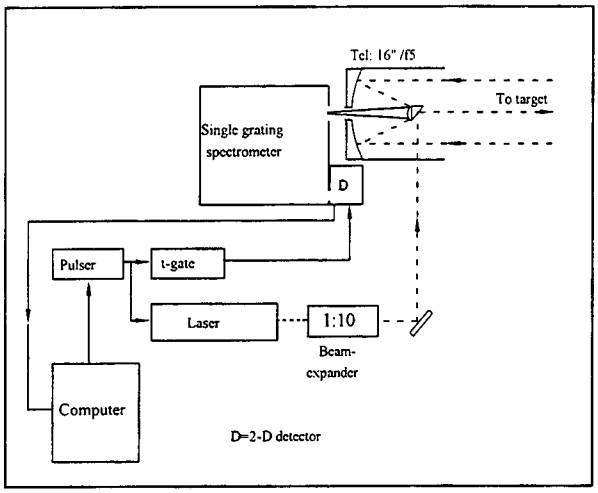

Figure 5. Schematic of Open-Path RaDIAL System

the creation and subsequent loss of the OH radical. The study of this reaction will be conducted on-site at BNL, as well as near various industrial park settings (i.e., power plant operations, etc.) where the microenvironments are very different.

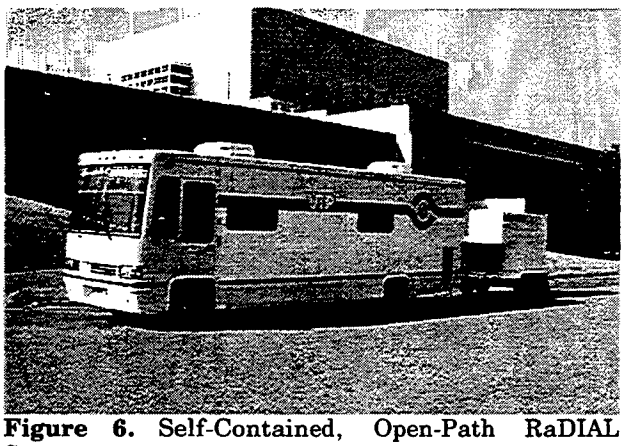

Figure 6. Self-Contained, Open-Path RaDIAL System

Figure 6. Self-Contained, Open-Path RaDIAL System

Due to the fact that the $O(^1D)/H_2O$ reaction will be examined *in situ*, the expected temporal behavior of the OH transient, both on a short time scale (100s ns) and long time scale (ms) must be addressed. Fortunately, this issue has been examined in detail by the theoretical studies of Clericetti et al. [2] and Smith and Crosley [1]. Smith and Crosley's interest in reaction 3 was in an effort to understand and potentially quantitate the interferences that the LIF probe laser photolysis of O_3 would have on a study of ambient OH concentration levels and temporal behavior. This detailed analysis is complete in that it accounts for reactive channels, quenching channels, rotational and vibrational relaxation pathways as well as additional absorption and competing radiative processes. The predicted transient lifetimes by Clericetti et al. [2], on the order of ms, is well within the temporal resolution of our LIDAR instrument. It is the goal of this investigation to elucidate this issue and its dependence on microenvironments.

Literature Cited

1. Smith, G. P. and Crosley, D. R., J. Geophy. Res. 95, (1990), p. 16,427.

2. Clericetti, A., Calpini, B, Durieux, E.,van den Bergy, H., and Rossi. M.J. SPIE 1714 Lidar for Remote Sensing, (1992) p. 291.

3. Renaut, D., Pourny J.C. and Capitini R., Optics Lett **5** (6) (1980) 233.

ACCOMPLISHMENTS:

During the course of this first year of funding, the PI approached DOE/NN-20 to discuss the potential applications of the RaDIAL technique towards the detection of trace effluents. DOE provided funding of $200,000 towards conducting a series of field tests at the Remote Sensing Test Range (RSTR) on the Nevada Test Site (NTS). This work for NN-20 differs from the current LDRD work in that it will deal with the ability to detect effluents related to proliferation activities and is in support of our general national security interests rather than the current atmospheric related project.

In addition, a patent on this idea for chemical sensing is currently being pursued. A manuscript describing the RaDIAL technique, along with results from the proof-of-principle experiments carried out at NTS, is in the final stages of preparation. Finally, although a proposal based on this idea and submitted to DOE's Office of Health and Environmental Research in response to the Atmospheric Chemistry Program's call for proposals (OER Notice 97-12) was not funded, solicitation for outside funding of this proposal will continue.

LDRD FUNDING:

FY 1997	$ 99,066
FY 1998 (est.)	100,000
FY 1999 (est.)	100,000

Molecular Biological Markers as Potential Prognostic Indicators for BNCT

Jacek Capala *97-70*
Jeffrey A. Coderre
Arjun D. Chanana
Aidnag Z. Diaz
Darrel D. Joel

PROJECT DESCRIPTION:

Thirty-five patients have been treated with BNCT since September 1994. Although palliation of the tumor was achieved in all cases, the time to progression could not be correlated with clinical prognostic indicators. In this project we search for molecular markers that could be of use in predicting the course of the disease and to correlate their presence in samples of tumors (formalin fixed, paraffin embedded sections) obtained from BNCT patients with clinical outcome.

Studies by Hoshino, et al. (1) indicate that the survival of patients with intracranial glioma appears to correlate inversely with the proliferative potential (determined by in-vivo BrdUrd labeling) of the tumor. Hoshimo's group conducted another designed study determined by using a monoclonal antibody (Ki-67) to a non-histone nuclear matrix antigen. This antigen is present in late G1, G2, S and M phases of the cell cycle and is absent in Go and early G1 phases. Good correlation was demonstrated. Use of Ki-67 antibody requires frozen sections. However, another monoclonal antibody to this antigen (MIB-1) can be used on formalin-fixed and paraffin-embedded sections following the antigen retrieval by microwave heating (2).

Cytogenetic and molecular genetic studies of malignant gliomas have documented abnormalities in many autosomes especially the loss of heterozygosity for loci of chromosomes 10 and 17 (p53) and amplification of EGFR gene (chromosome 7). The amplification of the gene for EGFR protein is found over expressed in most malignant gliomas, especially in GMB (3). Patients expressing p53 (product of the tumor suppressor gene on chromosome 17) have significantly reduced survival. Both EGFR gene product and p53 protein can also be evaluated on formalin-fixed, paraffin-embedded sections.

TECHNICAL PROGRESS AND RESULTS – Fiscal Year 1997:

Purpose: The aim of this work is to evaluate the biological markers in formalin fixed, paraffin embedded, tumor sections obtained from BNCT patients that could help to predict responsiveness to BNCT and explain the variations in the clinical outcome. If such factors are identified, then they could be used to identify patients that would optimally respond to BNCT and those for whom alternative treatments should be offered.

Approach: The specific goals of this project are:

a) to establish immunohistochemical laboratory;
b) to identify the possible biological markers, which have been shown to characterize tumor malignancy;
c) to develop and test protocols for detection and quantification of these markers;
d) to analyze the presence of these markers in tissue samples obtained from BNCT patients.

Technical Progress and Results:

a) A laboratory for immunohisto-chemical studies has been established in Medical Department;
b) Antigens, such as Ki67, p53 mdm2, EGFR, whose abnormal presence in tumor cells correlates with poor prognosis have been identified through literature studies and communication with leading scientist;
c) Protocols for immunohistochemical detection of Ki67, p53 and EGFR have been developed and tested on commercially available samples;
d) Brain autopsies of two BNCT patients were carried out in collaboration with the Department of Pathology, Stony Brook University Hospital. Representative samples of tumor, normal brain and transition regions, where both tumor and normal cells are present, have been obtained and prepared for immunohistochemical analysis. These samples are being currently used for final testing and fine-tuning of our methodologies.

ACCOMPLISHMENTS:

A laboratory for immunohistochemical studies has been established in Medical Department, which will be used to analyze the presence of biological prognostic factors in tumor samples obtained from BNCT patients.

REFERENCES:

1. Hoshino, T., et al. Int.J. Cancer 53, 550 (1993)

2. Onda, K., et al. Cancer 74, 1921 (1994)

3. Jaros, E., et al. Brit.J.Cancer, 66, 373 (1992)

LDRD FUNDING:

FY 1997	$99,822
FY 1998(est.)	$117,000

Note: This project involves animal vertebrates or human subjects.

LABORATORY DIRECTED RESEARCH AND DEVELOPMENT

1998 PROPOSED PROGRAM*

*New projects authorized for funding as of October 1, 1997.

Project Number 98-23

Beam Enhancement in a High Brightness Electron Linac

E. Johnson

"BNL has a leadership position in the development on concepts for the generation of vacuum ultra-violet radiation with Free Electron Lasers. The long-range target is to implement a Chirped Pulse FEL operating in the UV synchrotron radiation for a broad range of research. In this LDRD project we seek to undertake an experimental program to study the preservation of a low-electron beam emittance to the full energy of the accelerator and to test pulse compression schemes and emittance correction techniques."

FY 1998 Funding $250,000

Project Number 98-27

Novel Mechanisms of Hydroxy Fatty Acid Biosynthesis

J. Shanklin

"Crop plants vary in their fatty acid composition in terms of the degree of desaturation and in the chain length of the fatty acids. There are uncommon plants with unusual fatty acids such as hydroxy and epoxy groups. These fatty acids are desirable because the functional groups are stereospecific and can be easily derivitized and, therefore, used for specific industrial starting materials such as lubricants and plasticizers (which are currently obtained from petrochemicals)."

FY 1998 Funding $100,000

Project Number 98-42

AGS Spallation Neutron Source

J. Hastings

"The Brookhaven National Laboratory AGS Complex has many advantages as a facility for both the development and productive use of spallation neutron targets moderators and state-of-the-art neutron instrumentation. Chief among these advantages is that the existing AGS complex is capable of providing an average of 140 kW of proton beam power for a spallation neutron source (SNS) equal to the best in the world. The proposed program will study aspects of a working SNS using the AGS as a proton driver including target/ moderator design."

FY 1998 Funding $100,000

Project Number 98-58

Sensitive Detection and Rapid Identification of Biological Agents by Single Molecule Detection

M. Wu

"The project proposes to combine the techniques of capillary electrophoresis, immunofluorescence, and single-molecule detection for the creation of a portable system to perform rapid and reliable identification of biological agents."

FY 1998 Funding $100,000

Program Note: Due to a number of issues affecting Brookhaven National Laboratory, the LDRD Program will initially be reduced from current levels. BNL is in a period of financial uncertainty due to the termination and subsequent bidding process for a new contractor. Should the situation become more stable, funding levels would likely be restored.

Report Number (14) BNL--52351-97/12-Rev.

Publ. Date (11) 199712

Sponsor Code (18) DOE, XF

UC Category (19) UC-900, DOE/ER

no 1332.15 in folder

DOE